

**LANTHANIDS AND TRANSITION METALS
SATURABLE ABSORBER FILM FOR SHORT PULSE
FIBER LASER GENERATION AT 1.0 AND 1.55 MICRON
REGION**

MOHAMAD FAIZAL BIN BAHAROM

**FACULTY OF ENGINEERING
UNIVERSITY OF MALAYA
KUALA LUMPUR**

2021

LANTHANIDS AND TRANSITION METALS
SATURABLE ABSORBER FILM FOR SHORT PULSE
FIBER LASER GENERATION AT 1.0 AND 1.55 MICRON
REGION

MOHAMAD FAIZAL BIN BAHAROM

THESIS SUBMITTED IN FULFILMENT OF THE
REQUIREMENTS FOR THE DEGREE OF DOCTOR OF
PHILOSOPHY

FACULTY OF ENGINEERING
UNIVERSITY OF MALAYA
KUALA LUMPUR

2021

UNIVERSITY OF MALAYA
ORIGINAL LITERARY WORK DECLARATION

Name of Candidate: MOHAMAD FAIZAL BIN BAHAROM

Matric No: KVA170013

Name of Degree: DOCTOR OF PHILOSOPHY

Title of Project Paper/Research Report/Dissertation/Thesis (“this Work”):

LANTHANIDS AND TRANSITION METALS SATURABLE ABSORBER
FILM FOR SHORT PULSE FIBER LASER GENERATION AT 1.0 AND 1.55
MICRON REGION

Field of Study: PHOTONIC

I do solemnly and sincerely declare that:

- (1) I am the sole author/writer of this Work;
- (2) This Work is original.
- (3) Any use of any work in which copyright exists was done by way of fair dealing and for permitted purposes and any excerpt or extract from, or reference to or reproduction of any copyright work has been disclosed expressly and sufficiently and the title of the Work and its authorship have been acknowledged in this Work;
- (4) I do not have any actual knowledge nor do I ought reasonably to know that the making of this work constitutes an infringement of any copyright work;
- (5) I hereby assign all and every rights in the copyright to this Work to the University of Malaya (“UM”), who henceforth shall be owner of the copyright in this Work and that any reproduction or use in any form or by any means whatsoever is prohibited without the written consent of UM having been first had and obtained;
- (6) I am fully aware that if in the course of making this Work I have infringed any copyright whether intentionally or otherwise, I may be subject to legal action or any other action as may be determined by UM.

Candidate’s Signature

Date:

Subscribed and solemnly declared before,

Witness’s Signature

Date:

Name:

Designation:

**LANTHANOIDS AND TRANSITION METALS SATURABLE ABSORBER
FILM FOR SHORT PULSE FIBER LASER GENERATION AT 1.0 AND 1.55
MICRON REGION**

ABSTRACT

As pulsed laser technology has found expanding application in material processing, telecommunications, medical diagnostics and numerous other areas, the desire for inexpensive and robust laser sources has grown. Until recently, various passive saturable absorbers (SAs) have been introduced in developing Q-switched and mode-locked fiber lasers. However, tremendous research effort has been devoted to searching new alternative SA materials which accompany with high operation performance and simple SA fabrication method. This thesis proposed and demonstrated novel SA devices based on lanthanoid and metal oxides for developing various Q-switched and mode-locked fiber lasers operating at ~1 and 1.5 μm regions. New passive SAs based on three different materials: vanadium pentoxide (V_2O_5), lutetium oxide (Lu_2O_3) and nickel oxide (NiO) have been successfully fabricated and characterized in this work. V_2O_5 and NiO materials were embedded into polyethylene glycol (PEG) while Lu_2O_3 was embedded into polyvinyl alcohol (PVA) to compose a film absorber, which was then sandwiched between two fiber ferrule connectors with a fiber adapter to form a fiber compatible SA. The V_2O_5 , Lu_2O_3 and NiO based SA has a modulation depth of 7 %, 10 % and 9%, respectively. Various Q-switched and mode-locked fiber lasers have been successfully demonstrated in both 1- and 1.5-micron regimes by using the newly developed SAs in both 1- and 1.5-micron regimes. For instance, a Q-switched YDFL operating at 1067.8 nm was demonstrated using the Lu_2O_3 SA. The laser generates a stable pulses train with a pump power range from 116 mW to 151 mW with the maximum repetition rate of 46.68 kHz, the shortest pulse width of 4.6 μs and the highest pulse energy of 128 nJ. A soliton mode-locked Erbium-doped fiber laser (EDFL) operating at 1561.4 nm with a pulse width as short as 710 fs was also

successfully realized using the NiO based SA by optimizing the cavity design to operate at anomalous cavity dispersion of -0.282 ps^2 .

Keywords: Erbium-doped fiber, Ytterbium-doped fiber, Q-switching, Mode locking, Metal Oxide

Universiti Malaya

**LANTHANOIDS DAN LOGAM PERALIHAN BAGI FILEM PENYERAP TEPU
YANG SESUAI UNTUK GENTIAN LASER DENYUT PENDEK PADA
KAWASAN 1.0 DAN 1.55 MIKRON**

ABSTRAK

Teknologi laser denyut telah digunakan secara meluas dalam aplikasi pemrosesan bahan, telekomunikasi, diagnostik perubatan dan sebagainya, apabila diketahui umum bahawa sumber lasernya adalah lebih murah dan kukuh. Sehingga kini, pelbagai *passive saturable absorbers* (SAs) telah diperkenalkan dalam membangunkan laser gentian *Q-switched* dan *mode-locked*. Walau bagaimanapun, usaha penyelidikan yang lebih spesifik telah dijalankan untuk mencari bahan-bahan SA alternatif baru yang mempunyai sifat pengoperasian berprestasi tinggi dan kaedah fabrikasi SA yang lebih mudah. Tesis ini mencadangkan dan memperkenalkan peranti SA berdasarkan *lanthanoid* dan *metal oxide* untuk membangunkan pelbagai laser gentian *Q-switched* dan *mode-locked* di sekitar kawasan ~ 1 dan $1.5 \mu\text{m}$. SA pasif yang baru adalah berasaskan kepada tiga bahan yang berbeza: *vanadium pentoxide* (V_2O_5), *lutetium oxide* (Lu_2O_3) dan *nickel oxide* (NiO) telah berjaya difabrikasikan dan dikelaskan dalam operasi ini. Material V_2O_5 dan NiO telah tertanam ke dalam *polyethylene glycol* (PEG) manakala Lu_2O_3 telah tertanam ke dalam *polyvinyl alcohol* (PVA) untuk menghasilkan penyerap filem, yang kemudiannya diapit di antara dua penyambung gentian *ferrule* bersama penyesuai gentian untuk membentuk *fiber SA* yang sepadan. V_2O_5 , Lu_2O_3 dan NiO berasaskan SA mempunyai kedalaman modulasi masing-masing sebanyak 7%, 10% dan 9%. Pelbagai laser gentian *Q-switched* dan *mode-locked* telah berjaya dibuktikan dalam kedua-dua kawasan 1- dan 1.5 mikron dengan menggunakan SA yang baru dibangunkan dalam kedua-dua kawasan 1- dan 1.5 mikron. Sebagai contoh, dengan menggunakan Lu_2O_3 SA, telah dibuktikan bahawa *Q-switched* YDFL boleh beroperasi pada 1067.8 nm. Laser tersebut telah menjana *pulse train* stabil dengan julat kuasa pam dari 116 mW hingga 151 mW dengan kadar

pengulangan maksimum 46.68 kHz, lebar nadi terpendek 4.6 μ s dan tenaga nadi tertinggi 128 nJ. Dengan menggunakan NiO berasaskan SA, *Soliton mode-locked Erbium-doped fiber laser* (EDFL) yang beroperasi pada 1561.4 nm dengan lebar nadi sesingkat 710 fs juga telah berjaya direalisasikan dengan mengoptimumkan reka bentuk rongga untuk beroperasi pada penyebar rongga *anomalous* -0.282 ps².

Kata Kunci: Erbium-doped fiber, Ytterbium-doped fiber, Q-switching, Mode locking, Metal Oksida

Universiti Malaysia

ACKNOWLEDGEMENTSBLESS

In the name of Allah, the Most Gracious, the Most Merciful

First and foremost, praises and thanks to the Allah s.w.t, the Almighty, for His blessings throughout my research work to complete the research successfully.

I would like to express my deep and sincere gratitude to my research supervisor, Prof. Ir. Ts. Dr. Sulaiman Wadi Harun for giving me the opportunity to do research and providing invaluable guidance throughout this research. His dynamic, vision, sincerity and motivation have deeply inspired me. He has taught me the methodology to carry out the research and to present the research work as clearly as possible. It was a great privilege and honor to work and study under his guidance.

I would like to express my gratitude to my parents for their love, prayers, caring and sacrifices for educating and preparing me for my future. I am very much thankful to my wife and my children for their love, understanding, prayers and continuing support to complete this work.

I am extremely grateful to my seniors Ir Ts Dr Anas and Ir Ts Dr Mohd Fauzi for their motivation and invaluable ideas in managing my research works. Their immense knowledge and plentiful experiences have encouraged me in all the time. I also owe my appreciation to my friends and all photonics laboratory members in University of Malaya for their genuine support throughout this research work.

Finally, my special thanks goes to Universiti Teknikal Malaysia Melaka (UTeM) and Ministry of Higher Education Malaysia (MOHE) for giving financial aids for my PhD program under SLAB scholarship.

TABLE OF CONTENTS

Abstract	iii
Abstrak	v
Acknowledgement.....	vii
Table of Contents	viii
List of Figures	xi
List of Tables.....	xiv
List of Symbols and Abbreviations.....	xv
List of Appendices	xvii
CHAPTER 1: INTRODUCTION.....	1
1.1 Background and Motivation	1
1.2 Thesis Objectives.....	4
1.3 Thesis Overview	4
CHAPTER 2: LITERATURE REVIEW.....	6
2.1 Introduction.....	6
2.2 Principle of optical fiber laser.....	7
2.2.1 Ytterbium doped fiber laser.....	8
2.2.2 Erbium doped fiber laser	10
2.3 Pulsed fiber laser.....	12
2.3.1 Principle of Q-switching	12
2.3.2 Formation of Q-switched pulses and their important parameters	14
2.3.3 Principle of mode-locking	18
2.4 Propagation of optical pulses in a fiber	20
2.4.1 Dispersion.....	20

2.4.2	Nonlinear Effect	23
2.4.3	Self-phase modulation	24
2.5	Saturable Absorber	27

CHAPTER 3: VANADIUM OXIDE FILM AS PASSIVE Q-SWITCHER AND MODE LOCKER DEVICE 30

3.1	Introduction.....	30
3.2	Preparation and Characterization of V ₂ O ₅ SA.....	32
3.3	Q-Sswitched laser operating at 1-micron region with V ₂ O ₅ SA.....	37
3.4	Q-switched laser operating at 1.5-micron region with V ₂ O ₅ SA.....	45
3.5	Mode-locked laser operating at 1.5-micron region with V ₂ O ₅ SA.....	51
3.6	Summary.....	57

CHAPTER 4: LUTETIUM (III) OXIDE FILM AS PASSIVE Q-SWITCHER AND MODE LOCKER DEVICE 59

4.1	Introduction.....	59
4.2	Lutetium Oxide Film Fabrication and Characterization.....	61
4.3	Q-switched EDFL with Lu ₂ O ₃	65
4.4	Inducing Q-switching operation at 1-micron all fiber laser via Lu ₂ O ₃ film SA....	71
4.5	Inducing mode-locking operation with Lu ₂ O ₃	76
4.6	Summary.....	82

CHAPTER 5: MICROSECOND AND FEMTOSECOND PULSE GENERATION WITH NICKEL OXIDE SATURABLE ABSORBER..... 83

5.1	Introduction.....	83
5.2	Preparation of Characterization of Nickel Oxide Film SA.....	84

5.3	Microsecond Q-switched Pulse Generation in 1-Micron region Nickel Oxide Nanoparticles Saturable Absorber	87
5.4	Q-switched microsecond pulse in 1.5-micron spectral range with NiO SA.....	94
5.5	Mode-locked femtosecond pulse in 1.5-micron spectral range with NiO SA.....	100
5.6	Summary.....	105
CHAPTER 6: CONCLUSION AND OUTLOOK		107
6.1	Conclusion.....	107
6.2	Future Work.....	112
	References	113
	List of Publications and Papers Presented	132
	Appendix	134

LIST OF FIGURES

Figure 2.1: Energy level of Ytterbium doped silica fibers.....	9
Figure 2.2: The absorption and emission cross-section of a silica fiber	10
Figure 2.3: Simplified energy levels of Erbium ions in EDF.....	11
Figure 2.4: The formation of Q-switched fiber laser	15
Figure 2.5: The cycle of the formation of Q-switched fiber laser.....	15
Figure 2.6: Phenomenological description of spectral broadening of pulse due to SPM. (Gangwar et al., 2007).....	26
Figure 3.1: (a) yellowish-brown V_2O_5 compound and (b) its XRD profile	33
Figure 3.2: (a) A light yellow solid thin film of V_2O_5 (b) FESEM image (c) the film placed onto a fiber ferrule tip (d) all-fiber V_2O_5 SA device.....	34
Figure 3.3: (a) linear absorption curve (b) the nonlinear measurement setup (c) nonlinear saturable absorption curve for the V_2O_5 -SA film.....	37
Figure 3.4: Configuration of the Q-switched YDFL with V_2O_5 SA thin film	38
Figure 3.5: pump powers; (a) 96.1 mW (b) 130.5 mW and (c) 171.8 mW	41
Figure 3.6: Q-switched pulse characteristics at the pump power of 171.8 mW, showing (a) optical output spectrum and (b) RF spectrum	42
Figure 3.7: (a) Pulse width and repetition rate and (b) pulse energy and average output power corresponding to the pump power.....	44
Figure 3.8: Configuration of the Q-switched EDFL with V_2O_5 SA thin film.....	46
Figure 3.9: (a) Output spectral and (b) RF spectrum characteristics of the Q-switched EDFL at at a pump power of 138.7 mW	47
Figure 3.10: (a) Output spectral and (b) RF spectrum characteristics of the Q-switched EDFL at at a pump power of 138.7 mW	49
Figure 3.11: Q-switching performances of the V_2O_5 based EDFL against pump power (a) Repetition rate and pulse width (b) Average output power and single pulse energy.....	50
Figure 3.12: Schematic diagram of the experimental setup for the mode locked EDFL with V_2O_5 SA	52

Figure 3.13: The spectral and temporal characteristics of the V ₂ O ₅ based mode locked EDFL (a) Output spectrum (b) Oscilloscope trace (c) Autocorrelator trace (d) RF spectrum.....	55
Figure 3.14: Output power and single pulse energy versus pump power for the V ₂ O ₅ based mode locked EDFL	56
Figure 4.1: The proposed fabrication process of the Lu ₂ O ₃ thin film SA.....	62
Figure 4.2: The image and important characteristics of the Lu ₂ O ₃ film SA (a) real image (b) EDS profile (c) SEM image (d) Linear absorption profile.....	64
Figure 4.3: The nonlinear absorption profile of the Lu ₂ O ₃ film SA	65
Figure 4.4: Schematic diagram of the EDFL in ring-cavity configuration.....	66
Figure 4.5: The spectral and temporal characteristics of the Q-switched EDFL (a) Output spectrum (b) Oscilloscope trace (c) RF spectrum.....	69
Figure 4.6: Q-switched EDFL performances. (a) Output power, and pulse energy responses. (b) Pulse repetition rate, pulse width, and peak power responses.	71
Figure 4.7: Schematic diagram of the proposed Q-switched YDFL cavity.....	72
Figure 4.8: The spectral and temporal performances of the Q-switched YDFL (a) Output spectrum. (b) Repetition rate and pulse width (c) Oscilloscope train. (d) RF spectrum.....	75
Figure 4.9: Output power and pulse energy	76
Figure 4.10: The proposed EDFL mode-locked experimental setup.....	77
Figure 4.11: Mode-locked EDFL via Lu ₂ O ₃ film SA important characteristics at 145 pump power (a) Output spectrum (b) Oscilloscope trace (c) Autocorrelator trace (d) RF spectrum, while the inset shows the fundamental frequency in detail.....	80
Figure 4.12: The output power, pulse energy and peak power of the mode-locked EDFL as a function of pump power (145-187 mW).....	81
Figure 5.1: The fabrication process of NiO nanoparticles thin film (a) synthesis of NiO nanoparticles (b) Embedding the nanoparticles into the PEG film.....	84
Figure 5.2: (a) Image of the fabricated NiO PEG thin film image (b) FESEM image (c) XRD pattern of the NiO nanoparticles embedded on the PEG thin film (d) The NiO film attached onto a fiber ferrule tip.	86
Figure 5.3: The nonlinear saturable absorption curve for the NiO PEG film	87

Figure 5.4: The schematic diagram of the proposed Q-switched YDFL with NiO based SA.....	88
Figure 5.5: Output spectrum of the Q-switched YDFL at 89.2 mW pump power	89
Figure 5.6: Temporal characteristics of the Q-switched YDFL at pump powers of (a) 89.2 mW (b) 158.7 mW and (c) 226 Mw.....	91
Figure 5.7: The Qwitching performance of the YDFL (a) Repetition rate and pulse width (b) average pump power and single pulse energy against the pump power.....	93
Figure 5.8: RF spectrum at 226 mW pump power.....	93
Figure 5.9: Configuration of the Q-switched microsecond EDFL.....	94
Figure 5.10: Typical output pulse train at pump powers of (a) 143.8 mW, 191 mW and (c) 239.6 mW	96
Figure 5.11: Spectral and temporal characteristics of the Q-switched EDFL (a) Measured optical spectrum (b) RF spectrum on a 600 kHz span where the fundamental frequency is 58.85 kHz. Inset of (b) indicates the RF spectrum of fundamental frequency on a 60 kHz span.	97
Figure 5.12: Q-switching performance of the NiO based EDFL (a) Variation of the repetition rate and pulse width with pump power (b) Variation of the average output power and pulse energy with pump power	99
Figure 5.13: Configuration of the soliton mode-locked femtosecond EDFL	101
Figure 5.14: Output performance of the soliton EDFL based on NiO PEG film SA: (a) measured optical spectrum centred at 1561.4 nm (b) typical output pulse train with a spacing of 303 ns; (b) (c) autocorrelation trace of the 710 fs output pulses together with a sech ² fit; (d) RF spectrum showing the signal-to-background contrast of 72 dB.	104
Figure 5.15: Average output power and pulse energy as functions of pump power.....	105

LIST OF TABLES

Table 2.1: summarizes various 2D materials groups, which were recently discovered. In this work, V_2O_5 , Lu_2O_3 and NiO based SA are developed and proposed for Q-switching and mode-locking applications.(Geim et al., 2013)	29
Table 3.1: Performance comparison of mode-locked EDFL using various SA materials	57
Table 6.1: Comparison of Q-switching performances	111
Table 6.2: Comparison of mode-locking performances.....	111

Universiti Malaysia

LIST OF SYMBOLS AND ABBREVIATIONS

Al_2O_3	:	Aluminium Oxide
BP	:	Black Phosphorus
CNT	:	Carbon Nanotube
CPM	:	Cross phase Modulation
CW	:	Continues Waveform
EDF	:	Erbium Doped Fiber
EDFA	:	Erbium Doped Fiber Amplifier
EDFL	:	Erbium Doped Fiber Laser
EDS	:	Energy Dispersive Spectroscopy
Er^{3+}	:	Erbium
FESEM	:	Field Emission Scanning Electron Microscope
FWHM	:	Full Width Half Maximum
GVD	:	Group Velocity Dispersion
LD	:	Laser Diode
Lu_2O_3	:	Lutetium Oxide
MoS_2	:	Molybdenum Disulfide
NH_4VO_3	:	Ammonium Metavanadate
NiO	:	Nickel Oxide
NLDR	:	Nonlinear Dispersive Regime
OPM	:	Optical Power Meter
OSA	:	Optical Spectrum Analyzer
OSC	:	Oscilloscope
PD	:	Photodetector
PEG	:	Polyethylene Glycol

PVA	:	Polyvinyl Alcohol
RBW	:	Resolution Bandwidth
RF	:	Radio Frequency
RFSA	:	Radio Frequency Spectrum Analyzer
SA	:	Saturable Absorber
SBS	:	Stimulated Brillouin Scattering
SEM	:	Scanning Electron Microscope
SESAM	:	Semiconductor
SMF	:	Single Mode Fiber
SNR	:	Signal to Noise Ratio
SPM	:	Self-Phase Modulation
SRS	:	Stimulated Raman Scattering
TBP	:	Time Bandwidth Product
TiO	:	Titanium Oxide
TMD	:	Transition Metal Dichalcogenides
TMO	:	Transition Metal Oxide
V ₂ O ₅	:	Vanadium Oxide
VBW	:	Video Bandwidth
VOA	:	Variable Optical Attenuator
WDM	:	Wavelength Division Multiplexing
WS ₂	:	Tungsten Disulfide
XRD	:	X-ray Diffraction
YDF	:	Ytterbium Doped Fiber
YDFL	:	Ytterbium Doped Fiber Laser
ZnO	:	Zinc Oxide

LIST OF APPENDICES

Appendix: Publications

134

Universiti Malaya

CHAPTER 1: INTRODUCTION

1.1 Background and Motivation

Despite the impressive success of the titanium sapphire laser as a source of ultrashort pulses, solid-state lasers are limited in real-world applications due to their cooling requirement, size, cost and need for precise alignment of bulk optical components (Bourzeix et al., 1993; Walsh et al., 1997). Fiber lasers have surfaced in the last decade as an alternate approach to generate high energy short pulses (Walsh et al., 1997). They use a rare-earth doped fiber as a gain medium, and thus have many advantages over its solid-state counterparts. The large ratio of the surface area to the volume of the fiber eliminates the need for water cooling of the laser medium. In addition, the waveguide nature of optical fiber enables perfect overlap of the pump and signal in the gain medium, and thus eliminate the need for optical alignment. The single mode properties of optical fiber ensure excellent beam quality. Practically, fiber lasers tend to be less expensive than solid-state lasers, enabling laser technology to be more widely adopted in various industries.

Pulsed lasers have become an essential part of optical communications (Salehi et al., 1990), micromachining (Gattass et al., 2008), medical diagnostics (Nagy et al., 2009; Plamann et al., 2010), multiphoton imaging (C. Xu et al., 2013), spectroscopy and microscopy (Freudiger et al., 2014). Pulse generation can be realized by either Q-switching or mode-locking method. As the name would imply, Q-switching is a process where the quality factor of the cavity (energy stored in the cavity divided by energy loss per round trip) rapidly switches between high values and low values. The result is that the cavity stores light and energy while the Q factor is high before rapidly dissipating it as a pulse of durations ranging from microseconds to nanoseconds when the Q factor is low (Adachi et al.).

Mode-locking is another method of producing ultrafast pulses in a fiber laser that uses saturable absorbers (SAs) (Haus, 2000). A mode-locked laser can be realized by placing a SA material inside the laser cavity that absorbs a (proportionally) large percentage of light at low intensities but allows higher intensity light to pass through with reduced absorption. When a laser is not mode-locked, the intensity of the light that bounces around the cavity fluctuates semi-randomly due to the constructive and destructive interference between allowed modes. A SA placed in the cavity will attenuate the higher intensity fluctuations to a lesser degree than the lower intensity ones. After many such attenuations, the low intensity fluctuations are absorbed away entirely, and a pulse train forms. Even then, the saturable absorber improves the pulses. The low-intensity leading, and trailing parts of each pulse are attenuated more strongly than its high-intensity pulse center. This makes the newly formed pulses shorter and shorter over several iterations until a pulse-width as short as femtoseconds is attained. The width of this pulse then depends on the gain bandwidth of the gain material and on the response time of the SA. The more frequencies that the gain material produces in a laser (i.e., the more modes generated inside the laser cavity), the narrower a pulse can be. Similarly, as a general trend, the faster a saturable absorber can respond to light, the shorter the pulse can be.

Optical fiber provides a suitable platform for the development and monolithic combination of laser technology. Over the past decade, fiber laser technology has been rapidly developed especially on pulse generation. In the early years, semiconductor saturable absorption mirrors (SESAMs) (Gomez, 2004; Z.-C. Luo et al., 2010), carbon nanotubes (CNTs) (Ahmed et al., 2014; Set et al., 2004), and graphene SAs (Sun et al., 2010; Zhang et al., 2009) have been successfully used as the passive SA in both Q-switched and mode-locked fiber lasers. SESAMs which debuted in 1992 (Okhotnikov et al., 2004), quickly became the most prominent SA for some years. However, these devices have certain drawbacks including relatively high production cost, narrow

absorption bandwidth and considerably bulky for a fiberized laser source. In addition, CNTs have an operating wavelength based on their nanotube diameter which has a low damage threshold. Graphene, on the other hand, has a relatively low optical absorption per layer that limits its usability.

So far, many new SA materials were proposed and demonstrated to realize passive Q-switched and mode-locked pulses trains. For instance, BP is one of the most attractive SA materials for pulse generation due to their excellent conductive properties, ultrafast non-linear optical response wide bandwidth application (Y. Chen et al., 2015). However, BP is a hydrophilic material that easily interacts with water, as well as a polarization dependent material; thus, integrating BP as SA requires a complex preparation as well as careful handling. Thus, in recent years, several other new materials (Al-Hiti et al., 2019; Guo et al., 2018; Nizamani et al., 2020) with relatively easy preparation techniques have been proposed as SA candidates in promoting reliable and stable pulsed fibre lasers.

Despite many other materials were proposed and demonstrated, transition metal oxide (TMO) based materials are rarely being investigated for Q-switching and mode-locking applications. This type of material has high potential and significant advantages due to its high absorption capacity. For example, zinc oxide (ZnO) (Harith Ahmad, Lee, et al., 2016), nickel oxide (NiO) (M. Rusdi et al., 2019), titanium dioxide (TiO₂) (Harith Ahmad, Reduan, et al., 2016) and lately aluminum oxide (Al₂O₃) (Al-Hayali et al., 2017) have been demonstrated as a SA device in many laser cavities. This thesis focuses on developing Q-switched and mode-locked fiber lasers utilizing new materials based on vanadium pentoxide, lutetium oxide and nickel oxide.

1.2 Thesis Objectives

Q-switched and mode-locked fiber lasers have been widely researched due to their applications in micromachining, optical communication, metrology, medicine, and others.

This thesis aims to develop new saturable absorber devices, which can be fabricated by a simple, low cost and straight forward process and demonstrate high performance Q-switched and mode-locked lasers. This study focuses on the use of new materials based on lanthanoid and metal oxides for developing these lasers. Several objectives have been outlined to guide the research direction toward the goal:

- a) To fabricate and characterize new passive SAs based on three different materials: vanadium pentoxide (V_2O_5), lutetium oxide (Lu_2O_3) and nickel oxide (NiO).
- b) To demonstrate various Q-switched fiber lasers based on the newly developed SAs in both 1- and 1.5-micron regimes.
- c) To demonstrate various mode-locked fiber lasers based on the newly developed SAs.
- d) To optimize the cavity design of the mode-locked laser to generate soliton femtosecond pulses.

1.3 Thesis Overview

This thesis contains 6 chapters in which a comprehensive study on Q-switched and mode-locked pulse generations by using the newly developed SAs is presented. Chapter 1 presents a background, motivation, and objectives of this study. Chapter 2 is intended to provide the background theory for fiber laser and pulse generation technology as well as the introduction to the saturable absorber materials.

Chapter 3 proposes and demonstrates a new type of passive SA based on V_2O_5 film, which was composed by the embedding of the V_2O_5 material into polyethylene glycol (PEG). The fabricated V_2O_5 PEG film is used as nonlinear optical modulator in both Ytterbium- and Erbium-doped fiber laser (EDFL) cavities. By sandwiching the SA film between two fiber ferrules and incorporates into the laser cavity, Q-switched and mode-locked fiber lasers are realized.

In chapter 4, a new SA based on Lu_2O_3 PVA composite thin film is developed. The SA is then integrated into fiber laser ring cavity for realizing both Q-switched and mode-locked pulses. Stable and reliable Q-switched pulses are realized by integrating the Lu_2O_3 thin film SA into EDFL and YDFL cavity to operate at 1570 nm and 1067.8 nm, respectively. A mode-locked pulse train operating at 0.97 MHz is obtained by integrating Lu_2O_3 thin film SA in the extended EDFL cavity. The pulsed laser operates at 1564 nm wavelength with the highest peak power of 3.61 kW is obtained at 187 mW pump power.

In chapter 5, Q-switched and mode-locked fiber lasers operating in microsecond and femtosecond regime, respectively are demonstrated using a saturable absorption property of NiO nanoparticles. The NiO PEG film with a modulation depth of 9% at 1550 nm was developed in this chapter. Microsecond Q-switched pulses are obtained in both YDFL and EDFL cavities by using the NiO PEG film-based SA. A mode locked EDFL with a soliton pulse of 710 fs is demonstrated in a modified laser cavity with anomalous cavity dispersion of -0.282 ps^2 by integrating the NiO PEG film inside the laser cavity.

Chapter 6 concludes the thesis and presents a summary of the research findings. future direction of this work is also discussed in this chapter.

CHAPTER 2: LITERATURE REVIEW

2.1 Introduction

In the industrial revolution 4.0 era, a laser is one of the most advanced inventions in optics development and application (Hecht, 2010). The use of laser has opened several new scientific fields such as photonics, fiber-optics, optoelectronics, and nonlinear optics. The development of photonics technologies has been changing in every aspect and to the other progress of scientific fields, such as medical research, information technology, biological science, etc. A laser is coined from "light amplification by stimulated emission of radiation" and thus it operates based on the stimulated emission of electromagnetic radiation. It is a device that emits photons through a process of optical amplification. In 1917, Albert Einstein described the theory of "stimulated emission" in which, the matter may lose energy by emitting the same photon when it encounters a photon. This is the first explanation on the concept of laser operation. However, it was not until 1960 that the first laser was demonstrated by Theodore Maiman (Maiman, 1960). This laser was built based on a ruby crystal that was pumped by a flash lamp in a Fabry-Perot cavity. After that, a large variety of lasers were demonstrated using different types of materials including helium neon (Javan et al., 1961), neodymium crystal (Johnson et al., 1962), semiconductor, CO₂ (Patel, 1964), Nd: YAG (Geusic et al., 1964), dye (Sorokin et al., 1966), titanium sapphire (Moulton, 1986), etc. In 1964, E. Snitzer and his acquaintances have produced the earliest type of fiber laser as well (Koester et al., 1964)

The first optical fiber was proposed and fabricated by Charles K. Kao in 1965 (Kao et al., 1966), where he discovered that the high losses were due to impurities in the glass rather than the technology itself. After that, the optical fiber fabrication technology has rapidly progressed where the optical fiber losses have improved significantly from thousand dB/m to losses below 1 dB/km. To date, it is used in a vast number of applications mainly within the fields of communication and sensors. In communication

applications, the deteriorated optical signals as they travel along the transmission lines, are needed to be amplified. In the late 1980s, David N. Payne has pioneered the fiber amplifier by using an erbium-doped fiber (EDF) as the gain medium (Mears et al., 1987). The success of the EDF amplifier (EDFA) has led to the rapid development of fiber lasers, which used the similar concept of doping active ions in optical fibers.

The work presented in this thesis is focused on developing pulsed optical sources operating in microsecond to femtosecond regime at two wavelength regions: 1-micron and 1.5-micron. To this end, three metal-oxide materials: vanadium pentoxide, lutetium oxide and nickel oxide are used as saturable absorber to initiate Q-switching and mode-locking process for pulse generation. This chapter is intended to provide the background theory for fiber laser and pulse generation technology as well as the introduction to the saturable absorber materials.

2.2 Principle of optical fiber laser

The optical fiber lasers are defined as a device that generates photons based on amplification of light in a coherent, monochromatic, and unidirectional manner in the optical spectrum region. The photons are generated through the population inversion of active gain medium in a laser cavity. Three basic requirements must be met to develop a laser. First, the laser should contain an active gain medium. Secondly, the gain medium should be placed in between the reflective optical cavity to allow the circulation of photons. For the third one is an external pump source is required to produce a population inversion. All optical fiber lasers are set up with these three basic elements. As in the current case, we specifically use the all-fiber laser resonator setup configured with ring-cavity. Two types of the gain media will be used for this research as described in the next subsection.

2.2.1 Ytterbium doped fiber laser

Ytterbium is one of the chemical compounds that belong to a group of rare earth metals. It provides optical amplification and gains around 1 μm wavelength (Rudiger Paschotta et al., 1997). As an optically active element, it is already well known and has been rather intensively studied during the last two decades. Initially, Yb-activated glass was proposed for laser material as early as 1962 (Etzel et al., 1962; Gandy et al., 1965; Snitzer, 1966). However, the first Yb-based silica gain fiber was demonstrated 26 years later, in 1988 (Koponen et al., 2006). Since then, Yb-doped fibers have been extensively employed to create efficient, high power, and pulsed fiber lasers. These lasers operating at 1 μm find various applications in the fields of laser welding (Alexy et al., 2017; Aydın, 2014; Kumar et al., 2019; Osellame et al., 2012), material processing (Bachmann, 2003; Minoshima et al., 2001; Steen et al., 2010), eye surgery (Hermens et al., 2013; Moghissi et al., 2017; Watanabe et al., 1994) and other biomedical applications (Y. C. Chen et al., 2019; Keiser et al., 2014; Kong et al., 2017).

Figure 2.1 shows a sub-level in the energy diagram of Yb ions in Ytterbium-doped silica fiber (YDF). The sub-level splitting is depended on the position and concentration of Yb ions in the glass (Zervas et al., 2014). Typically, Ytterbium ions absorb the pump radiation and transfer the excitation energy to erbium ions. Although the erbium ions could absorb radiation directly at 980 nm, ytterbium co-doping can be useful because of the higher ytterbium absorption cross-sections and the higher possible ytterbium doping density in typical laser glasses, it is essential to receive a much shorter pump absorption duration and a higher gain. Ytterbium co-doping is also sometimes used for praseodymium-doped up conversion fiber lasers.

YDF lasers are very efficient sources. As shown in Figure 2.1, YDF has a very simple electronic level structure, with only one excited state manifold ($^2F_{5/2}$) within the reach from

the ground-state manifold ($^2F_{7/2}$). The simple electronic structure does not include the absorption of excited states as well as various adverse cooling processes. The upper state lifetimes are typically in the order of 10 to fs, which is beneficial for Q-switching and mode-locking pulses. The Yb ion possesses several emission transitions within the 950 - 1100 nm wavelength range. The emission wavelength can be selected by a careful choice of the pump wavelength. The homogeneous and inhomogeneous broadening of these transitions within a glass host leads to a wide and continuous emission spectrum in the 1-micron band. The gain of an YDF can be well modelled by a Gaussian function with full-width half-maximum (FWHM) of about 40 nm and with a central wavelength at around 1030 nm. Lifetimes of the emission and absorption spectrum depend on the host materials (Weber et al., 1983).

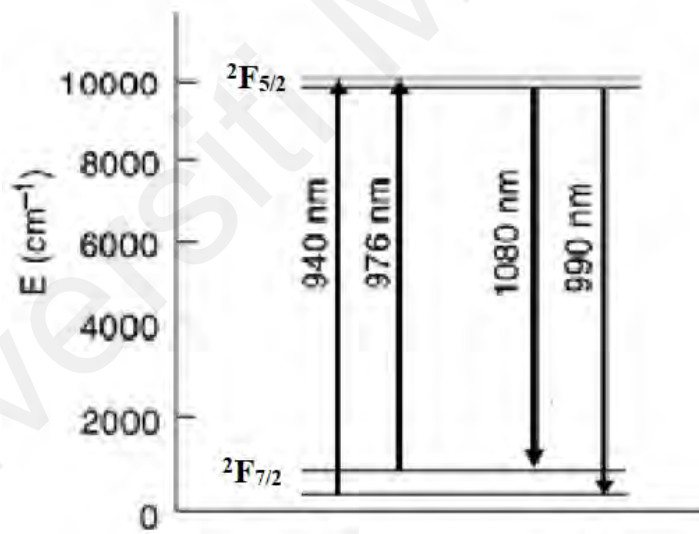


Figure 2.1: Energy level of Ytterbium doped silica fibers.

2.2.2 Erbium doped fiber laser

Erbium (Er^{3+}) ion is usually used as an active element since it can operate at a low loss region of 1.55-micron which suitable for optical communication applications. The absorption and emission cross-section of a silica fiber are shown in Figure 2.2. The EDF can be used in both amplifier (Erbium-doped fiber amplifier, EDFA) and laser (Erbium-doped fiber laser, EDFL) devices, and both devices are operated based on a similar mechanism. EDFA can be transformed into an EDFL device by incorporating a feedback system in the configuration. The EDF is usually used as a gain medium for ultra-short pulses generation due to its fiber gain spectrum, which is in a wide range and the fiber dispersion at the 1.55-micron region is anomalous. This anomalous dispersion works with the nonlinearity in the fiber promising a good self-stable pulses generation that can be used in different types of practical applications, especially in telecommunications window for wavelength division multiplexing (WDM) network (Tanabe, 2002).

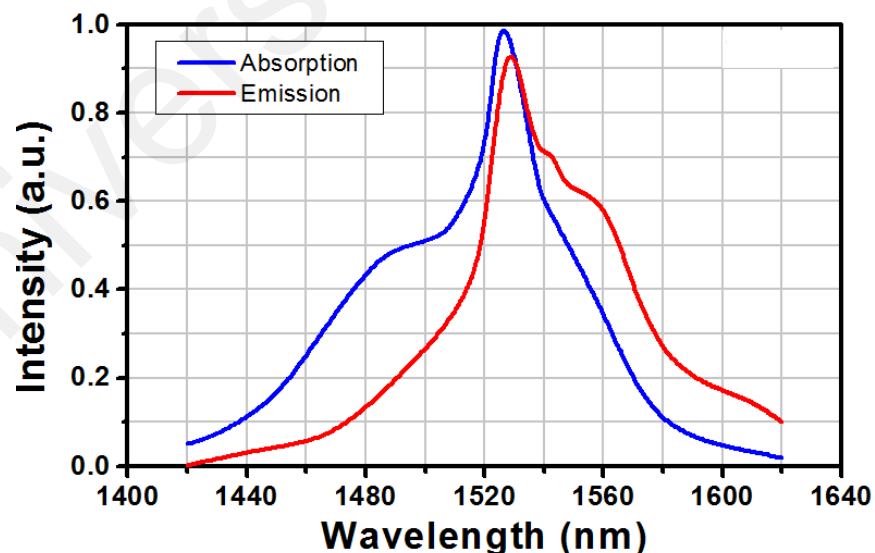


Figure 2.2: The absorption and emission cross-section of a silica fiber.

EDF has emerged as a strong candidate for employment as the gain medium in a fiber ring laser, with desirable properties such as the broad gain bandwidth of typically tens of nanometers due to lack of sharpness in its energy level (Zhang et al., 2009).). Figure 2.3 illustrates the energy level of the Er^{3+} in silica fibers. The energy level $^4\text{I}_{15/2}$ corresponds to a ground state for laser transition. When the pump photon is absorbed, the Er^{3+} ion is excited to a level of $^4\text{I}_{11/2}$ or $^4\text{I}_{13/2}$, depending on the pump wavelength used. In this research, erbium is excited by photons at 980 nm, and it has a nonradiative decay to a state $^4\text{I}_{13/2}$ where it can stay excited about relatively extended periods of time (lifetime ~ 10 ms) since the pump is provided from a 980 nm laser diode pump. This property is extremely important because the quantum efficiency of the device is dependent on how long it can stay in that excited state. If it relaxes too early, more photons are required to keep it excited, which means more input pump power is needed to make the amplifier work. (Desurvire, 1994). Erbium can also be excited by photons at 1480 nm (energy level $^4\text{I}_{13/2}$). When excited that way, both the energy pumping process and the stimulated emission of the signal occurs in the same wavelength and energy band.

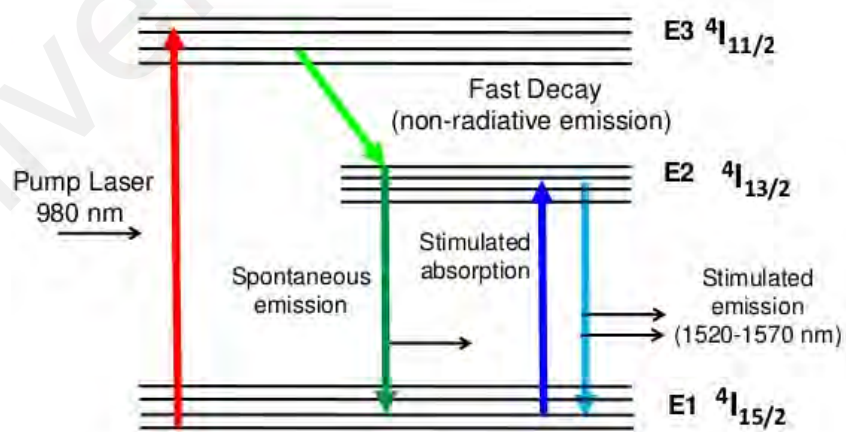


Figure 2.3: Simplified energy levels of Erbium ions in EDF.

2.3 Pulsed fiber laser

Many applications require the use of modulated lasers or well known as pulsed lasers. There is a variety of pulsed laser applications in the area of optical communication, range finding, spectroscopy, and micromachining. The pulsed laser has been proposed soon after the first demonstration of a single-mode CW fiber laser. The first Q-switched and mode-locked fiber lasers were reported by Alcock et al.,(Alcock et al., 1986). The pulsed formation has been realized by using an acousto-optic modulator which generated a pulse width of 200 ns and ~1 ns for Q-switching and mode-locking, respectively. The pulsed formation can be successful using several techniques plus the simplest way is to directly modulate the CW lasers. Light can escape from the cavity for a short period by placing the fast modulator into the cavity. However, by using this method, the loss of the produced light is high when the modulator is in a closed state. Thus, more sophisticated techniques have been used such as cavity dumping, gain switching, mode-locking, and Q-switching. The two latter techniques provide a more reliable, robust, and superior style for pulsing the lasers.

2.3.1 Principle of Q-switching

Q-switching laser involves the technique of modulating the losses of the laser resonator by any method. The term Q represents the quality of the laser resonator which contains information regarding the cavity losses. The quality factor (Q-factor) portrays the ability of a laser cavity to preserve its energy. A higher Q indicates a lower intracavity loss. The Q-switching phrase describes the idea of switching the laser configuration from a low to high Q to create a short pulse duration. Originally, the Q-factor is kept at a low level (i.e. high losses), preventing any potential for lasing. The gain medium provides an accumulation of spontaneous emission in the cavity by constant pumping; thus, energy is stored. At this moment, the Q-factor is suddenly switched to a high level and the desired amount of energy is stored, spontaneous emission grows into lasing and a laser pulse is

beginning to build up in the laser cavity. The pulse grows stronger until the gain equals the losses. When the pulse peak power is reached and depletes the gain completely, the laser is no longer able to oscillate. The Q-switcher is open again (low Q), and the process starts from the beginning to build up more inversion for the next consecutive pulse. It is useful to have a long upper state lifetime of a gain medium to store more gain, so that it does not disappear as fluorescence emission before the Q-switcher is opened.(Digonnet, 2001).

The Q-switched laser can be realized by active and passive means. The common devices of active Q-switching are electro-optic and acousto-optic modulators. In addition, a revolving mirror or prism may also be used. Inactive Q-switching, the repetition rate can be controlled and exhibit low timing jitter due to the exemption of movable parts in the cavity (Hjelme et al., 1992; J. Zayhowski et al., 1995) Basically, timing jitter cannot be avoided due to the oscillating photon originating from spontaneous emission from the gain medium. Typically, the pulse width in active Q-switching reduces and the pulse energy rises with the increase in pump power (Eichhorn et al., 2007). The pulse width depends on the two factors which are the gain and the cavity round trip time whereas the pulse energy depends on the repetition rate (J. Zayhowski et al., 1991). Since the repetition rate in the active Q-switched can be controlled by driving the modulator with different seed signal, increasing the pulse energy to a certain rate reduces, the gain will be divided by fewer pulses, thus individual pulses will receive more gain.

A passive Q-switching offers a simpler method in providing a compact setup and is more cost-effective. It does not need external modulation incorporated in the setup, thus the saturable absorber (SA) has been used to self-modulate the cavity losses and the gain. Saturable absorbers are made up of materials and methods such as semiconductor compounds (Spühler et al., 1999) and crystal doped (Y.-F. Chen et al., 2000; Tsai et al., 2000). Other reported works focused on the generation of Q-switching using doped fiber (S. D. J. A. O. Jackson, 2007; Kurkov, 2011). The transmission and reflection of the saturable absorber are based on the light intensity. It absorbs the light up to a certain limit which is determined by the absorber saturation fluence (U. J. N. Keller, 2003). When the energy reaches the limit, a pulse is released.

2.3.2 Formation of Q-switched pulses and their important parameters

Figure 2.4 shows the formation of the Q-switched fiber laser of one pulse cycle (Spühler et al., 1999). The saturable absorber with bleach, '0', unbleached conditions ' q_0 ' and a saturable absorber loss coefficient $q(t)$, have been considered and the total cavity loss within one cavity round trip is l . As can be seen in the figure, in Phase 1, the pulse starts to emerge when the gain, $g(t)$ reaches the total cavity loss condition (low Q) at the saturable absorber unbleached conditions. At this point, the power increases until the gain are capable to bleach the absorber. The intracavity power $P(t)$ grows when gain $g(t)$ reaches l in which saturable absorber is saturated before grows significantly.

When the induced power causes the absorber to bleach in phase 2, the gain $g(t)$ is at the high Q until the gain starts to deplete to the loss level $q(t) + l$. The maximum pulse occurs when the gain $g(t)$ is equal to the total cavity loss l at the bleach condition. Then in Phase 3, the gain $g(t)$ depletion continues and reaches the negative value, therefore the intracavity power $P(t)$ decreases. Finally, the absorber recovers its unbleached state in Phase 4 due to the recovery time of the shorter absorber relative to the gain (t). The

continuous pumping of the gain medium will provide sufficient gain to attain the threshold level to start over for the next consecutive pulse which is going back to Phase 1. Phase 1 starts when gain $g(t)$ reaches the unsaturated loss as shown in Figure 2.5.

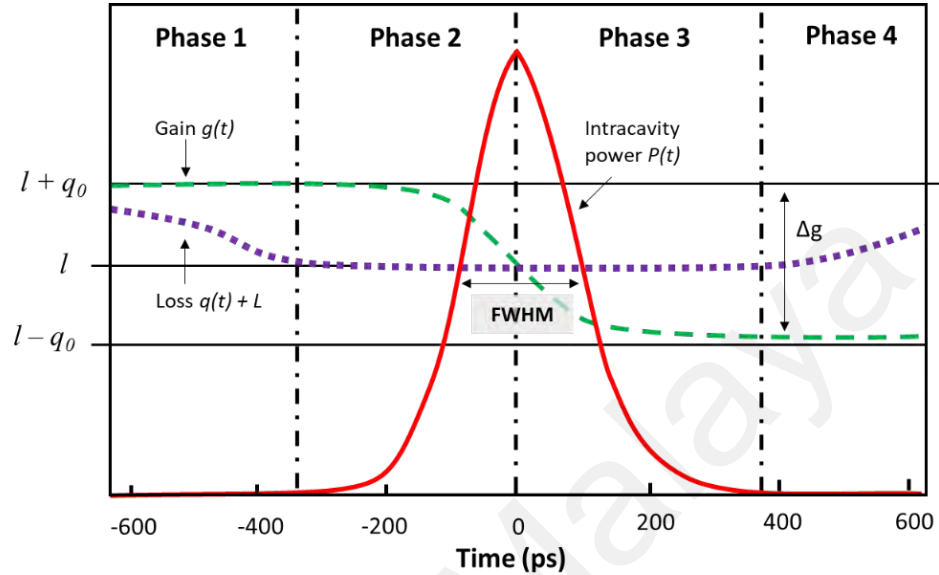


Figure 2.4: The formation of Q-switched fiber laser.

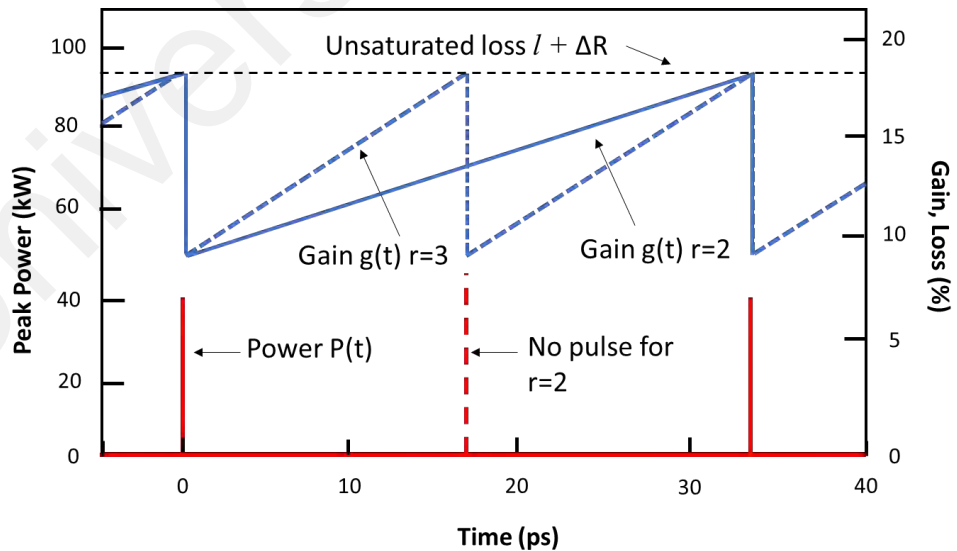


Figure 2.5: The cycle of the formation of Q-switched fiber laser.

The stored energy in the gain medium for optical pumping or formation in Q-switching can be defined as;

$$E_{stored} = AL_G N_2 h\nu_1 \quad (2.1)$$

where N_2 is excitation energy, $h\nu_1$ is photon energy at the pumping wavelength, AL_G is pumped gain volume.

In passive Q-switching, pulse width and pulse energy are independent of the pump power (Spühler et al., 1999). However, the pulse width usually decreased as the pump power increased as explained by (Herda et al., 2008). The pulse width (which is sometimes called pulse duration) of the Q-switching can also be observed in Figure 2.4. The FWHM of the pulse determines the pulse width. According to (J. J. Zayhowski et al., 1994) and based on Figure 2.4, the pulse width can be expressed as:

$$\tau_p = \frac{S_p T_r}{q_0} \left[\frac{\delta(1 + \delta)\eta}{\Delta - \ln(1 + \delta)} \right] \quad (2.2)$$

where $S_p \sim 0.88$ is the pulse shape factor, T_r is the cavity round-trip time, η is the energy extraction efficiency of a light pulse and δ is the ratio between saturable and unsaturable cavity loss. The pulse width is proportional to the cavity round-trip time and inversely proportional to the saturable losses of the cavity.

The repetition rate is defined as the number of emitted pulses per second or the inverse of an adjacent pulse. It can be measured directly from the oscilloscope by observing the duration between the output pulse trains. The repetition rate is commonly observed to be linearly dependent on the pump power and normally in the range of 1–100 kHz. This has also been confirmed by various experiments using fiber lasers (S. D. Jackson et al., 2007).

The average power of the Q-switched laser is measured directly from the power meter. Since average power is calculated while the laser is Q-switching, to determine the pulse energy, the repetition rate at which the measurement was taken should be considered. An equation for the pulse energy is determined by dividing the average power, P_{avg} by the repetition rate, f_{rep} :

$$E_p = \frac{P_{avg}}{f_{rep}} \quad (2.3)$$

According to (Spühler et al., 1999), the pulse energy depends on the amount of energy stored in the gain medium. Therefore, the lifetime of the gain medium and the absorber saturation loss is crucial. This is due to their relationship as shown in Figure 2.3. Nevertheless, passive Q-switching suffers from the timing jitter (Huang et al., 1999). This is due to variations in pump strength, temperature, losses, and much more. In a fiber laser, the large amount of intracavity spontaneous emission is significant to produce jitter in a pulse.

The peak power of an optical pulse is defined as the maximum occurring optical power of a pulse. For long pulse duration, the peak power can be measured directly from the oscilloscope (OSC) with a photodiode. For short pulse duration in the picosecond and femtosecond region, the peak power of a pulse can be calculated by the following equation where E_p is the pulse energy and τ_p is the pulse width:

$$P_{peak} = \frac{E_p}{\tau_p} \quad (2.4)$$

2.3.3 Principle of mode-locking

Mode-locking is a method used to produce an ultra-short pulse laser. The pulse duration range can be between picoseconds (10^{-12} s) to femtoseconds (10^{-15} s). An ultra-short pulse can be generated when all the longitudinal modes have a fixed phase relationship, hence the term “mode-locking” or “phase-locking”. The fixed phase superposition between all the modes oscillating inside a laser cavity causes the continuous wave (CW) laser to be transformed into a train of the pulse. The number of longitudinal modes that can simultaneously lase is dependent on the gain linewidth, $\Delta\nu_g$ and the frequency separation between modes. Under sufficiently strong pumping, we can expect that the number of modes, M oscillating in the cavity is given by

$$M = \frac{\Delta\nu_g}{c/2L} = \frac{2L}{c} \Delta\nu_g \quad (2.5)$$

where c is the speed of light and L is the length of a linear cavity. The shortest pulse duration that we can expect to obtain by a given gain linewidth is

$$\tau_{min} = \tau_M = \frac{2L}{cM} = \frac{1}{\nu_g} \quad (2.6)$$

From above equation, the shortest attainable pulse width is a reciprocal of gain line width (in Hz) (Peter et al., 2010)

Mode-locking involves periodic modulation of resonator loss. Once the resonator loss is modulated, all the laser modes phase can easily be fixed. In the time domain, the mode-locked laser generates the equidistance pulse train, while the T_R specifies the round-trip time of a pulse within the laser cavity while pulse length is indicated by τ_p . In the frequency domain, a phase-locked frequency's comb can be obtained with constant mode-

spacing, ν_R , that is equal to $1 / T_R$. The pulse duration, τ_p , is inversely proportional to the spectral width of the envelope of the frequency comb, $\Delta\nu_g$.

In a homogeneously broadened gain medium, the laser normally lases at one axial mode at the peak of the gain. Periodic loss modulation, however, moves the additional energy phase-locked to the adjacent mode divided by the modulation frequency. This modulation frequency is normally referring to the cavity round-trip frequency. Consequently, the frequency comb has an equidistance axial mode-locked together in phase forms a short pulse in the time domain. A mode-locked laser's basic repetition rate is determined by its cavity duration, as described in the following equations:

$$\text{Repetition rate (for linear cavity)} = \frac{c}{2Ln} \quad (2.7)$$

$$\text{Repetition rate for ring cavity} = \frac{c}{Ln} \quad (2.8)$$

where L , c and n are defined as the length of the cavity, speed of light and refractive index respectively. As the round-trip time, T_R , is the inverse of repetition rate, therefore,

$$T_R = \frac{Ln \text{ or } 2Ln}{c} \quad (2.9)$$

2.4 Propagation of optical pulses in a fiber

Because of the difference between the refractive indices of the core and the cladding, it is possible to transmit light inside the fiber. The refractive index of the core must be always higher than the refractive index of the cladding. The modal theory can explain the existence of an angle of incidence that enables the phenomenon of total internal reflection (Y. Jiang et al., 2010). Light, while propagating in the fiber, can be seen as an electromagnetic phenomenon, and the whole propagating mechanism, which can be described by the electromagnetic optical fields associated with it, is governed by Maxwell equations (Agrawal, 2013). While propagating in an optical fiber, especially in the linear regime, any pulse suffers from the effect of time dispersion, which causes its expansion and can interfere between symbols, which can greatly limit the bandwidth of the signal to be transmitted.

Pulse propagation in a nonlinear regime is affected by the optical Kerr effect. The propagation of impulses is controlled simultaneously by the SPM and group velocity dispersion (GVD) in the Nonlinear Dispersive Regime (NLDR) (Agrawal, 2013). In the anomalous dispersion region, the SPM effect is contrary to the GVD, thereby allowing the propagation of pulses very interesting because it does not change its shape over propagation in the fiber. These pulses are called a soliton. In this section, the dispersion phenomena, SPM, and soliton generation are briefly discussed.

2.4.1 Dispersion

The light-wave travels at a constant speed c when propagating through free space. However, when light travels through a material its speeds are slowed down due to interaction between the light's electromagnetic field and the material's electron cloud. The degree to which the light is slowed down is represented as a material refractive index n , which relates to the speed of the light in the material by

$$v_m = \frac{c}{n} \quad (2.10)$$

Since the interaction of the electromagnetic field with the material depends on the frequency of the light (wavelength), the refractive index also depends on the frequency of light. This property is referred to as chromatic dispersion. Chromatic dispersion is also called material dispersion and is given by

$$D_M(\lambda) = \frac{\lambda}{n} \frac{d^2 n}{d\lambda^2} \quad (2.11)$$

in which the refractive index n is a function of wavelength λ . Chromatic dispersion plays a critical role in the propagation of laser pulses. If the laser pulses contained only one frequency component, it would travel through the material without any distortion. In practical, pulse is consisted of a range of different frequencies. The shorter the pulse (time domain) the wider the range of frequency it covers (frequency domain). Unfortunately, different frequency components will travel at different speeds; some travel faster, some lag behind. This making pulse width become broadening.

Besides chromatic dispersion, the light also experiences an additional dispersion caused by the structure of the optical fiber. It is known as waveguide dispersion and can be described as

$$D_w(\lambda) = -\frac{n_2(\lambda)\Delta}{c\lambda} V \frac{d^2(Vb)}{dV^2} \quad (2.12)$$

where $n_2(\lambda)$ is the refractive index of the fiber core, Δ is the refractive index different, b is the normalize propagation constant and V is the normalized frequency. The total dispersion of the fiber is the combination of chromatic dispersion and waveguide dispersion:

$$D(\lambda) = D_M(\lambda) + D_w(\lambda) \quad (2.13)$$

The propagation of a laser pulse in a fiber is characterized by a mode propagation constant β . The mode propagation constant β can be expanded in a Taylor series about the center frequency ω_0

$$\beta(\omega) = \frac{n(\omega)\omega}{c} = \beta_0 + \beta_1(\omega - \omega_0) + \frac{1}{2}\beta_2(\omega - \omega_0)^2 + \dots \quad (2.14)$$

where

$$\beta_m = \left. \frac{d^m \beta}{d\omega^m} \right|_{\omega=\omega_0} \quad (m = 0, 1, 2, \dots) \quad (2.15)$$

The pulse envelope moves at the group velocity ($v_g = 1/\beta_1$) (while the parameter β_2 is responsible for pulse broadening. β_2 is generally referred to as the GVD parameter and relates to the chromatic dispersion parameter D by

$$\beta_2 = -\frac{\lambda^2 D}{2\pi c} \quad (2.16)$$

The fiber is said to exhibit normal dispersion for $\beta_2 > 0$, and to exhibit anomalous dispersion for $\beta_2 < 0$. In the normal dispersion regime, high frequency (blue-shifted) components of an optical pulse travel slower than the low frequency (red-shifted) components. The opposite occurs in the anomalous dispersion regime.

Pulse broadening induced from dispersion degrades the initial pulse's intensity, which can cause two adjacent pulses to overlap. This leads to errors at receiver in fiber optic communication systems. However, combined dispersion and SPM effect can lead to the formation of an optical soliton on the good side, where the wave is stable and unchanged during its propagation through the fiber.

2.4.2 Nonlinear Effect

Nonlinear effect phenomena occur in any dielectric medium as a consequence of the modification of the optical properties of a material system by the presence of sufficient intense laser light. These phenomena are "nonlinear" in the sense that they arise when a material system's reaction to an applied optical field depends on the strength of the optical field in a nonlinear manner. Therefore, the dielectric medium behaves like a nonlinear medium. A year after Maiman demonstrates the first working laser in 1960 (Maiman, 1960) Franken et al. discover a second-harmonic generation and thus become a stepping stone to the field of nonlinear optics (Franken et al., 1961).

An optical nonlinearity can be considered as to how the polarization $\tilde{P}(t)$ of a material system depends on the strength $\tilde{E}(t)$ of an applied optical field (Agrawal, 2013).

At first, the induced polarization depends linearly on the field strength which can be described as

$$\tilde{P}(t) = \epsilon_0 \chi^{(1)} \tilde{E} t \quad (2.17)$$

where the constant of proportionality $\chi^{(1)}$ is referred to as the linear susceptibility and ϵ_0 is the permittivity of free space. From Equation 2.17, the nonlinear effect can be expressed in the polarization $\tilde{P}(t)$ as a power series in the field strength $\tilde{P}(t)$ as

$$\tilde{P}(t) = \epsilon_0 [\chi^{(1)} \tilde{E}^1(t) + \chi^{(2)} \tilde{E}^2(t) + \chi^{(3)} \tilde{E}^3(t) + \dots] \quad (2.18)$$

The amounts $\chi^{(2)}$ and $\chi^{(3)}$ are referred to as the second-and third-order nonlinear optical susceptibilities. The quantities and the nonlinear optical susceptibilities of the second and third-order, respectively, are known. Only in non-centrosymmetric crystals can second-order nonlinear optical interactions occur (crystals that do not display

inversion symmetry). Since liquids, gases, amorphous solids (such as glass), and even several crystals exhibit inversion symmetry, $\chi^{(2)}$ disappears in the same way for such media, and as a result, such materials cannot generate second-order nonlinear optical interactions. On the other hand, third-order nonlinear optical interactions described by $\chi^{(3)}$ susceptibility can occur for both centrosymmetric and non-centrosymmetric media.

In the optical fibre, nonlinear effects occur either because of the strong dependence of the silica glass medium's refractive index or because of the inelastic-dispersing phenomenon. For the Kerr effect, the power dependence of the refractive index is responsible. This Kerr-nonlinearity expresses itself in three separate effects, e.g. self-phase (SPM) modulation, cross-phase (CPM) modulation and mixing of four waves (FWM). For the inelastic-scattering phenomenon, silica glass medium can induce stimulated Brillouin-scattering (SBS) and stimulated Raman-scattering (SRS) at the only high-power level. In this thesis, only the relevant nonlinear effects including SPM are discussed.

2.4.3 Self-phase modulation

Inside the optical fiber, the fiber refractive index is not only varied with wavelength but also varied with the intensity of the propagated light. The interaction between light and the material electron cloud increases nonlinearly with the light intensity, so the high-intensity light travels slower than the low-intensity one. As a result, the fiber refractive index increases with the intensity of light and can be described as

$$n_{eff} = n_l + n_{nl}I \quad (2.19)$$

where n_{eff} is the effective refractive index, n_l is the linear refractive index, n_{nl} is the nonlinear refractive index, and I is the light intensity inside the fiber.

SPM is one of the most concern effects of the fiber nonlinearity on the pulse propagation theory. Under the SPM effect, the optical pulse experiences a phase shift induced by the intensity-dependent refractive index while the pulse shape remains unchanged. The nonlinear phase constant ϕ_{nl} introduced by a field \tilde{E} over a fiber length L is

$$\phi_{nl} = \frac{2\pi}{\lambda} n_{eff} L \quad (2.20)$$

where λ is the operating wavelength of pulse laser propagating in fiber of effective refractive index n_{eff} along the optical path length of L .

Inside the fiber, the propagated light intensity is time varying and thus it produces a time varying refractive index. So, the leading edge of a pulse will experience a positive refractive index gradient ($+dn/dt$) which leads to red shift, and for trailing edge of a pulse, a negative refractive index gradient leads ($-dn/dt$) to blue shift. This temporally varying index change results in a temporally varying phase change, as shown in Figure 2.6. The optical phase changes with time in exactly the same way as the optical signal.

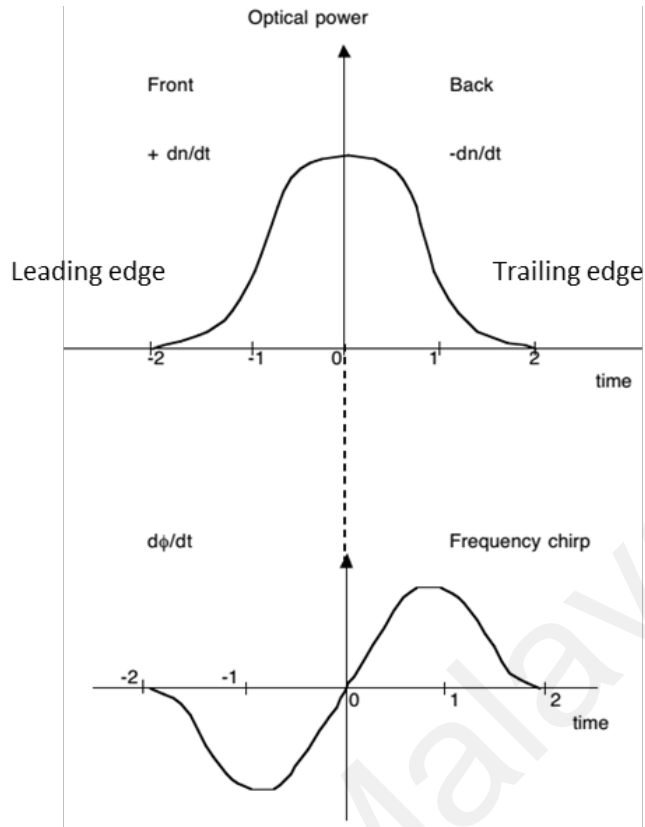


Figure 2.6: Phenomenological description of spectral broadening of pulse due to SPM. (Gangwar et al., 2007).

If intensity is time dependent, the wave is temporally modulated and phase ϕ will also depend on time. This variation in phase ϕ_{nl} with time is responsible for change in frequency spectrum ω , which is given by

$$\delta\omega = \frac{d\phi_{nl}}{dt} \quad (2.21)$$

The time dependence of $\delta\omega$ is referred as a frequency chirping. This chirping phenomenon is generated along the temporal pulse profile where ϕ_{nl} increases with the interaction fiber length. This denotes to the new instantaneous frequency generation at $\omega_0 + \delta\omega(t)$ as the pulse propagates inside a fiber and therefore leads to the spectral broadening of the pulse. Here, the SPM concept is used in soliton pulse generation.

2.5 Saturable Absorber

Passive Q-switching and mode-locking requires a saturable absorber (SA) device to provide an intensity dependent loss or gain in the laser cavity. SAs are intracavity elements that introduce lower loss for higher intensities. This can be used to discriminate between high intensity pulses and low intensity CW radiation. SAs can be classified as either slow or fast depending on their response time relative to the pulse duration. A slow SA recovers its absorption on a time scale longer than the pulse duration, and its transmission scales with the pulse fluence. A fast SA responds instantaneously to changes in the pulse intensity, and therefore its transmission scales with the pulse intensity. In general, both types of SAs help to form a net gain window that determines the pulse duration and stabilizes the pulse against perturbations.

Up to date, numerous passive SAs have been proposed and demonstrated for pulse generation. Semiconductor Saturable absorber mirror (SESAM) is one of the most popular SA in solid-state lasers (Zitter, 1969). Although the device parameters such as saturation energy, absorption wavelength, and recovery time can be accurately controlled with modern semiconductor technology, SESAM requires a complex and costly fabrication process. Therefore, many researchers have also shifted their interest to other passive materials such as single-walled carbon nanotubes (CNT) and graphene (H Ahmad et al., 2012; Harun et al., 2012; Tan et al., 2013). For instance, Liu et. al reported a multi-wavelength mode-locked laser operation using CNTs SA (X. Liu et al., 2013). On the other hand, graphene, a single atomic layer of carbon atoms has also gained tremendous interest as an excellent SA since it has zero bandgap energy. It can be exfoliated from graphite and has attracted particular interest in recent years since its 2D structure and zero bandgaps enable wideband optical operation. However, its weak absorption resulted in a low modulation depth. Besides graphene, more recently many new emerging and promising material have been proposed as SA including transition metal dichalcogenides

(TMDs), topological insulators (TIs), and black phosphorus (BP). All of these materials offer distinct, yet complementary properties (Latiff et al., 2016; Henan Li et al., 2015; Sobon, 2015; Woodward et al., 2015) and hence, new opportunities for optical applications in fiber-based systems. The possibility of combining layers of 2D materials to form van der Waals heterostructures also offers an exciting prospect for a wide range of new engineerable photonic devices (Geim et al., 2013), as does the potential to vary nanomaterial properties through their growth conditions, doping and electronic control (Lee et al., 2015; Lin et al., 2015).

Transition metal oxides (TMOs) are also considered as another 2D material that has the potential to be utilized as SA. For instance, Vanadium Oxide (V_2O_5) has been recently discovered as a new class of 2D material. Vanadium can be viewed as a single layer of vanadium oxide (V_2O_5), much in the same way as graphene is a single layer of graphite. Moreover, V_2O_5 having a small and tunable bandgap due to the dependence of its film thickness. The bandgap of V_2O_5 can be fine-tuned by adjusting the number of the layer in V_2O_5 material. V_2O_5 consists of Van der Waals forces which attract the individual of the atomic layer by layer since it is the most stable vanadium in the group. The interesting properties of V_2O_5 have attracted the attention of plenty of researchers.

Very recently, a rare earth material lutetium oxide (Lu_2O_3) has demonstrated its good thermal and mechanical ability, high melting point and phase stability which broadband nonlinear absorption ability at 1030 nm and 515 nm (Rahimi-Nasrabadi et al., 2017). Their results show that Lu_2O_3 exhibits a much stronger SA response, high threshold damage, and simpler than graphene at both wavelengths. Also, inspired by the success of NiO in nonlinear fiber lasers, other researcher has tried their best efforts to demonstrate the real broadband SA of multi-layer Lu_2O_3 ranging from the visible (400 nm) towards mid-infrared region (at least 1930 nm) (Ordin et al., 2010; Wiktorczyk, 2001). With the demonstrations

of Lu_2O_3 's SA characteristics, it is foreseeable and prospective that they could also be used in nonlinear optics as other layered structure materials.

Likewise, NiO has been discovered huge attention due to its properties of transport and optical, a layered structure atom is attached between two layers of sulfur atoms in a 2D hexagonal lattice that possesses an optical property and thickness-dependent electronic. By determining the unique symmetry of its lattice structure, the few-layer NiO demonstrates a suitable orientation-dependent third-order optical nonlinearity, which is different from graphene which possesses very weak second-order nonlinearity (Usha et al., 2018). There are many types of methods that have been investigated to produce a NiO. In 2021, the NiO nanosheets exhibited well saturable absorber than graphene-based on the technique of open aperture Z-scan (Pepe et al., 2021). Besides that, the electron transition process by hydrothermal and spin coating method was used to synthesize the few-layer NiO which had a saturable intensity of 22.59 MW/m^2 and modulation depth of 1.48 % at 1065 nm (B. Sun et al., 2018). By introducing suitable defects, the pulse laser deposition technique was used to fabricate broadband NiO SAs (Bouessay et al., 2002)

Table 2.1: summarizes various 2D materials groups, which were recently discovered. In this work, V_2O_5 , Lu_2O_3 and NiO based SA are developed and proposed for Q-switching and mode-locking applications.(Geim et al., 2013).

Graphene family	Graphene	hBN 'white graphene'	BCN	Fluorographene	Graphene oxide
2D chalcogenides	MoS ₂ , WS ₂ , MoSe ₂ , WSe ₂		Semiconducting dichalcogenides: MoTe ₂ , WTe ₂ , ZrS ₃ , ZrSe ₂ , and so on	Metallic dichalcogenides: NbSe ₂ , NbS ₂ , TaS ₂ , TiS ₂ , NiSe ₂ , and so on	
				Layered semiconductors: GaSe, GaTe, InSe, Bi ₂ Se ₃ , and so on	
2D oxides	Micas, BSCGO	MoO ₃ , WO ₃	Perovskite-type: LaNb ₂ O ₇ , (Ca,Sr) ₂ Nb ₃ O ₁₀ , Bi ₂ Ti ₃ O ₁₂ , Ca ₂ Ta ₂ TiO ₁₀ and so on		Hydroxides: Ni(OH) ₂ , Eu(OH) ₂ and so on
	Layered Cu oxides	TiO ₂ , MnO ₂ , V ₂ O ₅ , TaO ₃ , RuO ₂ , and so on			Others

CHAPTER 3: VANADIUM OXIDE FILM AS PASSIVE Q-SWITCHER AND MODE LOCKER DEVICE

3.1 Introduction

Q-switched and mode-locked fiber lasers have gained considerable attentions in recent years owing to their inherent features of alignment-free structure, good mode confinement and high stability (Digonnet, 2001). They have many significant applications in many areas including material processing, microfabrication, range finding, remote sensing, optical communications, skin treatment and medical surgery (Adachi et al., 2002; Clowes, 2008; Eigenwillig et al., 2008; M. Jiang et al., 1997). Q-switched and mode-locked pulses can be generated by using an electro-optic or acousto-optic modulators to actively modulate the loss within the cavity (El-Sherif et al., 2003; Nikodem et al., 2008). However, this modulator is made of bulky and costly components, which increases the complexity and cost of production of the laser system. In contrast, the passive technique with saturable absorber (SA) offers a compact, low cost, simple and reliable alternative method to generate Q-switched or mode-locked pulses (Al-Hiti et al., 2019). Furthermore, the lightweight properties and low energy consumption have made it more suitable for the practical applications of some portable devices e.g., range finder.

Typically, semiconductor saturable absorber mirror (SESAM) (Okhotnikov et al., 2004) and carbon-based nanomaterials (Ahmed et al., 2015; Haris et al., 2020) are deployed into a laser cavity as SA for Q-switched or mode-locked pulse generation due to their exceptional nonlinear optical responses. However, the synthesis process of these materials is expensive and complicated. Additionally, SESAMs have the narrow operation wavelength band and thus reduced the applicability and flexibility of this SA. The carbon-based materials such as carbon nanotube (Ahmed et al., 2015), graphene (Fu et al., 2014) and graphene oxide (Haris et al., 2020) have their own shortcomings e.g. diameter control needed for carbon nanotube and lower modulation depth for graphene.

Therefore, tremendous research effort has been devoted to searching new alternative SA materials which accompany with high operation performance and simple SA fabrication method.

Recently, 2D nanomaterials such as TMDs and Black Phosphorus (BP) have also been reported as SAs in many laser systems (Luo et al., 2014) (R. Chen et al., 2016). TMDs have excellent physical properties such as fast response time, good electron mobility, and high superconductivity (Manzeli et al., 2017). For instance, Molybdenum disulfide (MoS_2) and tungsten disulfide (WS_2) have a relaxation time of about 30 fs and thus they were widely explored for pulse generation (Mao et al., 2015; Z. Wang et al., 2018). These materials require a special fabricating procedure based on mechanical exfoliation to obtain monolayer structure, which has a bandgap corresponds with the production of the near-infrared laser (Yuan et al., 2016). But this fabrication procedure is difficult because the mechanically exfoliated material contains an inconsistent powder-like layer that is difficult to handle. On the other hand, BP had these unique properties but it is sensitive to air and water which affects its performance (R. Chen et al., 2016).

Transition metal oxide (TMO) materials has also gained explosive grow of advertence in the past few years due to their excellent electronic and optical properties. They can enable high performance optoelectronic devices due to their high carrier mobility and broadband light absorption. TMO in their low-dimensional form demonstrated good abilities in the field of nonlinear optics. It is characterized by large third-order nonlinear interchangeability, ultrafast response time in a narrow range, a high damage threshold, and a wide absorption band (Mao et al., 2018). Besides, TMO bandgap can be set via the thickness and controlling particle size (Pang et al., 2019). Several TMO-SAs have been proposed for producing Q-switched or mode-locked pulses such as zinc oxide (Harith

Ahmad et al., 2019; Alani et al., 2018), titanium dioxide (M. F. M. Rusdi et al., 2017), copper oxide (Sadeq et al., 2018), and molybdenum oxide (W. Wang et al., 2018).

Vanadium pentoxide (V_2O_5) is one of the most important transition metal oxides (Yan et al., 2009). It was reported to have an excellent nonlinear optical absorption characteristic and thus suitable for SA applications (Molli et al., 2016). In this chapter, Q-switched and mode-locked fiber lasers are demonstrated using the newly developed V_2O_5 SA. The SA was prepared by the embedding of V_2O_5 material into polyethylene glycol (PEG) to compose a film absorber, which was then inserted between two fiber ferrules. The V_2O_5 PEG film could be used as nonlinear optical modulator in both Ytterbium- and Erbium-doped fiber laser cavities.

3.2 Preparation and Characterization of V_2O_5 SA

For this work, the ammonium metavanadate (NH_4VO_3) compounds were acquired from Sigma Aldrich Malaysia Sdn Bhd and used as a raw material. The compounds were purified by using a standard chemical reaction to obtain V_2O_5 compounds. In the process, 20 g of NH_4VO_3 was dissolved in 500 mL of deionized water. After that, 0.1 g of Triton X-100 surfactant was added in the above solution under constant stirring at $90^\circ C$ for one hour to complete the emulsification. Concentrated HNO_3 (35% Merck) was then added dropwise in the above mixture to acidify the solution. The dark brown precipitates were formed overnight, which were collected and washed with deionized water to remove acid and traces of surfactant. The precipitates were dried in hot air oven at $90^\circ C$ for 12 hours. Finally, dried powder was crushed and calcined at $500^\circ C$ for five hours in a box furnace at heating and cooling rate of $25^\circ C/min$ to obtain yellowish-brown V_2O_5 compound (Figure 3.1(a)). Figure 3.1 (b) shows the X-ray diffraction (XRD) profile of the V_2O_5 powder, which reveals the structural crystallinity and phase purity of V_2O_5 . The XRD pattern exhibits sharp peaks at many positions of 2θ degree. The peaks at 15.4, 20.3, 21.7, 26.2, 31, 32.4-, 34.4-, 47.4-

and 51.3-degree positions correspond to the lattice planes of (200), (010), (110), (101), (310), (011), (301), (600) and (002), respectively. All diffraction peaks for V_2O_5 can be indexed as an orthorhombic crystal phase (space group $P m n 2_1$, PDF 96-101-1226) without showing any impurity.

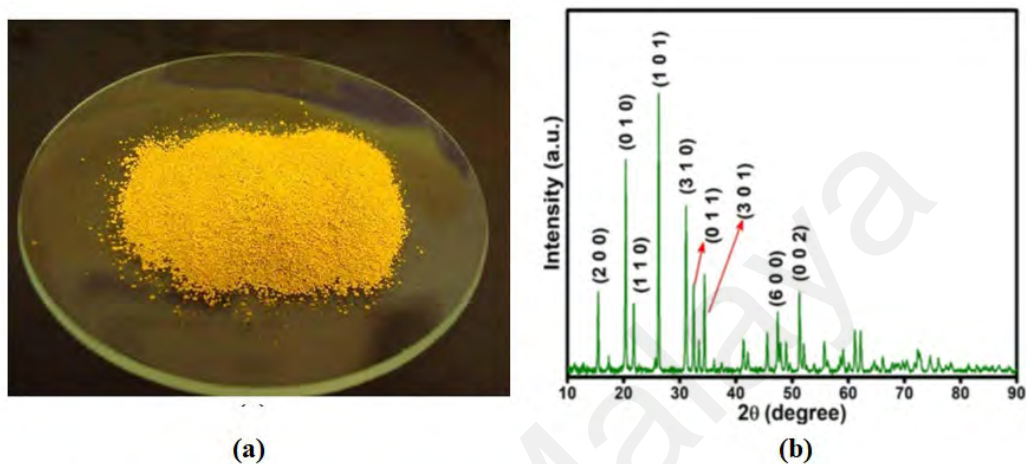


Figure 3.1: (a) yellowish-brown V_2O_5 compound and (b) its XRD profile

For the V_2O_5 compound to be integrated as an SA within the laser cavity, they were suspended in a thin polyethylene glycol (PEG) polymer film. The thin film was prepared by dissolving 1.0 g of PEO powder in 120 mL deionized water and put under stirring for 2 hours. Subsequently, an appropriate amount of the V_2O_5 compound was added into the prepared uniform transparent PEG solution and the mixture was kept under constant stirring for another 2 hours to obtain homogenous V_2O_5 PEG composite solution. The composite solution was cast on to the Teflon petri and dried in a vacuum oven at 60 °C for 24 hours to obtain light yellow solid thin film as shown in Figure 3.2 (a). The FESEM image of the V_2O_5 film is shown in Figure 3.2 (b), depicting the tubular shape of V_2O_5 . The tubular morphology is particularly attractive since it provides access to three different contact regions: inner and outer surface as well as the tube ends. Therefore, it holds a great advantage over other nanoparticles in that regard.

The SA itself is fabricated by simply sandwiching a small piece of the fabricated film with the suspended V_2O_5 compound between two conventional FC/PC fiber ferrules. The thin film is placed onto the face of one of the fiber ferrules with a help of index matching gel (Figure 3.2 (c), and then joined to a standard FC/PC adaptor. The other ferrule is then connected to the adaptor and the assembly secured, thus forming a fiber compatible SA device (Figure 3.2 (d)). A tiny amount of index matching gel was also applied in the connection to avoid spurious reflection in the SA device. The insertion loss of the SA is estimated to be less than 1 dB.

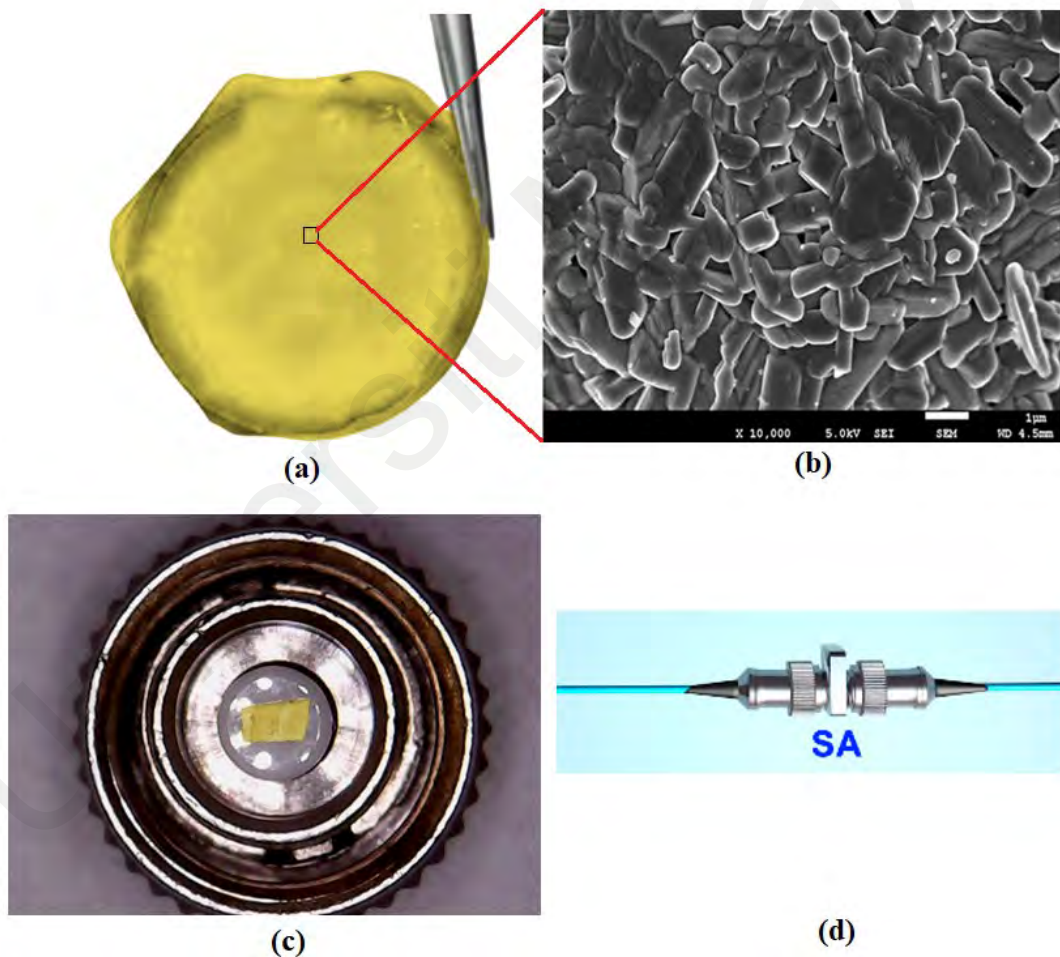
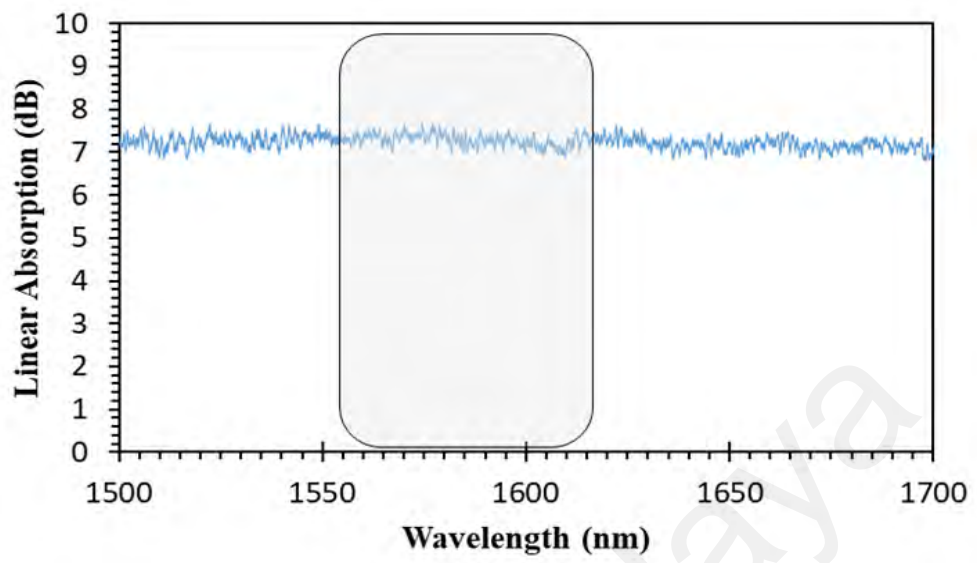


Figure 3.2: (a) A light yellow solid thin film of V_2O_5 (b) FESEM image (c) the film placed onto a fiber ferrule tip (d) all-fiber V_2O_5 SA device

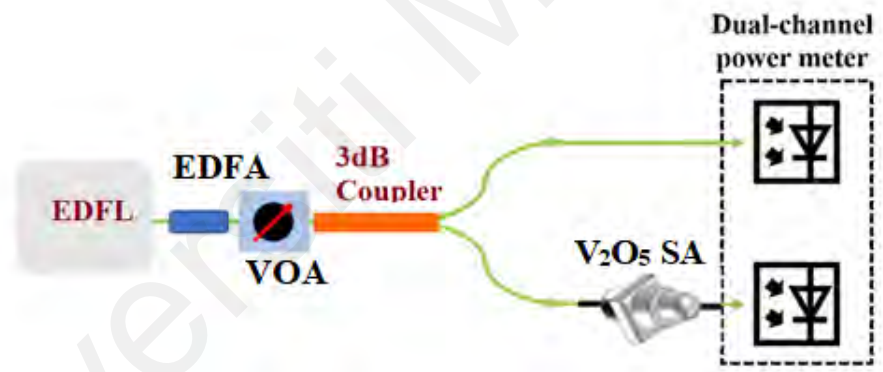
The linear absorption of the V₂O₅ PEG thin film was then evaluated as shown in Figure 3.3 (a). It was obtained by launching a broadband light from a white light source into the prepared film and recorded the output spectrum with an optical spectrum analyzer (OSA) with resolution of 0.07 nm. The linear absorption of about 7 dB was observed at 1550 nm wavelength region. The nonlinear absorption measurement was also gauged based on a twin-balanced detector technique using a homemade setup as shown in Figure 3.3 (b). The EDFL produced a mode-locked pulse train with a repetition rate of 1.809 MHz, a pulse width of 4.62 ps and a centre wavelength of 1559 nm, was used as a light source for this measurement. It is connected to an Erbium-doped fiber amplifier (EDFA) for amplification and then to a variable optical attenuator (VOA) for controlling the intensity. The attenuated signal is connected to a 3 dB coupler to separate the beam into two parts: One part is launched into the V₂O₅ film and the other is used as a reference. While varying the incident intensity on the V₂O₅ film under characterization, the absorption for different input intensities is measured by using an optical power meter. The nonlinear absorption profile is then plotted as illustrated in Figure 3.3 (c). A fitting curve is also plotted based on the saturation model as follows:

$$T(I) = 1 - q_0 \exp\left(-\frac{I}{I_{sat}}\right) - q_{ns} \quad (3.1)$$

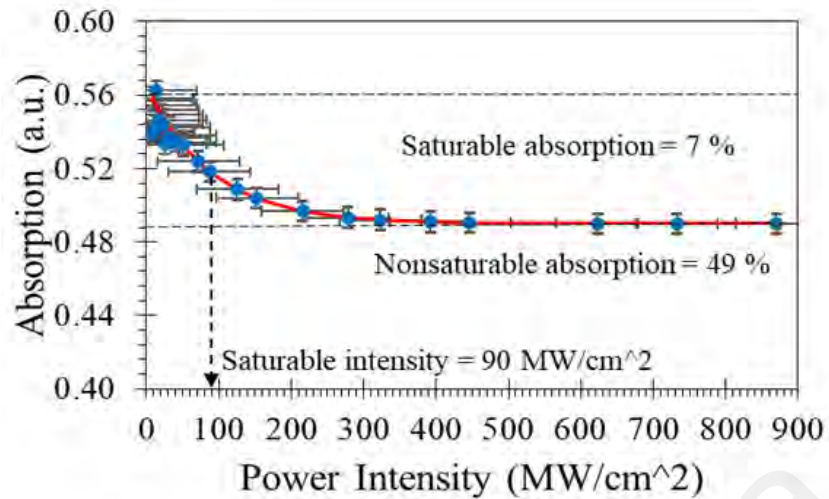
where $T(I)$ is the transmission, I is the input intensity, q_0 denotes the modulation depth of SA which represents the maximum change in absorption, I_{sat} represents the SA saturation intensity, and q_{ns} is the non-saturable absorption. As shown in Figure 3.3 (c), the saturation intensity of the V₂O₅ PEG film SA is 90 MW/cm² whereas its non-saturable absorption and modulation depth are 49 % and 7 %, respectively. The V₂O₅ nanoparticles are reported to have an optical bandgap of around 2.0 eV, which corresponds to the peak absorption in visible region (Srilakshmi et al., 2019). However, an absorption is also obtained in 1.5 μm region due to some defects in material morphology during the preparation.



(a)



(b)



(c)

Figure 3.3: (a) linear absorption cure (b) the nonlinear measurement setup (c) nonlinear saturable absorption curve for the V₂O₅-SA film

3.3 Q-Switched laser operating at 1-micron region with V₂O₅ SA

In this section, a Q-switched YDFL is demonstrated using a V₂O₅ based SA as a Q-switcher. The YDFL is configured in a ring cavity as shown in Figure 3.4. A laser diode operating at a wavelength of 974 nm is used as the YDFL's pump laser, and it is attached to the 980 nm port of a 980/1060 wavelength division multiplexer (WDM). The WDM marks the entry of the pump signal into the ring cavity, with its common port connected to a 1.5 long ytterbium doped fiber (YDF), which functions as a gain medium. The YDF has a core diameter of 4.0 μm, NA of 0.20 and cutoff wavelength of slightly shorter than 980 nm. The doping level of ytterbium ions in the fiber is 1500 ppm. The YDF's output is now connected to a 90:10 output coupler. The coupler is used to obtain a sample of the propagating signal for analysis via its 10% port, while the remainder of the signal is allowed to continue to propagate within the ring cavity by exiting the 90% port, which is spliced to the pre-fabricated V₂O₅ SA device. The SA device is in turn connected to a polarization insensitive optical isolator, which is optimized for operation in the 1-micron

wavelength region. The isolator ensures unidirectional propagation to the cavity to stabilize the system and reduce losses that may be incurred due to back-reflection, as well as prevent possible damage to the SA and the laser diode. The output pigtail of the isolator is then spliced to the 1060 nm port of the WDM and thus completes the cavity. Total length of the cavity was about 11 meters.

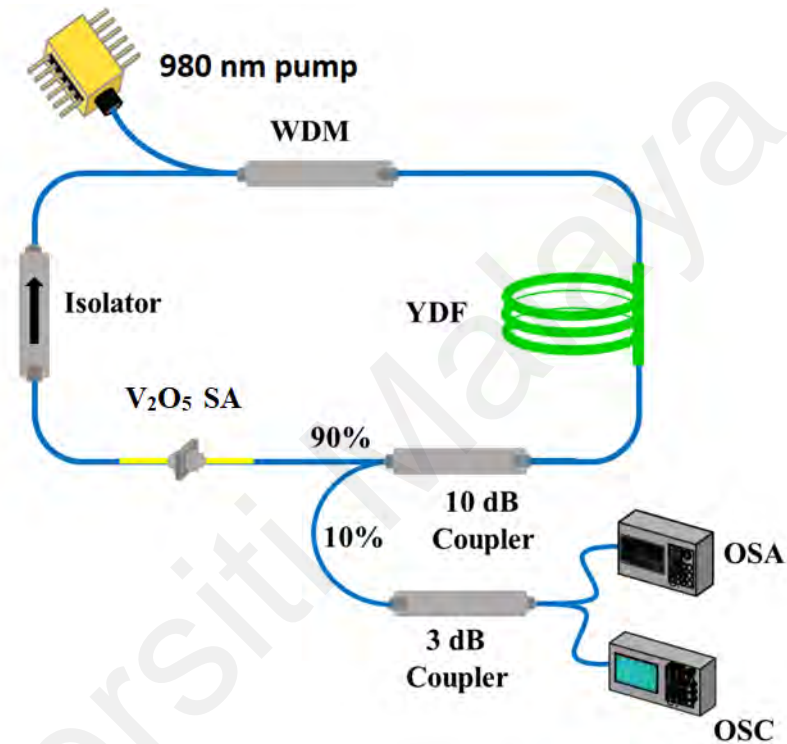
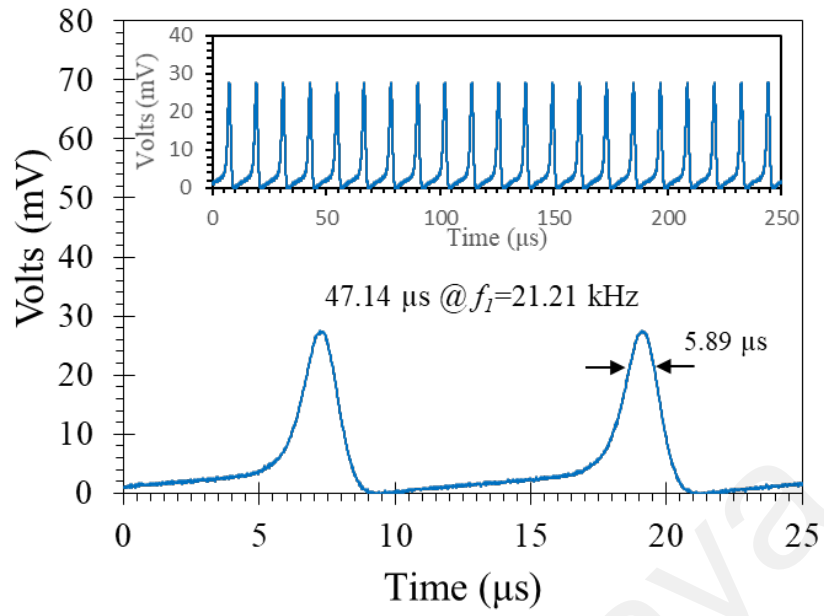


Figure 3.4: Configuration of the Q-switched YDFL with V₂O₅ SA thin film.

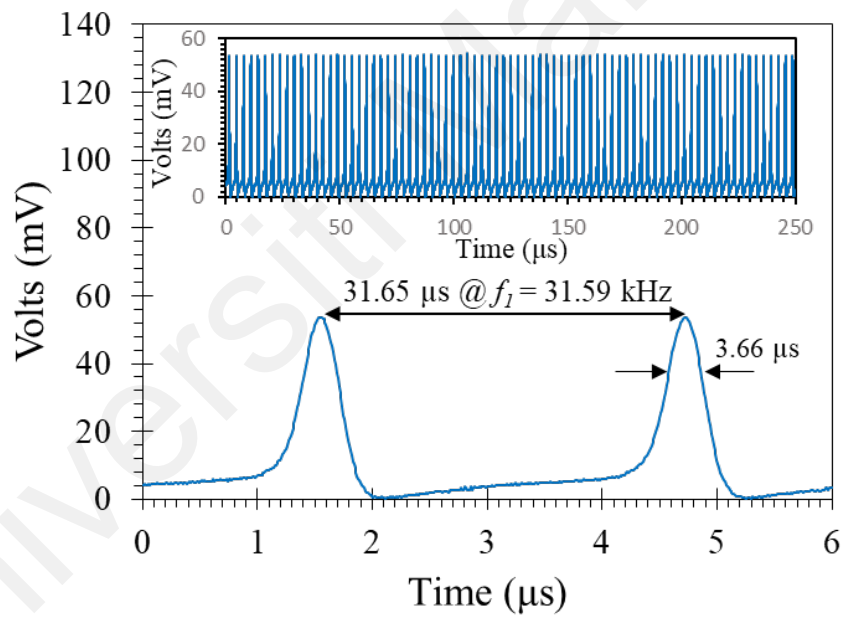
The signal extracted from the ring cavity is now split into two equal portions using another coupler with a coupling ratio of 50:50. The outputs from the 3dB coupler are used to analyse the optical and pulse characteristics of the generated signal. An optical spectrum analyzer (OSA), with a 0.07 nm resolution is employed to analyse the optical characteristics of the generated pulse. A 350 MHz oscilloscope is used for the measurement of the pulse characteristics via a 1.2 GHz photodetector. The oscilloscope

is then replaced with radio frequency spectrum analyzer (RFSA) to analyse the RF spectrum. The output power of lasing was measured using an optical power meter (OPM).

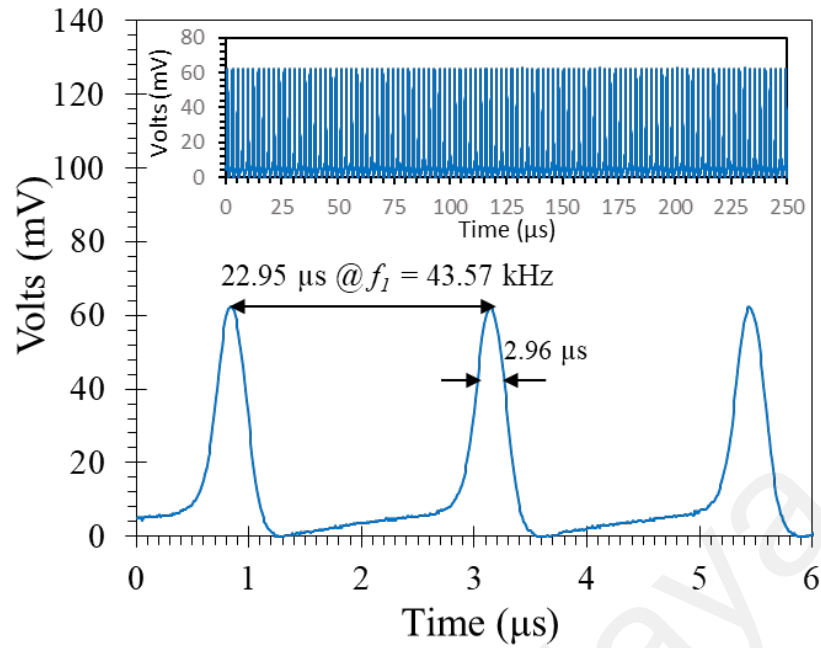
It should be noted that no Q-switched operation occurs without the V_2O_5 SA device connected in the laser cavity. This indicates that the Q-switched operation is mainly induced by the SA. The YDFL's lasing threshold is at approximately 75.4 mW, while its Q-switching threshold is approximately 96.1 mW. A stable Q-switched operation was observed up to the maximum pump power of 171.8 mW. Figures 3.5 (a), (b) and (c) show the typical Q-switched pulse train at pump powers of 96.1, 130.5 and 171.8 mW, respectively. As seen, the pulse repetition rate is 21.21, 31.59 and 43.57 kHz at pump power of 96.1, 130.5 and 171.8 mW respectively. The corresponding two pulses profiles were also displayed in Figure 3.5. It shows a full-width half maximum (FWHM) of 5.89, 3.66 and 2.97 μ s, at the pump powers of 96.1, 130.5 and 171.8 mW respectively. It indicates the feature of passive Q-switching state where the repetition rate is progressively increased while the pulse width decreases with pump power increment. There is also no amplitude fluctuation for the pulse within the tunable range of the repetition rate and no peak intensity modulation on pulse train, which indicates the high stability of the Q-switching state.



(a) 96.1 mWmW



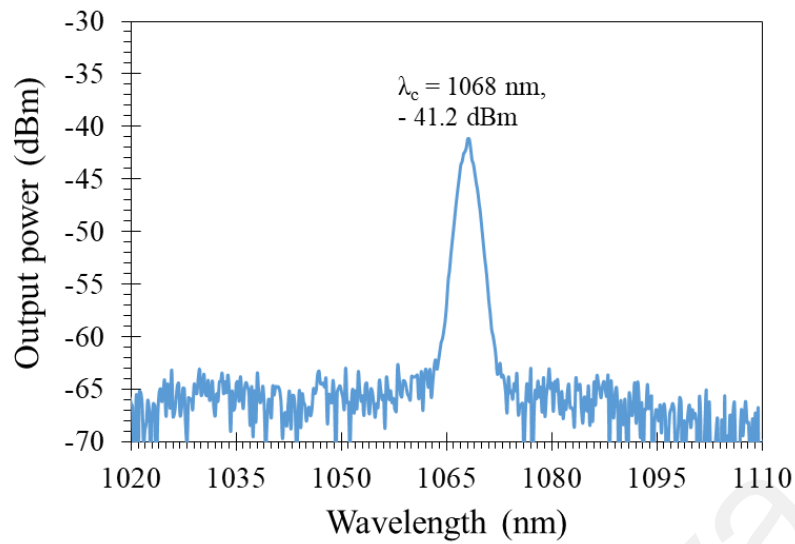
(b) 130.5 mW



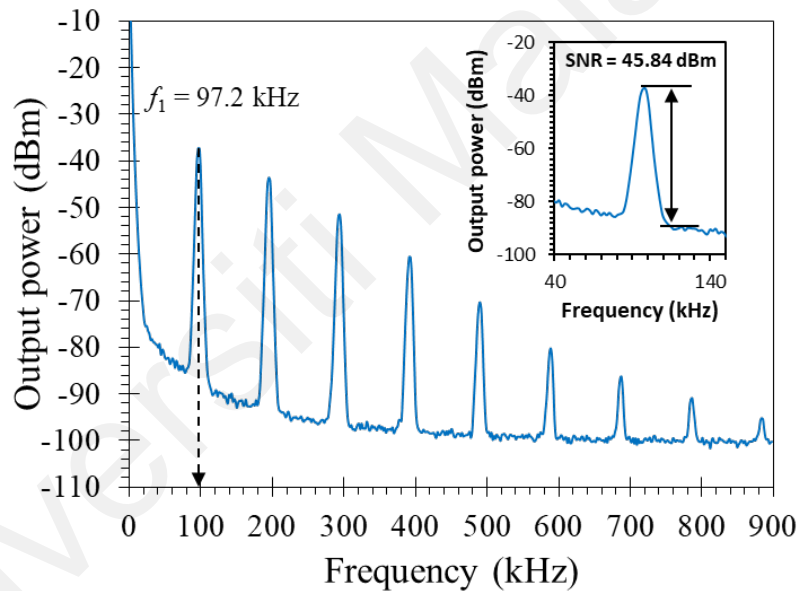
(c) 130.5 mW

Figure 3.5: pump powers; (a) 96.1 mW (b) 130.5 mW and (c) 171.8 mW

Figure 3.6 summarizes the typical spectral and frequency characteristics of the Q-switched pulse emitted from YDFL using V_2O_5 SA device as a Q-switcher at maximum pump power of 171.8 mW. Figure 3.6 (a) shows the optical spectrum of Q-switched YDFL, which operates at wavelength of 1068.2 nm. To investigate the stability of Q-switching pulses train in the proposed V_2O_5 SA based YDFL, RF spectrum was obtained at this pump power using an RF spectrum analyzer as shown in Figure 3.6 (b). The fundamental frequency was obtained at 97.2 kHz, which is in good agreement with the oscilloscope trace of Figure 3.5 (c). At the fundamental frequency, the signal to noise ratio (SNR) obtained was about 45.84 dB, which indicates the excellent stability of the laser. The proposed laser is observed to be highly stable, with no significant changes observed in any of the output parameters after two hours of operation, and repeated cycles of operation in the two days following.



(a) Output spectrum

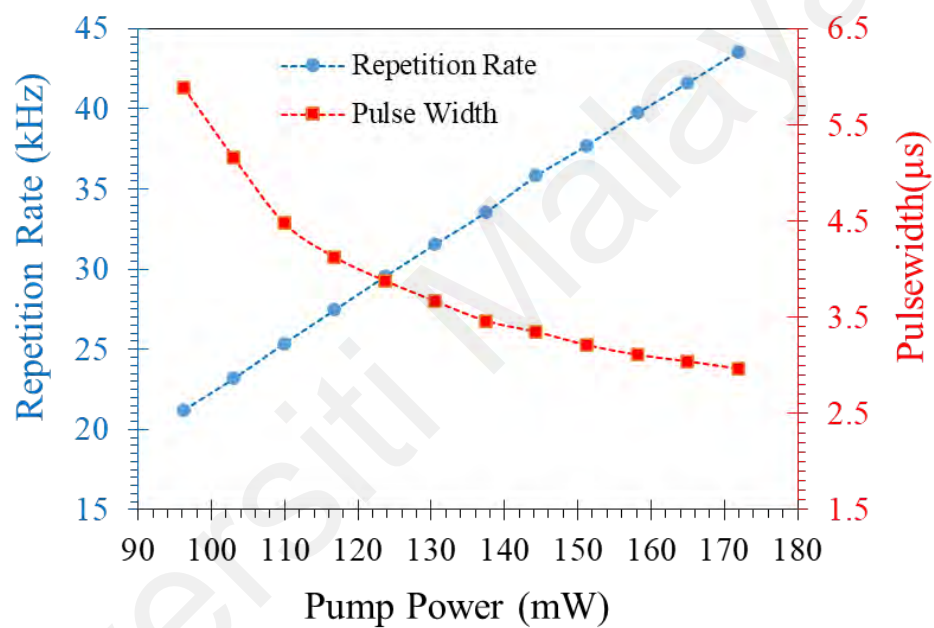


(b) RF spectrum

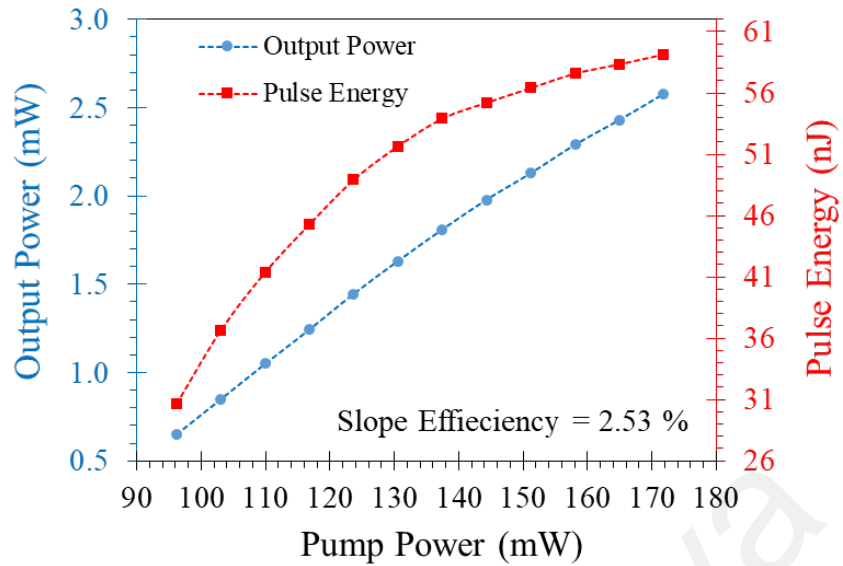
Figure 3.6: Q-switched pulse characteristics at the pump power of 171.8 mW, showing (a) optical output spectrum and (b) RF spectrum

Figure 3.7 (a) shows the repetition rate and pulse width against the pump power. The repetition rate increases in a linear fashion against the pump power, in agreement with the pulses train obtained from the oscilloscope as shown in Figure 3.5. The pulse width on the other hand decreases as the pump power increases, from a value of 5.89 μs at the

threshold pump power to the smallest pulse width of 2.97 μs at the maximum pump power of 171.8 mW. The pump rate for the upper laser level increases with increasing the pump power and causes the reduction of the pulse width and the increase of the repetition rate. The linear response of the repetition rate, which can be reproduced by repeating the experiment, shows that the SA has not exceeded its damage threshold, thus providing a relatively rugged and reliable platform for generating the sought-after Q-switched output in this region.



(a)



(b)

Figure 3.7: (a) Pulse width and repetition rate and (b) pulse energy and average output power corresponding to the pump power

Figure 3.7 (b) shows the average output power and pulse energy against the pump power. In the same manner as the repetition rate, the average output power and the pulse energy both increase in a linear fashion against the pump power. The highest average output power and pulse energy obtained were approximately 2.58 mW and 0.59 nJ respectively, at the maximum pump power. The average output power increases from 0.65 to 2.58 mW with a slope efficiency of 2.53% as the pump power is increased from 96.1 to 171.8 mW. The proposed Q-switched YDFL will have many advantages in providing high energy pulsed outputs for applications that operate at or near the 1-micron region, in particular sensing applications. Furthermore, optimizing the design of the cavity, including reducing the cavity length and cavity losses as well as optimizing its cavity structure and using higher quality V_2O_5 based SAs, will allow for better Q-switched pulses to be obtained. While use of the YDFL to generate pulsed and non-pulsed outputs at this region is not new, the use of the V_2O_5 based SA to achieve Q-switching in this configuration is to the knowledge of the authors, this is the first time such an approach

has been demonstrated, and opens up new possibilities for applications that require a compact yet rugged and cost-effective platform capable of operating in that wavelength region.

3.4 Q-switched laser operating at 1.5-micron region with V₂O₅ SA

In this section, passively Q-switched pulses are generated in an EDFL cavity using the V₂O₅ SA as a Q-switcher. An EDFL is constructed to study the performance of the V₂O₅-PEG SA, as shown in Figure 3.8. The ring cavity is formed by splicing 2 m EDF, a polarization-insensitive isolator, a V₂O₅-PEG SA, a 90/10 fiber-fused optical coupler, and a 980/1550nm WDM. An optical isolator was placed in between the gain medium and the SA to allow unidirectional light propagation inside the ring resonator. The prepared V₂O₅ PEG film was sandwiched between two FC/PC fiber ferrules and inserted into the laser cavity to function as Q-switcher. 10% of the output pulses were extracted through a 90:10 coupler for analysis. The output spectrum of the laser has been detected by an optical spectrum analyzer (OSA, Yokogawa AQ6370B) with a spectral resolution of 0.02 nm. The frequency and time-domain of the signal can be detected by a 1.3 GHz photodetector (Thorlabs, DET10D/M) in conjunction with a 7.8 GHz RF spectrum Analyzer (Anritsu) and a 350 MHz digital oscilloscope (GWINSTEK: GDS-3352), respectively. The total length of the cavity for Q-switching operation is about 5 m.

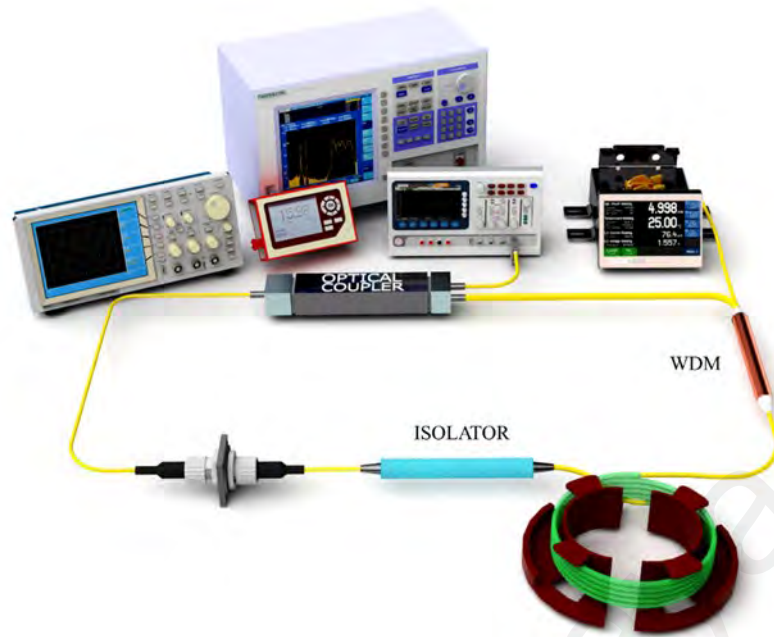
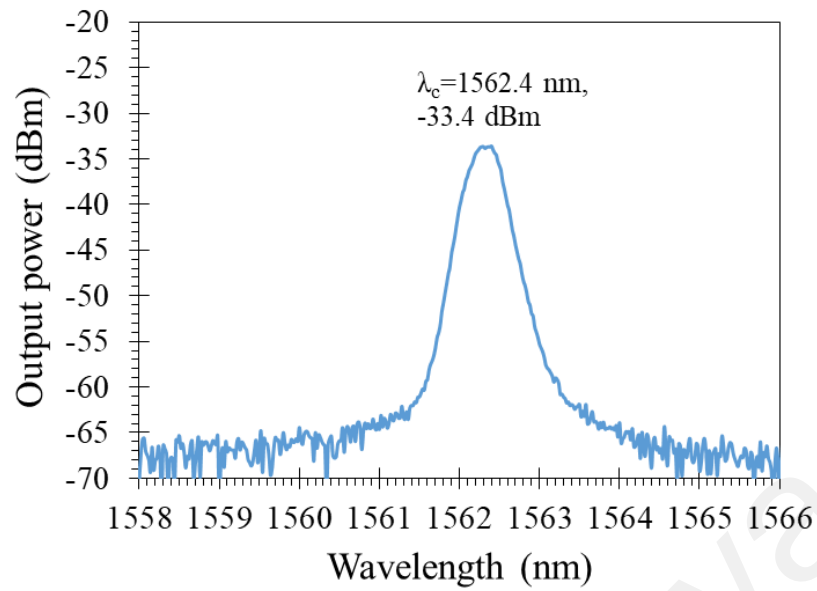
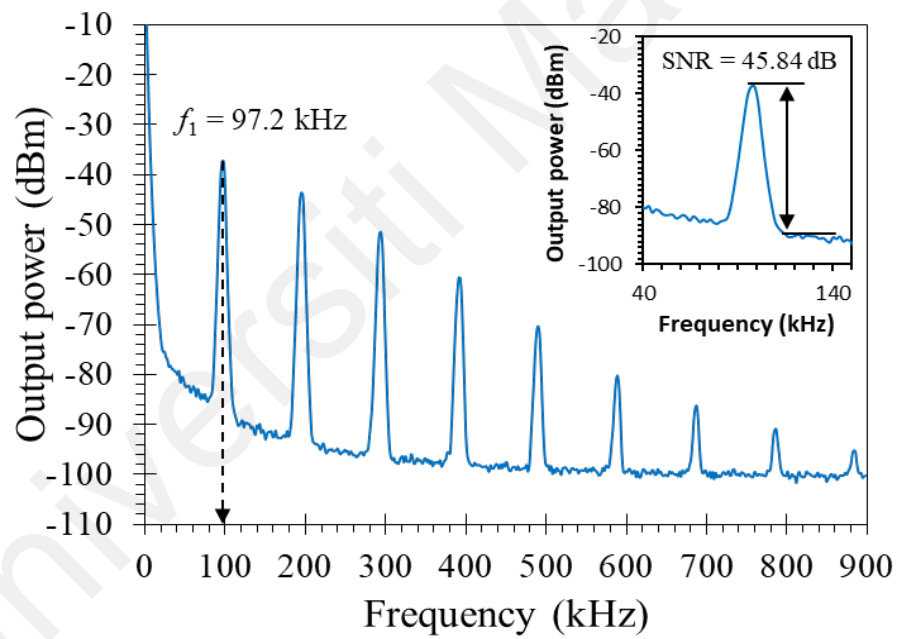


Figure 3.8: Configuration of the Q-switched EDFL with V₂O₅ SA thin film.

After inserting the V₂O₅-PEG SA into the cavity, a free running continuous wave laser is firstly generated in the EDFL at pump power of 40 mW. Further increasing the pump power to 110.9 mW, the EDFL delivers a train of Q-switched microsecond laser pulses. Figure 3.9 (a) shows the output spectrum of the laser at a pump power of 138.7 mW. The laser wavelength is centered at 1562.4 nm with a 3-dB bandwidth of 0.4 nm. Figure 3.9 (b) illustrates the corresponding RF spectrum, which indicates that the repetition rate of the pulses is 97.2 kHz at 138.7 mW pump power. The signal-to-noise ratio of the fundamental frequency is observed to be higher than 45 dB, which confirms the stability of such Q-switched operation. Figures 3.10 (a), (b) and (c) plot the typical oscilloscope traces at pump powers of 110.9, 138.7 and 166.5 mW, respectively. As seen, all pulses trains have a uniform profile and intensity. The pulse periods are given as 10.90, 10.29 and 7.82 μ s, which correspond to repetition rates of 91.7, 97.2 and 128.2 kHz, respectively. The zoom-in images of triple pulses are shown in Figures 3.10 (a), (b) and (c), giving a pulse width of 10.6, 9.5 and 4.7 μ s, respectively.

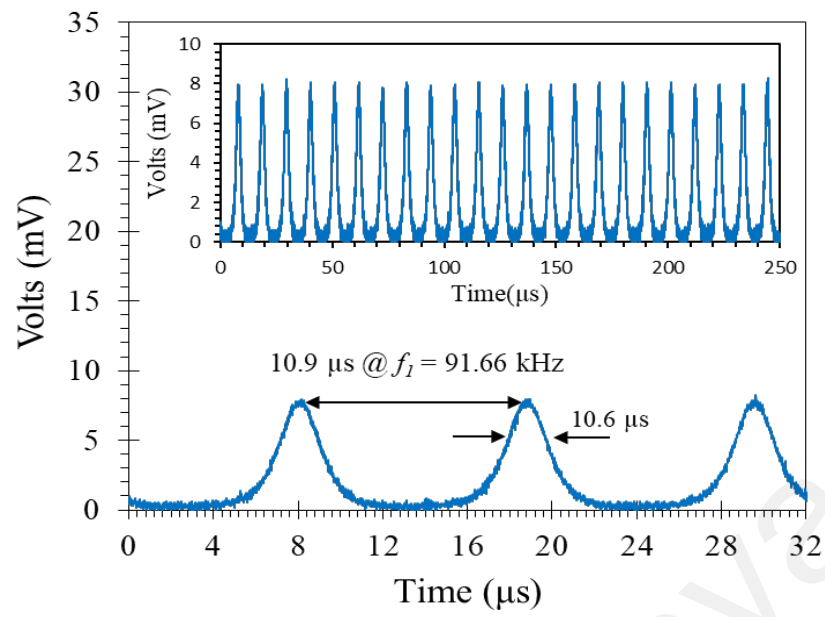


(a)

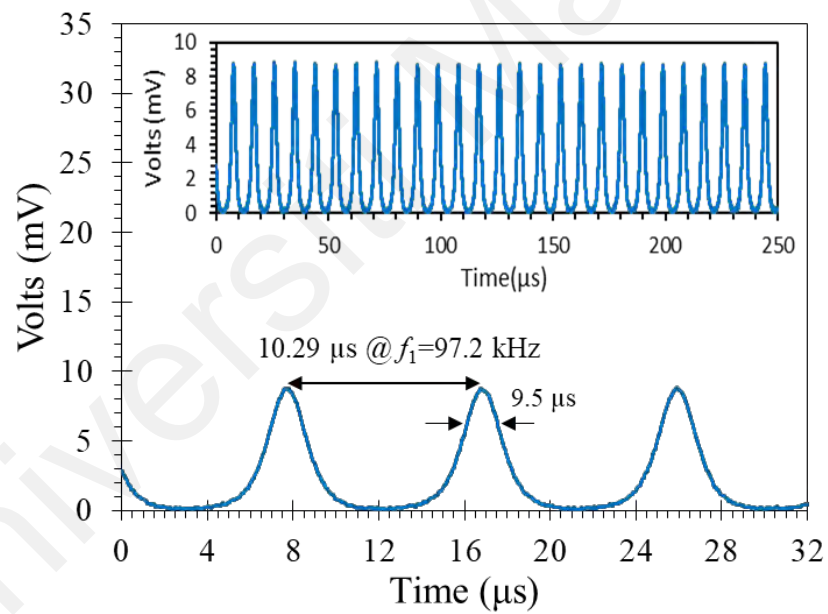


(b)

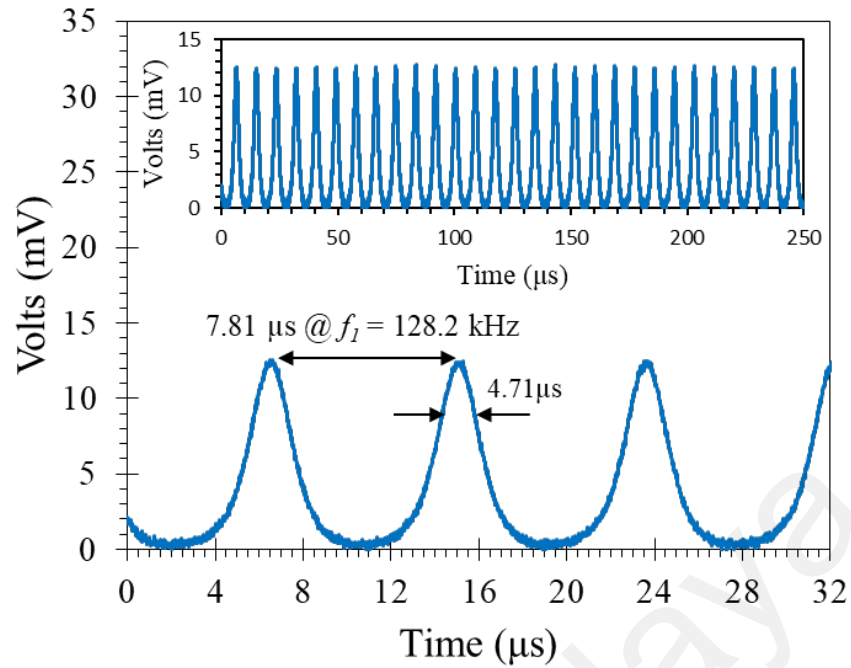
Figure 3.9: (a) Output spectral and (b) RF spectrum characteristics of the Q-switched EDFL at a pump power of 138.7 mW



(a) 110.9 mW



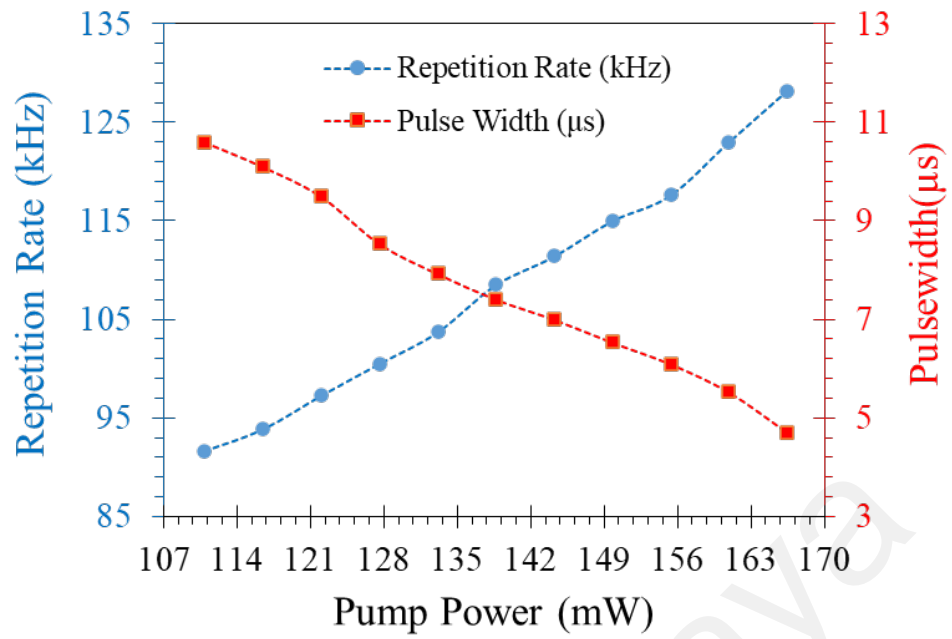
(b) 138.7 mW



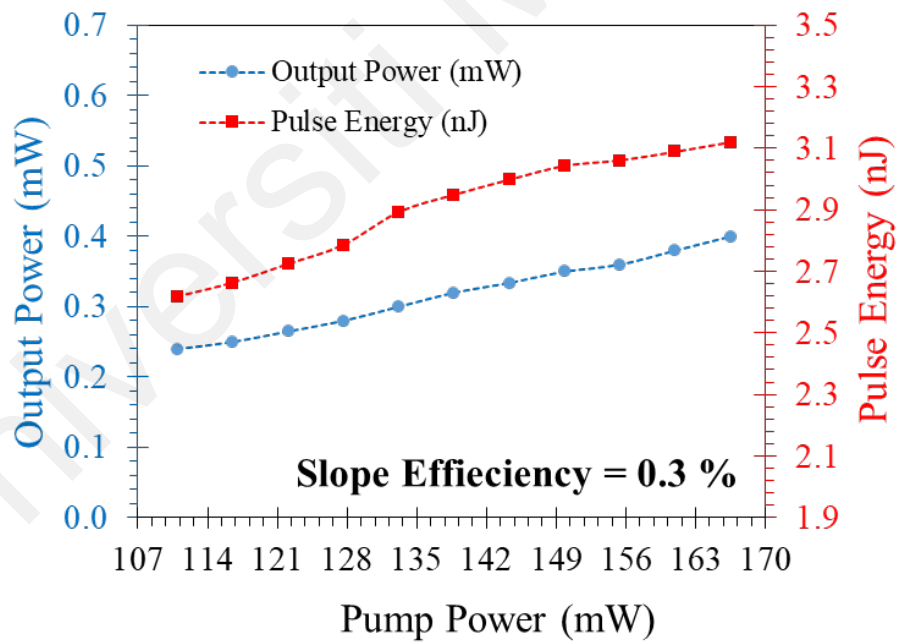
(c) 166.5 mW

Figure 3.10: (a) Output spectral and (b) RF spectrum characteristics of the Q-switched EDFL at a pump power of 138.7 mW

The evolution of the Q-switched pulses with the change of pump power is also investigated as shown in Figure 3.11. As illustrated in Figure 3.11 (a), by gradually varying the pump power from 110.9 mW to 166.5 mW, the repetition rate enlarges from 91.7 kHz to 128.2 kHz while the pulse duration shortens from 10.90 μs to 7.81 μs , which is the typical characteristic of the passively Q-switched operation. However, this operation becomes unstable and a continuous wave appears on the top of the spectrum at higher pump powers. The average power and calculated single pulse energy of the Q-switched EDFL versus pump power are described in Figure 3.11 (b). One can observe that the output power almost increases monotonously from 0.24 mW to 0.40 mW and the single pulse energy increases from 2.6 nJ to 3.2 nJ. The maximum value of light conversion efficiency is about 0.3 %. The low efficiency might be due to the large cavity loss induced by the SA film.



(a) Repetition rate and pulse width versus pump power



(b) Average output power and single pulse energy versus pump power

Figure 3.11: Q-switching performances of the V_2O_5 based EDFL against pump power (a) Repetition rate and pulse width (b) Average output power and single pulse energy

To confirm whether the Q-switching operation is purely induced by the V₂O₅ PEG film, the SA was replaced with a pure PEG film. However, Q-switched pulses were not observed in any cases, in despite of tuning laser diode over a full range. By changing the length of EDF and incorporating additional SMF in the EDFL cavity, a mode-locking operation was also realized, confirming that V₂O₅-PEG film can also act as a mode-locker. The performance of the V₂O₅ based mode locked EDFL will be discussed in the next section.

3.5 Mode-locked laser operating at 1.5-micron region with V₂O₅ SA

In this section, a picosecond pulse generation is demonstrated utilizing a newly developed V₂O₅ SA as a mode-locker. The SA was prepared by the embedding of V₂O₅ material into polyethylene glycol (PEG) to compose a film absorber, which was then inserted between two fiber ferrules. The V₂O₅ PEG film could be used as nonlinear optical modulator in an Erbium-doped fiber laser (EDFL) cavity as it has a modulation depth of 7% with a saturation intensity of 90 MW/cm². A V₂O₅ SA was integrated into an EDFL cavity as shown in Figure 3.12 to generate a soliton mode-locked pulse. The fiber laser was constructed using a 4 m long EDF, which has a core diameter of 4 μm, numerical aperture of 0.23, a group velocity dispersion (GVD) of 27.6 ps²/km and peak absorption of 35 dB/m at 1531 nm. The EDF was pumped in forward direction by a 980 nm laser diode through a 980/1550 WDM, which has a 0.5m long pigtail of Corning HI1060 fiber with a GVD of -7 ps²/km. An optical isolator was inserted after the EDF to ensure unidirectional propagation of the laser light inside the EDFL cavity. An output coupler (OC) with a splitting ratio of 10:90 was used, so that 10% of the oscillated laser can be tapped out from the cavity for measurement. The additional 50 m long of single mode fiber (SMF) with a GVD of -22 ps²/km was used to assist the V₂O₅ SA in generating a self-starting mode-locked pulse by providing sufficient dispersion and nonlinearity inside the laser cavity. The total cavity length is about 55 m with a net cavity dispersion

of -1.004 ps^2 . This shows the cavity operates in anomalous dispersion and thus ensuring the laser operation in soliton regime. The laser measurement was carried out using an optical spectrum analyzer (OSA, Yokogawa AQ6370B) with a spectral resolution of 0.02 nm, a 350 MHz oscilloscope (GWINSTEK: GDS-3352), an autocorrelator (Alnair Labs, HAC-200), and a 7.8 GHz radio frequency (RF) spectrum analyzer (Anritsu) with a 1.3 GHz photodetector (Thorlabs, DET10D/M).

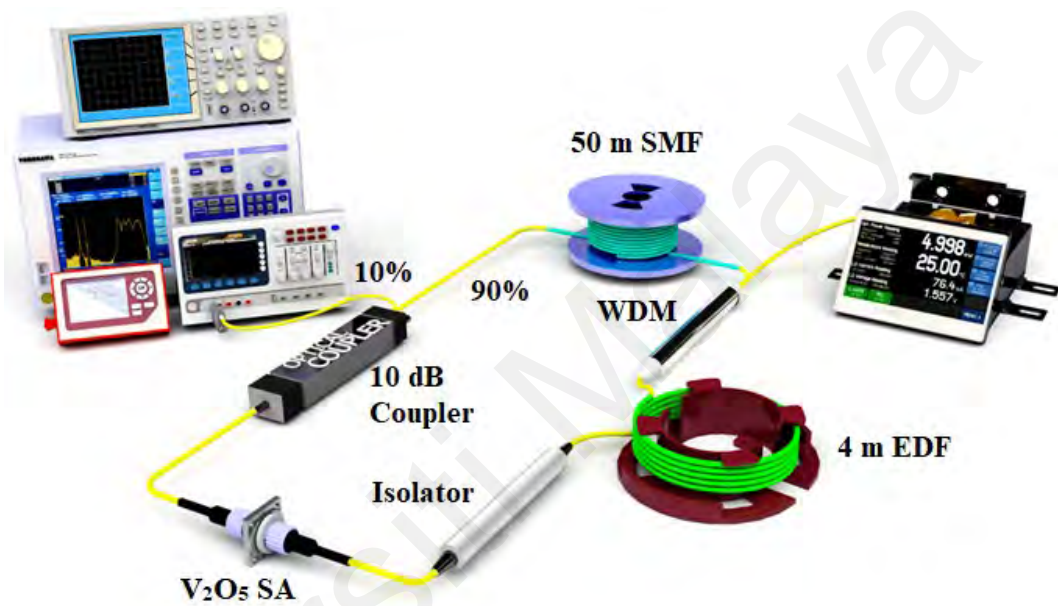
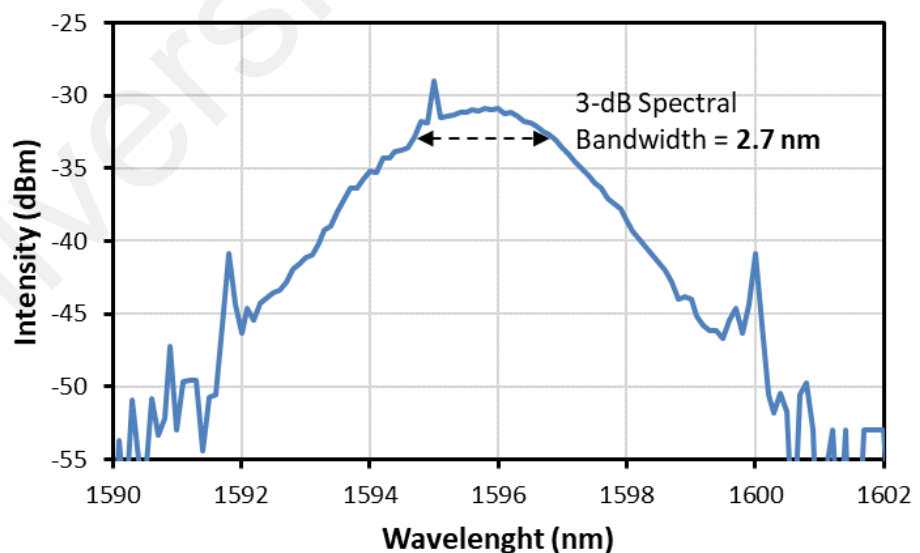


Figure 3.12: Schematic diagram of the experimental setup for the mode locked EDFL with V_2O_5 SA.

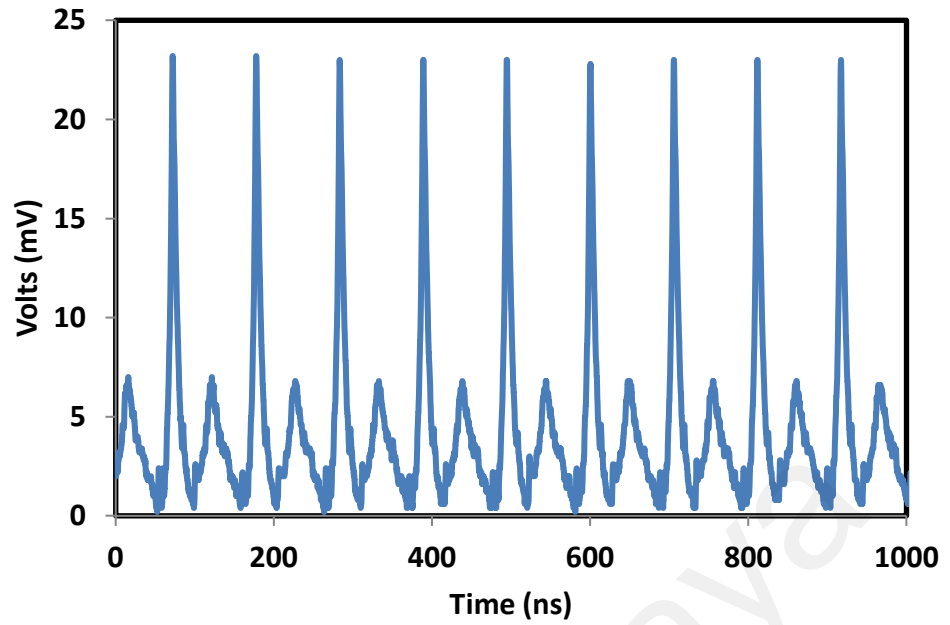
A self-starting mode locked pulse was generated when the pump power increased to 80.0 mW. The mode-locking operation was maintained as the pump power is further increased up to 106.6 mW. The mode-locked operation was initiated via absorption of light by V_2O_5 , which causes the cavity to modulate loss and produces picosecond pulses. The SA also functions to prevent a build-up of noise, thus allowing the self-started mode-locked with superior stability. Figure 3.13 (a) shows the optical spectrum of the generated mode-locked pulses at 106.6 mW pump power. It centered at a wavelength of 1595.4 with a 3 dB bandwidth of 2.7 nm. The Kelly side band was also observed in the spectrum,

which indicates that the laser operated in a soliton regime due to the anomalous dispersion of the cavity. The laser operates in L-band region due to the use of relatively long gain medium (4 m). The EDF absorbed C-band photons to emit at L-band region.

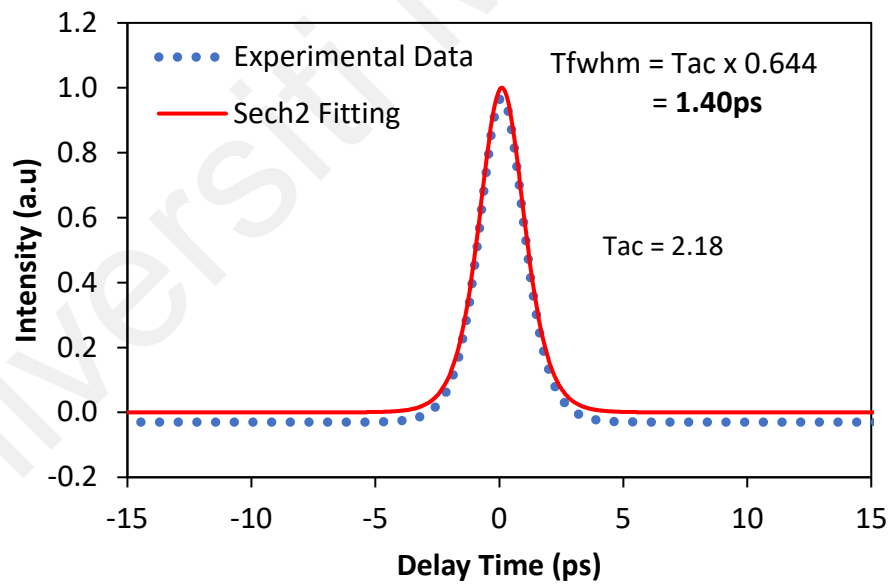
A typical oscilloscope trace is shown in Figure 3.13 (b) with a time interval between two pulses of 106.4 ns at pump power of 106.6 mW. The pulse train is stable with the pulse period corresponds to repetition rate of 9.4 MHz, which matches very well with the cavity length of 55 m. A small amplitude fluctuation of the pulse was visible due to the presence of timing jitter inside the laser cavity. The pulse width recorded on the oscilloscope is not the actual value due to the resolution limitation in the oscilloscope. Therefore, an autocorrelator was used to measure the pulse width and the experimental result is plotted in Figure 3.13 (c) in conjunction with sech^2 fitting. The figure indicates that the measured auto-correlator pulse trace has sech^2 pulse profile with FWHM of 1.40 ps.



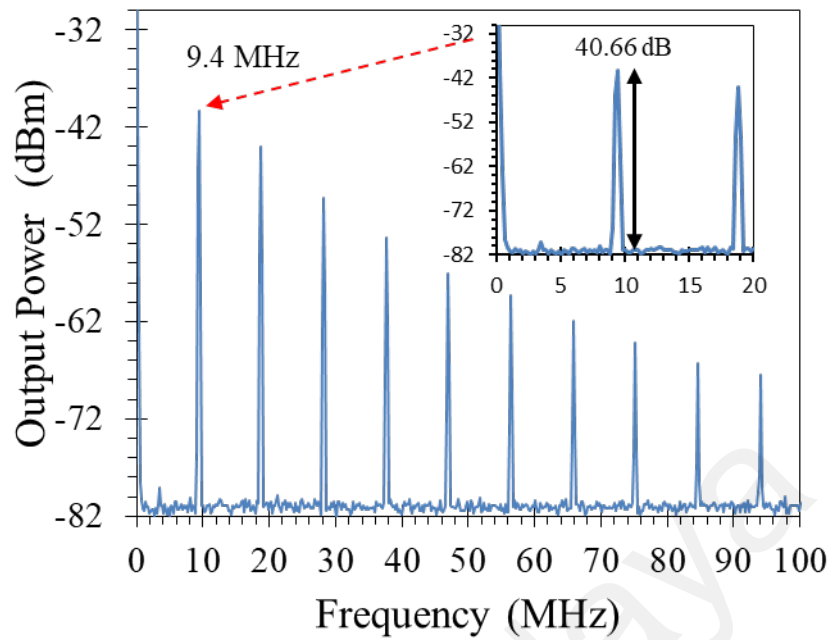
(a) Output spectrum



(b) Typical pulse train



(c) Autocorrelator trace



(d) RF spectrum

Figure 3.13: The spectral and temporal characteristics of the V_2O_5 based mode locked EDFL (a) Output spectrum (b) Oscilloscope trace (c) Autocorrelator trace (d) RF spectrum

The degree of suppression of the noises has been measured to investigate the stability of the pulse via RF spectrum as shown in Figure 3.13 (d). It shows that the fundamental frequency of the cavity is around 9.4 MHz and the noises are suppressed by 40.66 dB which confirms the stability of the pulse. Many harmonics were also recorded within a wide frequency span of 100 MHz, which indicates a low signal distortion inside the laser cavity and confirms the formation of mode-locked pulses with narrow pulse width. The relatively small signal to noise ratio (SNR) is due to the long cavity implementation. The generated RF spectrum might be improved by optimization of SA quality and cavity design to reduce loss. A time bandwidth product (TBP) was measured to be approximately 0.445, which indicates the pulses are chirped.

The output power and pulse energy of the generated mode-locked laser versus pump power have also been investigated as shown in Figure 3.14. The output power increases from 0.82 mW to 1.93 mW as the pump power is creased from 80.0 mW to 106.6 mW and so does the pulse energy. An optical-to-optical efficiency of the laser was obtained at 4.3%. The efficiency is relatively low due to the operation of the laser in L-band region. The maximum pulse energy of 205.3 pJ was obtained at 106.6 mW pump power. The confinement of photons inside a small diameter of the optical fiber core and long cavity length limits the pulse energy of the laser. Reducing the cavity length might decrease such effect and improves the maximum attainable pulse energy. The mode-locking performance was also comparable to other SAs as depicted in Table 3.1.

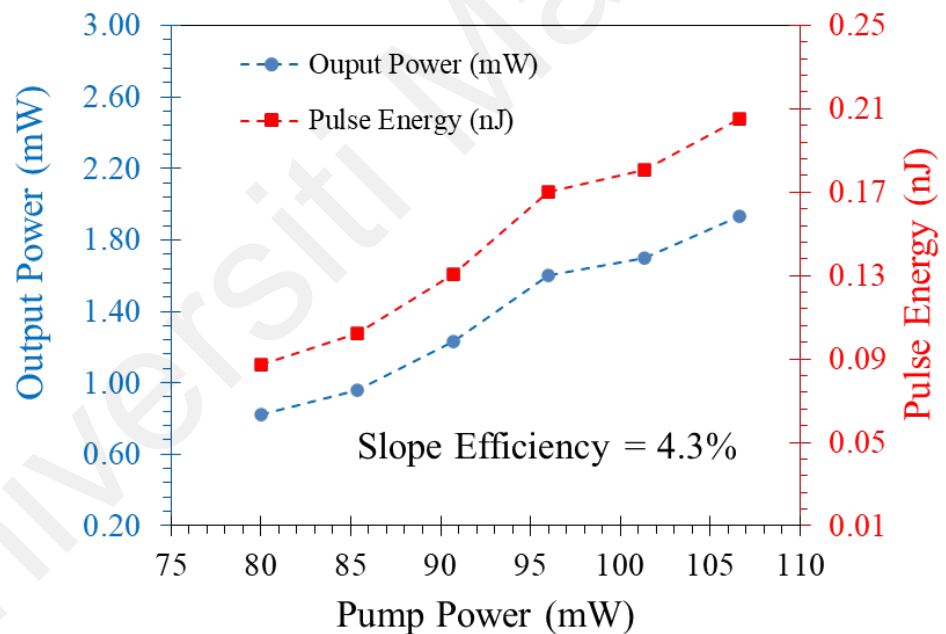


Figure 3.14: Output power and single pulse energy versus pump power for the V₂O₅ based mode locked EDFL.

Table 3.1: Performance comparison of mode-locked EDFL using various SA materials.

SAs	Modulation depth (%)	Threshold (mW)	Pulse width (ps)	Repetition rate (MHz)	3 dB bandwidth (nm)	Ref.
WS₂	1.8	190	1.20	8.96	3.1	(Mao et al., 2015a)
WSe₂	0.5	35	1.25	5.31	2.1	(Mao et al., 2016)
MoSe₂	0.4	-	1.18	5.03	2.2	(Mao et al., 2016)
SnS₂	5.0	45	1.63	4.397	1.6	(Yang et al., 2017)
V₂O₅	7.0	80	1.40	9.4	2.7	This work

3.6 Summary

Q-switched and mode-locked fiber lasers have been successfully demonstrated by using the V₂O₅ film as a SA. The SA was obtained by embedding the synthesized V₂O₅ into a PEG polymer film. It has a modulation depth, saturation intensity and non-saturable loss of about 7 %, 90 MW/cm² and 49 % respectively. At first, a Q-switched YDFL operating at 1068.2 nm was successfully realized by incorporating the SA in a YDFL cavity. A stable Q-switching pulses train was successfully generated at a threshold pump power of approximately 96.1 mW. The maximum output pulse energy of the proposed fiber laser is 0.59 nJ and minimum pulse width of 2.97 μs are obtained at the repetition rate of 43.57 kHz from the laser cavity when the input pump power is 171.8 mW. A Q-

switched EDFL by using V_2O_5 film as SA was then experimentally demonstrated. Q-switching operation was obtained from pump power range of 110.9 – 166.5 mW. The pulse repetition rate shows an increasing trend from 91.7 kHz to 128.2 kHz, whereas the pulse width exhibits a decreasing trend from 10.90 μ s to 7.81 μ s. The highest pulse energy of 3.2 nJ is obtained at pump power of 166.5 mW.

An ultrashort pulse laser operating in L-band region (1595.4 nm) was also experimentally achieved by incorporating the V_2O_5 film inside an EDFL cavity configured with 4 m long EDF and 50 m long additional SMF. The soliton mode locked pulses were successfully generated within a pump power of 80.0 mW to 106.6 mW. It operated at a repetition rate of 9.4 MHz and pulse width of 1.40 ps and produced a maximum output power of 1.93 mW and maximum pulse energy of 205.3 pJ. The pulses generated was stable as it has a SNR of 40.66 dB. The easy fabrication, good stability, and robust structure of V_2O_5 based SA will facilitate many more potential nonlinear photonic applications, which are expected to work towards ultrafast photonics and play key role in various optical telecommunications and measurement applications.

CHAPTER 4: LUTETIUM (III) OXIDE FILM AS PASSIVE Q-SWITCHER AND MODE LOCKER DEVICE

4.1 Introduction

Q-switched and mode-locked fiber lasers, particularly the ones achieved via passive techniques, have seized the attention of many researchers in recent years as they are easier to generate and more compact in setup (Harith Ahmad, Ruslan, et al., 2016). This is due to the flexibility and simplicity of the passive techniques that do not require an electronic controller to trigger the pulses. In particular, Q-switched erbium-doped fiber lasers (EDFL) have found many applications in telecommunication, medical diagnostics and treatments, sensing, material processing, and range finding (Hakulinen et al., 2007; U. Keller, 2003; Lucas et al., 2012; Martin E. Fermann, 2009; R Paschotta et al., 1999).

In the early years, semiconductor saturable absorbers (SESAMs) (Du et al., 2014; Keller et al., 1992), carbon nanotubes (CNTs) (Set et al., 2004; Zhou et al., 2010), graphene (Bao et al., 2011; J. Liu et al., 2012; Z. Luo et al., 2010; Popa et al., 2011) and black phosphorus (BP) (Y. Chen et al., 2015; Ma et al., 2015), among others (X. Jiang et al., 2018; Lu et al., 2018; Niu et al., 2017; R. Sun et al., 2018; Zhao et al., 2012) have been successfully used as intracavity-loss modulators to produce pulsed lasers passively or have been successfully used as intracavity-loss modulators to produce pulsed lasers passively or have been benefited many other photonics applications. After its debut in 1992 (Keller et al., 1992), SESAMs quickly became the most prominent SA for several years. However, they suffer from some drawbacks including narrow absorption bandwidth, relatively high production cost and considerably bulky size. The main drawback of CNT SAs is that their absorption efficiency and bandwidth are dependent on their diameter. As for graphene, its main issue is its relatively low optical absorption per layer that limits its usability. Meanwhile, BP is a polarization dependent and hydrophilic material that easily interacts with water (Island et al., 2015). Thus, constructing a BP SA

is challenging as it requires a complex preparation as well as careful handling. In recent years, other new materials that are relatively easy to prepare have been proposed as candidates for SAs to produce cheap and stable pulsed fiber lasers (Ab Rahman et al., 2018; Kang et al., 2018; Heping Li et al., 2015; Niu et al., 2017). In an earlier report, holmium oxide, a lanthanide material had been successfully revealed as a reliable SA candidate for inducing a stable Q-switched fibre laser at the 2-micron regime (Rahman et al., 2017).

Lutetium oxide (Lu_2O_3) or Lutecia, another lanthanide oxide element, is a thermally stable white compound material which is suitable for glass and optical applications. It is used as cracking, alkylation, hydrogenation, polymerization, X-ray application as well as the starting material in the production of laser crystals. Experimentally, it has been tested to have sufficient optical absorption in the $1.55 \mu\text{m}$ vicinity, suggesting a suitability to be used as a potential SA candidate for both Q-switched and mode-locked EDFL operations. By properly embedding the Lu_2O_3 element into the polyvinyl alcohol (PVA), a very thin Lu_2O_3 PVA film with a thickness of around $30 \mu\text{m}$ could be attained. The film SA can be easily incorporated into the laser cavity by sandwiching a small size ($1\text{mm} \times 1 \text{mm}$) of the film between two fibre ferrules before being closely fixed with a fibre adapter. Such a mechanism allows the realization of a simple, as well as flexible all-fiberized passively mode-locked laser system.

In this chapter, the developed Lu_2O_3 PVA composite thin film was integrated into fiber laser ring cavity for realizing both Q-switched and mode-locked pulses. The proposed Lu_2O_3 SA is quite easy to prepare, and shows relatively higher modulation depth of 10% than certain of 2D materials (B. Chen et al., 2015); MoS_2 (2.15%), MoSe_2 (6.73%), WS_2 (2.53%) and WSe_2 (3.02%). Unlike BP SA, which tends to react with water due to its hydrophilic property, the Lu_2O_3 SA is more reliable, simple and robust.

4.2 Lutetium Oxide Film Fabrication and Characterization

In this experiment, the PVA was chosen as the host material as it has excellent film-forming and adhesive properties. Furthermore, by embedding the Lu_2O_3 materials inside the PVA film, not only it would ease the film SA handling and integration into the laser cavity, but it would also securely protect the Lu_2O_3 materials from external contamination. The laser operation was conducted at considerably low or moderate pump power and therefore would not damage the film SA. The Lu_2O_3 powder (CAS No. 12032-20-1, 99.9 % traces metal basis) used in the Lu_2O_3 thin film SA fabrication was obtained from Sigma Aldrich (Malaysia) without further purification. The fabrication process of the Lu_2O_3 film SA is illustrated in Figure 4.1. The Lu_2O_3 solution was prepared by dissolving 5 mg Lu_2O_3 into 50 ml isopropyl alcohol (IPA). The solution was constantly stirred for 5 minutes using a magnetic stirrer. Then, the Lu_2O_3 solution was centrifuged for 6 hours using an ultrasonic bath machine. Upon completion of these processes, the supernatant containing Lu_2O_3 solution could be seen emerging on the surface of the Lu_2O_3 residue. The Lu_2O_3 solution was then transferred into a test tube for later use. On the other hand, the PVA solution was prepared by dissolving 1 g of PVA powder with 120 ml deionized (DI) water. The mixture was stirred at a stirring temperature of 90°C for 30 minutes. Then, the PVA solution was cooled down to room temperature. Next, the pre-prepared Lu_2O_3 solution was carefully mixed with the PVA solution. The mixed solution was ultrasonicated for 2 hours to form a homogenous composite precursor solution. The solution was then transferred onto a petri dish and left to dry at room temperature for 3 days, to form ~ 30 microns thick of Lu_2O_3 PVA composite film SA. For brevity, the composite film SA is regarded as Lu_2O_3 film SA in this chapter.

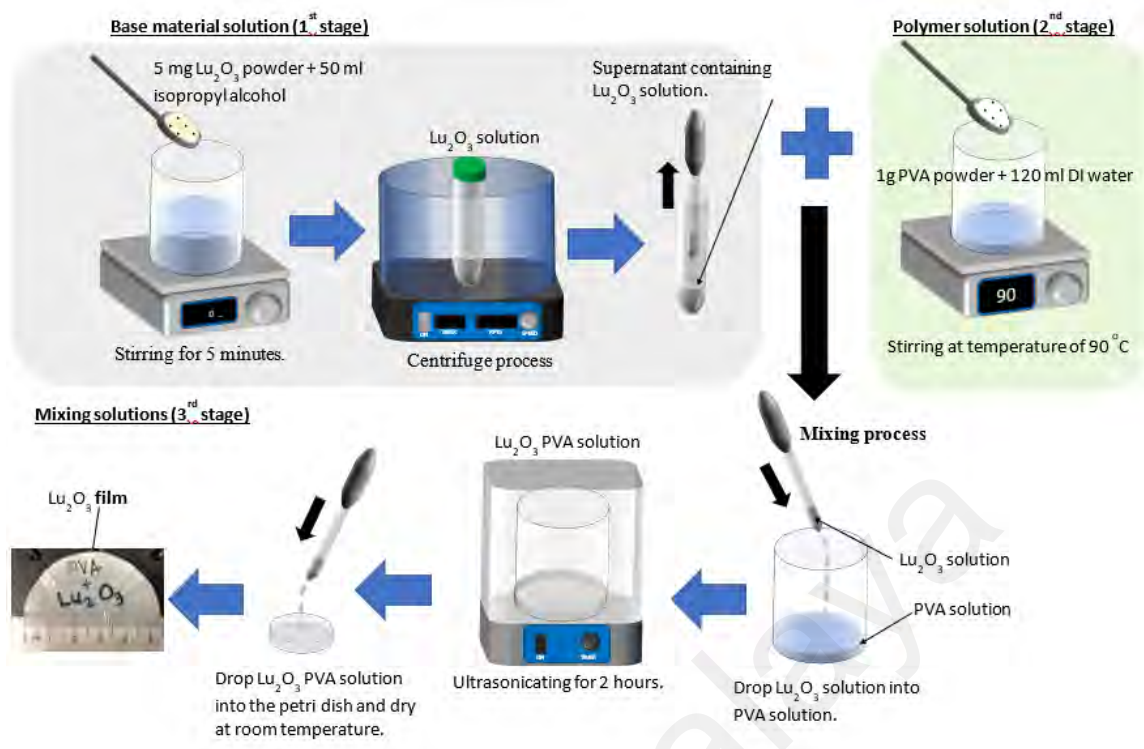
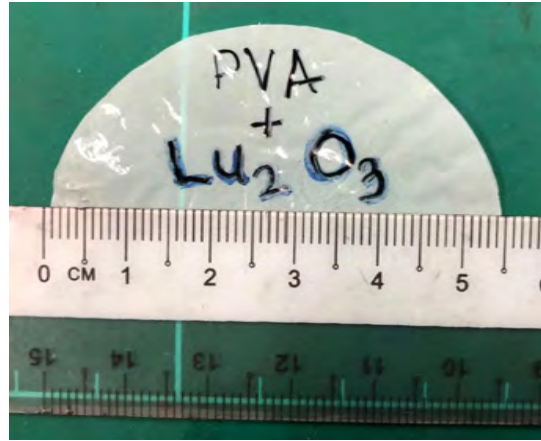
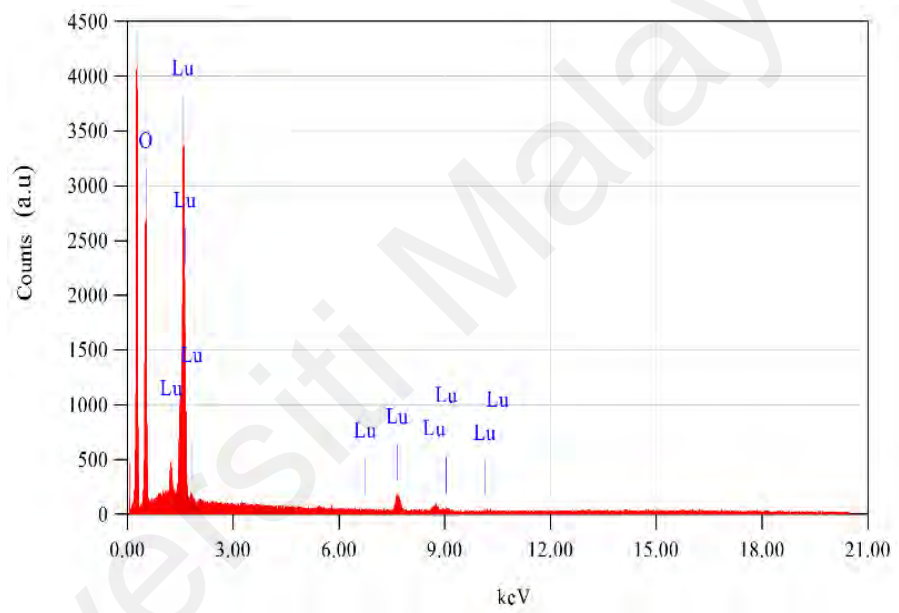


Figure 4.1: The proposed fabrication process of the Lu₂O₃ thin film SA.

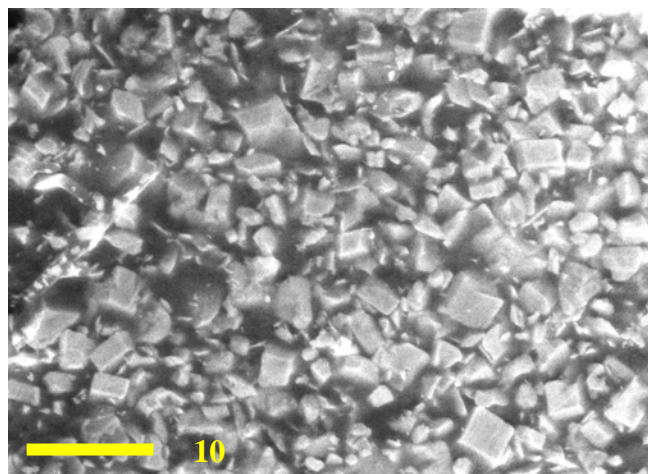
Figure 4.2 shows the image and important optical characteristics of the Lu₂O₃ film SA. Figure 4.2 (a) shows the real image of the Lu₂O₃ PVA thin film. The film is white in color and is partly transparent. The composition of the fabricated Lu₂O₃ film SA was investigated via energy dispersive spectroscopy (EDS). As provided in Figure 4.2 (b), the presence of the Lu₂O₃ is confirmed through several high peaks dominated by the Lu and O elements that appear on the plot. Figure 4.2(c) illustrates the scanning electron microscopy (SEM) image of the fabricated Lu₂O₃ film SA, which shows the Lu₂O₃ component randomly distributed in the polymer composite. The linear absorption profile of the Lu₂O₃ film SA is provided in Figure 4.2(d). As demonstrated, the peak absorption (20.7 dB) is observed to be at 1308 nm wavelength, while the optical absorption at the mode-locked operating wavelength (1564 nm) is found to be 4.6 dB. The inset of Figure 4.2(d) illustrates the set-up used for the linear absorption measurement.



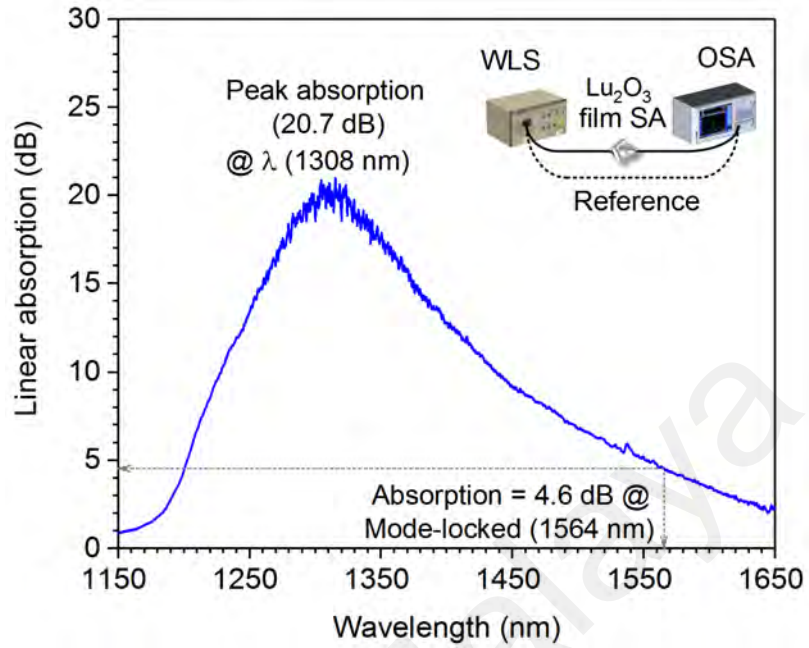
(a)



(b)



(c)



(d)

Figure 4.2: The image and important characteristics of the Lu₂O₃ film SA (a) real image (b) EDS profile (c) SEM image (d) Linear absorption profile

The film SA modulation depth was measured using twin detector measurement method. In the experiment, a stable 1 MHz amplified self-generated passively mode locked EDFL (1550 nm) with a constant 2 ps pulse width was used as the input pulse light source. The output powers from both detectors (with and without SA integrated into) were recorded as the optical power gradually increased. The results were then fitted with the Gamire et al. saturation model formula (Garmire, 2000),

$$\alpha(I) = \frac{\alpha_s}{1+I/I_{\text{sat}}} + \alpha_{\text{ns}} \quad (4.1)$$

where $\alpha(I)$ is the absorption rate, α_s is the saturable absorption or modulation depth, I is the input intensity, I_{sat} is the saturation intensity, and α_{ns} is the non-saturable absorption. As given in Figure 4.3 the Lu₂O₃ film SA has saturable absorption of 10%, saturation intensity of 100 MW/cm² and non-saturable loss of 58%, respectively. In comparison with certain 2D materials (B. Chen et al., 2015); MoS₂ (2.15%), MoSe₂ (6.73%), WS₂ (2.53%) and WSe₂ (3.02%), the obtained modulation depth of Lu₂O₃ film SA (10%) is relatively higher.

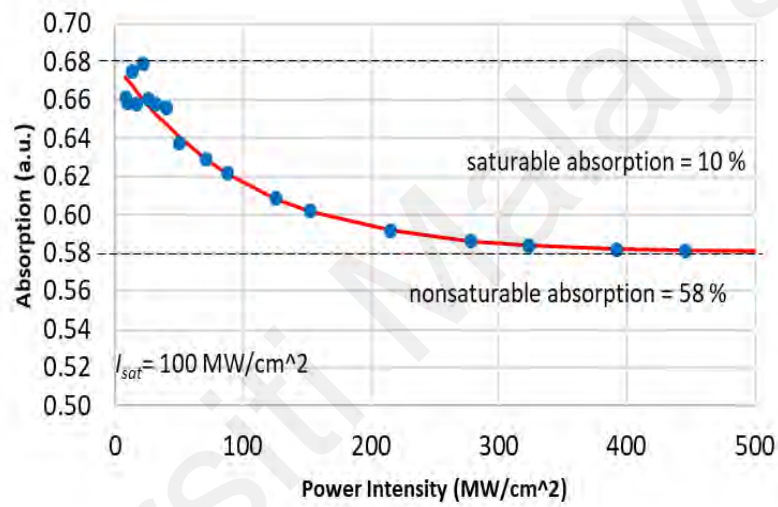


Figure 4.3: The nonlinear absorption profile of the Lu₂O₃ film SA.

4.3 Q-switched EDFL with Lu₂O₃

The proposed Lu₂O₃ based Q-switched EDFL configuration, in a forward-pumped ring cavity scheme, is illustrated in Figure 4.4. The laser cavity consists of 2.8 m long erbium-doped fiber (EDF) gain medium, a wavelength division multiplexer (WDM), an isolator and a 3dB coupler. The components are all connected via standard SMF. The EDF has a core diameter of 4 μm, a fiber diameter of 125 μm, an absorption coefficient in the range of 23-27 dBm at an operating wavelength of 980 nm and a numerical aperture (NA) of 0.23. It is pumped by a 980 nm single wavelength laser diode (LD) via the 980 nm port

of the 980/1550 nm wavelength division multiplexer (WDM). The other end of the gain medium is connected to the optical isolator which ensures unidirectional light propagation inside the cavity. Then the light goes into the thin-film SA that periodically switches the intracavity losses, as well as the Q-factor of the cavity. After the SA, the light passes through the 3dB coupler where 10% of the laser output is extracted while the rest (90%) is retained to circulate inside the cavity via the 1550 nm port of the WDM. An optical spectrum analyzer (OSA) with a 0.03 nm resolution is utilized to investigate the laser optical spectrum. Meanwhile, a radio frequency spectrum analyzer (RFSA) and a digital oscilloscope (OSC) that are pre-coupled with a fast photodetector (PD) are used to examine the appearance and quality of the pulsed signal in the time domain and frequency domain, respectively. An optical power meter is used to measure the output power of the pulsed laser.

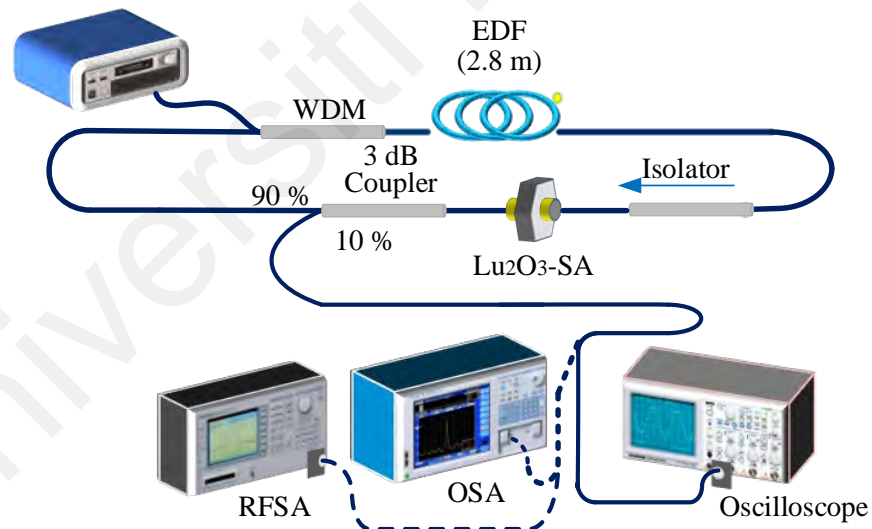
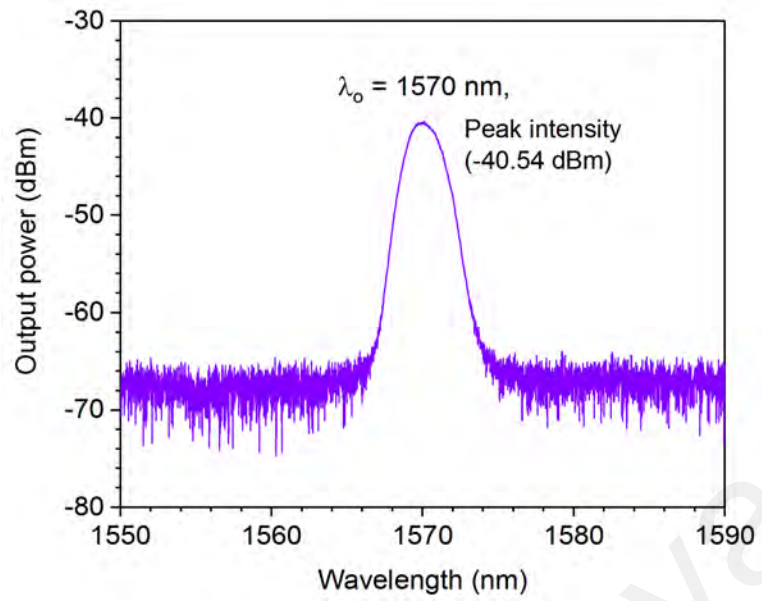


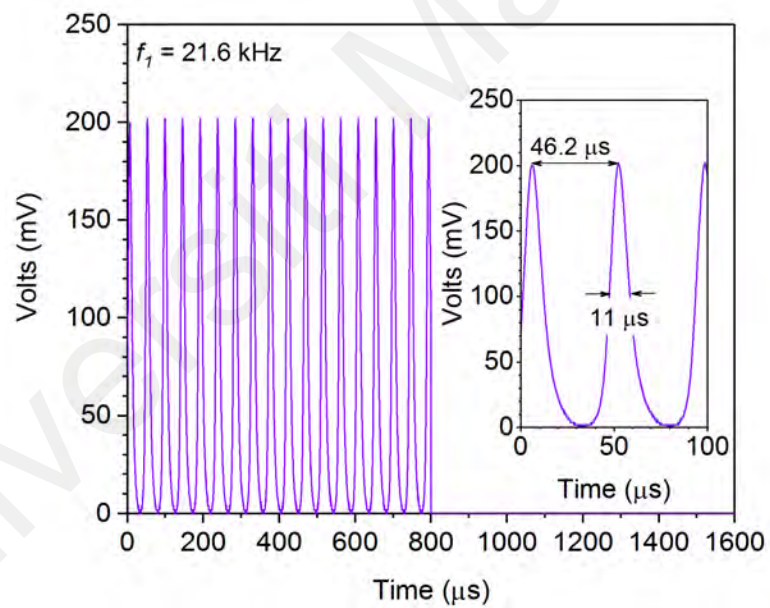
Figure 4.4: Schematic diagram of the EDFL in ring-cavity configuration.

The proposed laser started to transform into a stable Q-switched laser with an initial frequency of 18.4 kHz at a threshold pump power of 26.3 mW. The pulsed laser remains stable with the increase in pump power and its frequency rose steadily up to 30.4 kHz when the pump power reached 71.6 mW. Beyond this value, the pulsed laser started to destabilize and collapsed into a continuous wave (CW) operation. The optical spectrum of the Q-switched EDFL in Figure 4.5 (a) shows a single wavelength laser, centered at 1570 nm (λ_0) with a peak power intensity of -40.54 dBm. The optical signal-to-noise ratio (OSNR) is obtained at 33.46 dB, which is acceptable. Recently, several reports demonstrated wavelength-tunable fiber laser which particularly would benefit spectroscopy and biomedical research (Y. Chen et al., 2014; Li et al., 2016). Based on the obtained Q-switched laser spectrum, we believed that the central wavelength of the pulsed laser could be tuned within the spectral bandwidth of 1567-1573 nm. This can be achieved by employing a correct tunable wavelength filter and by providing sufficient pump power into the cavity.

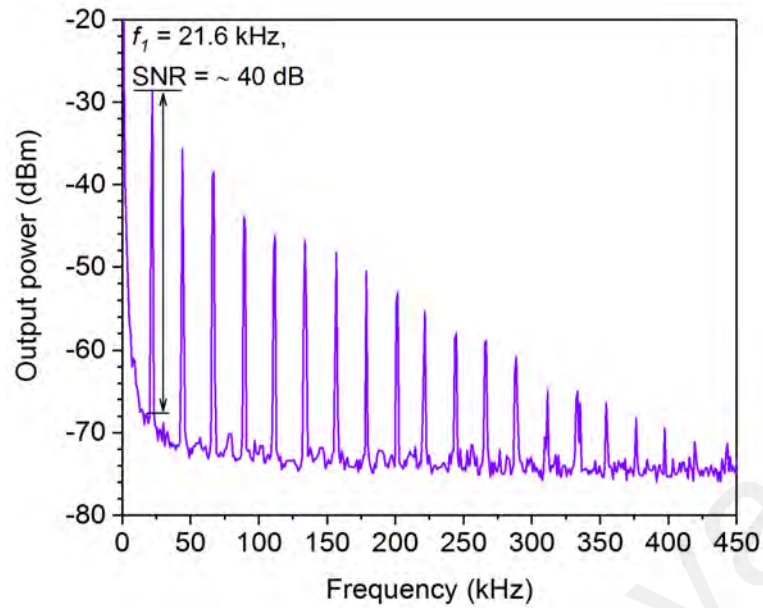
The oscilloscope trace of the pulsed laser at 38 mW pump power in Figure 4.5(b), shows nearly identical pulses with a repetition rate, f_r , of around 21.6 kHz. The inset of Figure 5(b) is an enlarged view of the pulses, indicating a peak to peak time interval that corresponds to a pulse period of 46.2 μ s. In addition to that, the pulse width taken at full wave half maximum (FWHM) is approximately 11 μ s. Meanwhile, the frequency domain of the Q-switched EDFL examined via the RFSA as depicted in Figure 4.5 (c), shows that more than ten frequency harmonics generated stably within the span of 450 kHz. As expected, the fundamental frequency (f_1) of both the time and the frequency domains are identical, thus technically confirming both optical measurements. The signal to noise ratio (SNR) of the fundamental frequency (21.6 kHz) is measured to be around 40 dB, indicating a stable Q-switching operation. In addition to that, the performances of the pulsed laser at different pump powers are demonstrated in Figure 4.6.



(a) Output spectrum at a threshold pump power of 26.3 mW.



(b) Oscilloscope trace at 38 mW pump power. Inset image shows the enlarged view of the enveloped pulses.

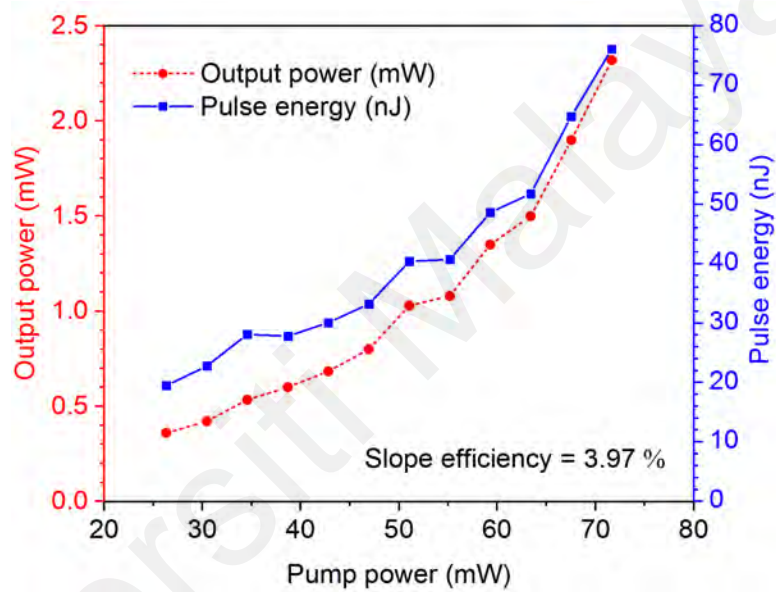


(c) RF spectrum within a 450 kHz span.

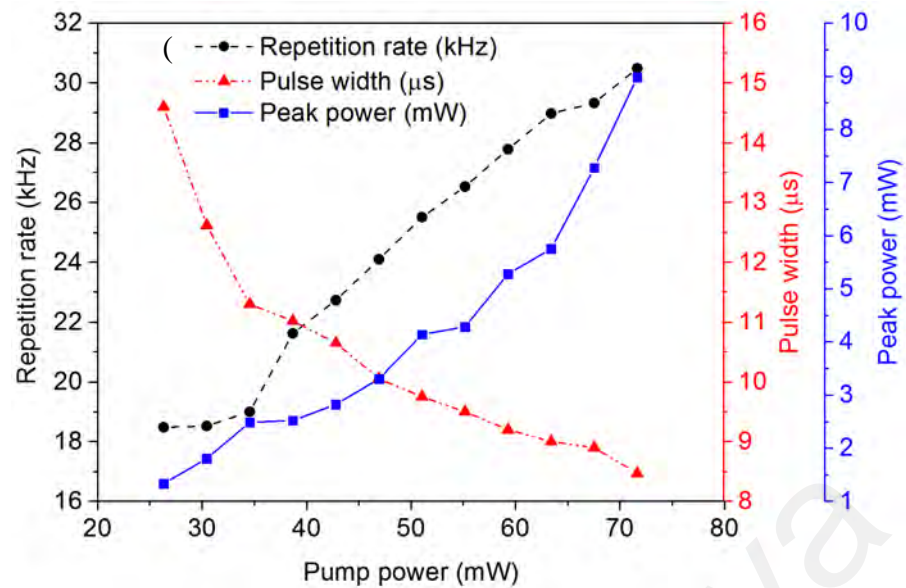
**Figure 4.5: The spectral and temporal characteristics of the Q-switched EDFL
(a) Output spectrum (b) Oscilloscope trace (c) RF spectrum**

The output power of the Q-switched EDFL is provided in Figure 4.6 (a). It increases from 0.36 mW to 2.32 mW with the rise of pump power from 26.3 mW to 71.6 mW. Meanwhile, the slope efficiency which is related to the output power response is obtained at 3.97 %, indicating an acceptable level of intra-cavity losses. The increase in pump power also increases the pulse energy from 19.4 nJ to the highest value of 76 nJ and the repetition rate from 18.4 kHz to the greatest value of 30.4 kHz as illustrated in Figure 4.6 (b). The pulse width, however, declines from 14.6 μ s to the shortest value of 8.47 μ s. In a typical Q-switched laser, by increasing the pump power, more gain is available, thus the threshold energy which is needed to saturate the SA is accomplished earlier, resulting in a higher pulse repetition rate and narrower pulse width. These changes (repetition rate and pulse width) cause the peak power to climb-up from 1.33 mW to a maximum of 8.98 mW. The experiment was then repeated without inserting the SA in the cavity, under the same condition and procedure. As expected, no pulsed laser was detected, confirming that the Q-switched laser was essentially induced by the film SA. In addition to that, the

experiment was conducted by increasing the pump power beyond its maximum available pump. No Q-switched pulse could be detected as the pump power rose beyond the maximum level of 76.1 mW. When the pump power decreased back to the Q-switched operating pump power (26.3-71.6 mW), a stable pulsed laser with almost similar Q-switching characteristics as demonstrated earlier emerged again. This phenomenon not only verified that the film SA was still in good condition but also suggested that the laser operation was conducted below the SA optical damage threshold.



(a)



(b)

Figure 4.6: Q-switched EDFL performances (a) Output power, and pulse energy responses (b) Pulse repetition rate, pulse width, and peak power responses

The long-term stability of the SA was examined by monitoring the condition of the Q-switching at a moderate pump power of 50 mW for several hours. Throughout the experiment, the Q-switched pulse remained stable without any sign of pulse destruction, indicating that the SA was still in a good condition.

4.4 Inducing Q-switching operation at 1-micron all fiber laser via Lu_2O_3 film SA

In this section, the passively Q-switched Yb-doped fiber laser (YDFL) based on Lu_2O_3 film SA is demonstrated. Figure 4.7 illustrates the all-fiber YDFL cavity in ring configuration. The 1.5 m long ytterbium-doped fiber (YDF) was used as a gain medium. The 980 nm laser diode pumped into the 4 μm core diameter of YDF via 980/1060 WDM. The YDF used is a single-clad fiber with a peak core absorption of 1200 dB/m at 976 nm wavelength. The insensitive polarization isolator was used to suppress back-scattering in laser cavity by allowing unidirectional light propagation. Q-switching operation laser can

only be generated when Lu_2O_3 film is inside the laser cavity. The fabricated Lu_2O_3 film was cut into a small piece of 1 mm x 1 mm. Then, it was sandwiched in between two fiber ferrules with index matching gel use to adhere the film onto fiber ferrule tip. The Q-switched laser performance then was tapped from 10 % of coupler port. Another 90 % of coupler port was used as a feedback to WDM. Finally, complete construction of ring configuration was attained to generate Q-switched YDFL.

To observe the Q-switched YDFL performance, we measured the laser output spectrum by using OSA with 0.05 nm resolution and output power by using a power meter. For temporal performance, the measured photon was converted into electrical signal by using 2 GHz photodetector (PD). Then, PD was connected to 350 MHz digital oscilloscope for time-domain analysis, and 7.8 GHz RF spectrum analyser (RFSA) for frequency-domain analysis. This PD has a rise and fall time of 150 ps.

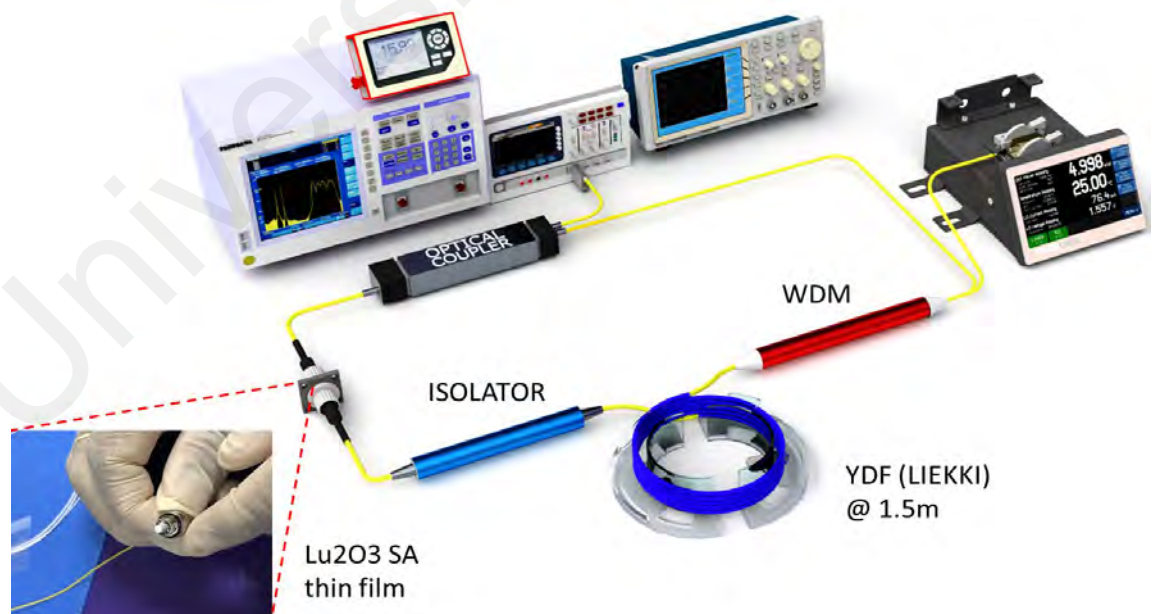
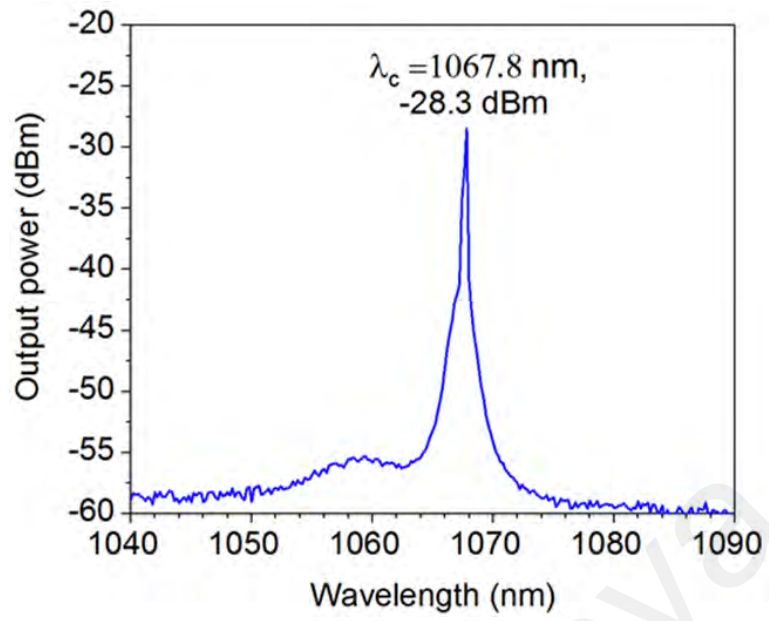


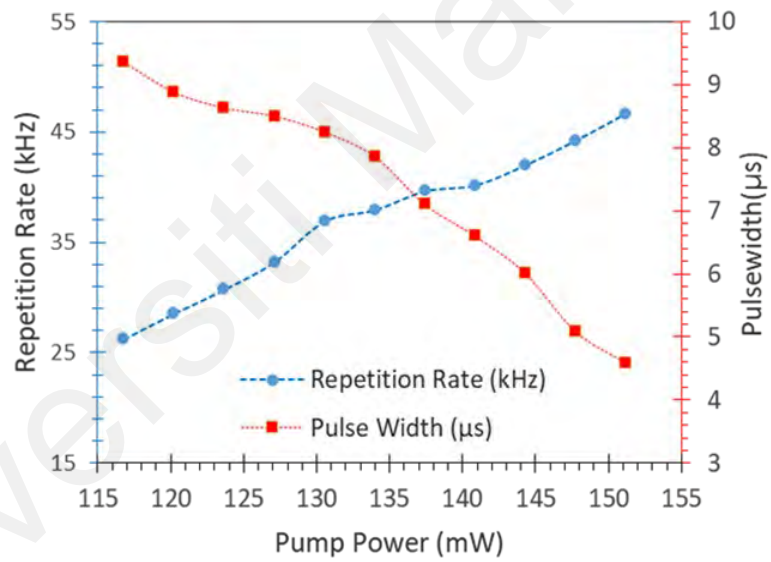
Figure 4.7: Schematic diagram of the proposed Q-switched YDFL cavity.

Figure 4.8 shows the spectral and temporal performances Q-switched YDFL using Lu_2O_3 film as SA. The output spectrum of Q-switched YDFL in Figure 4.8 (a) has a peak wavelength of -28.3 dBm at 1067.8 nm. It also shows the 3-dB spectral bandwidth is not too narrow, indicates the pulse width is short. The self-started Q-switching operation occurs at 116 mW pump power. The typical Q-switching operation stable until 151 mW pump power. Further increase the pump may eliminates the Q-switching operation. Figure 4.8 (b) shows the repetition rate and pulse width from 116 mW to 151 mW pump power. The typical repetition rate and pulse width pattern was plotted according to pump power. The repetition rate rises from 26.25 kHz to 46.68 kHz, while pulse width drops from 9.36 μs to 4.59 μs .

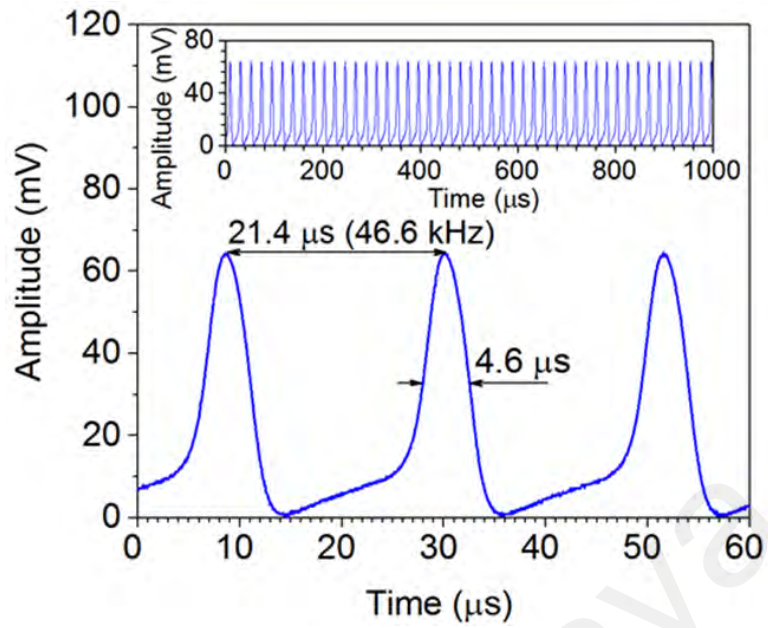
For temporal characteristics, oscilloscope train shows analysis of Q-switching operation in time-domain. Figure 4.8 (c) shows oscilloscope train of Q-switched YDFL at 151 mW pump power. It shows the separation between two adjacent pulse is 21.4 μs , corresponding to 46.6 kHz repetition rate. Each of single-pulse envelope has a full-wave half maximum (FWHM) of 4.6 μs . Insert image in Figure 4.8 (c) shows the stable oscilloscope train recorded from 0 s to 1000 μs . To confirm pulsing stability, the output laser was measured by using RFSA. The resolution used for RFSA is 3 kHz for both resolution bandwidth (RBW) and video bandwidth (VBW). Figure 4.8 (d) shows the RF spectrum consist of 9 harmonics within 450 kHz span. The fundamental frequency obtainable at 46.6 kHz, corresponding to pulse period of 21.4 μs in oscilloscope train. It has a signal-to-noise ratio of 42 dB. As we remove the Lu_2O_3 film from YDFL cavity, the laser only produces continues-wave operation.



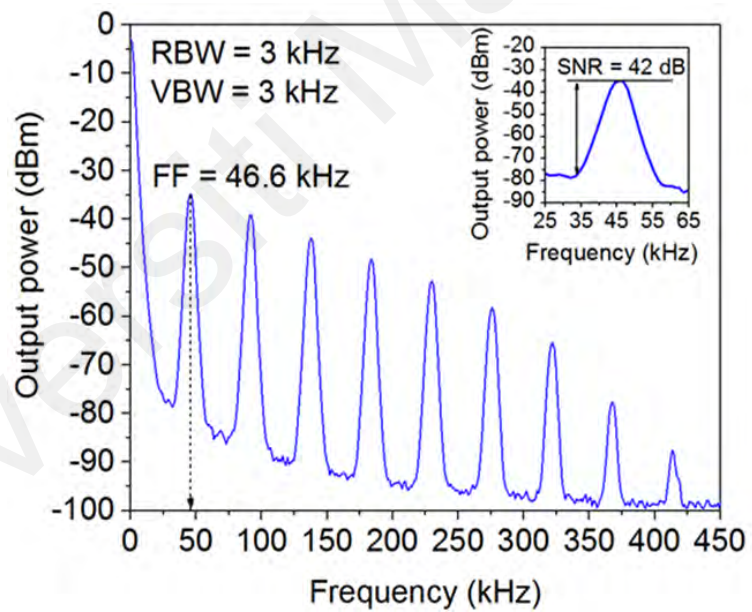
(a)



(b)



(c)



(d)

Figure 4.8: The spectral and temporal performances of the Q-switched YDFL
(a) Output spectrum. (b) Repetition rate and pulse width (c) Oscilloscope train. (d)
RF spectrum.

Figure 4.9 depicts the output power and pulse energy under Q-switching operation with operated pump power is from 116 mW to 151 mW. As shown in the figure, the output power increase linearly from 2.2 mW to 6.0 mW with a slope efficiency of 5.52 %. This indicates our YDFL cavity has a low intra-cavity loss. From output power and repetition rate, the pulse energy for every single-pulse envelope has relatively obtained from 85 nJ to 128 nJ.

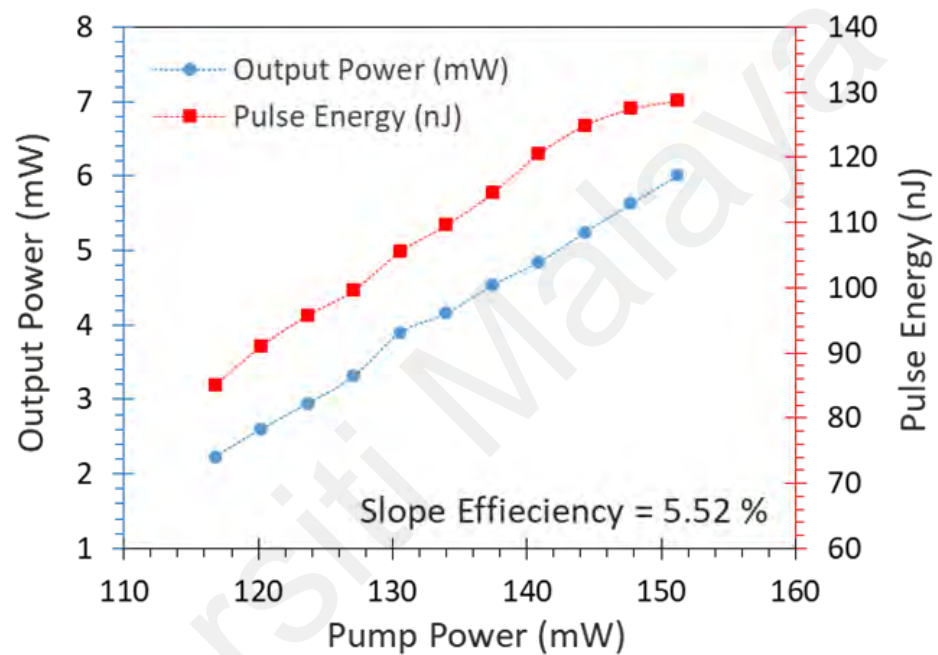


Figure 4.9: Output power and pulse energy

4.5 Inducing mode-locking operation with Lu_2O_3

The mode locked EDFL experimental configuration is illustrated in Figure 4.10. It employed the similar gain medium (2.8 m EDF, IsoGain I-25(980/125)) with the previous Q-switched EDFL setup. The EDF is optically pumped by a single wavelength 980 nm laser diode (LD) through a 980/1550 nm wavelength division multiplexer (WDM). The light is then channeled into an isolator and the Lu_2O_3 film SA. The isolator preserves unidirectional light propagation within the cavity, whereas the film SA promotes the necessary loss modulation. The integration of the Lu_2O_3 film SA into the cavity is done

by sandwiching the pre-cut film SA (1 mm x 1 mm) between two FC/PC fibre ferrules. The joining was then closely fitted with a clean fibre adapter. A small quantity of index matching gel was pre-applied onto the surface of the fibre ferrule where the film SA to be located. The application of the gel would minimize the unwanted parasitic reflections. After transmitting out from the SA, the light is then directed into a 90/10 optical coupler, where 10% of the laser output is channelled out into a 3dB coupler. The 3dB coupler further divides the laser output into 50:50 separations, enabling simultaneous data collections. In the meantime, 90% of the laser output (from the 90/10 coupler) is propagated through 200 m single mode fibre (SMF28). The laser is then directed into the WDM through the 1550 nm port for a complete closed-loop light propagation. The additional length of SMF28 is used to assist the Lu_2O_3 film SA for a stable self-starting mode-locked laser generation by providing sufficient dispersion and nonlinearity in the cavity. As in the mode-locked operation, both of these two parameters; dispersion and nonlinearity need to be well balanced. Furthermore, it would also enhance the pulse energy by slightly broadening the pulse width. This enhanced pulse energy would be sufficient enough to saturate the Lu_2O_3 film SA at a moderate pump power.

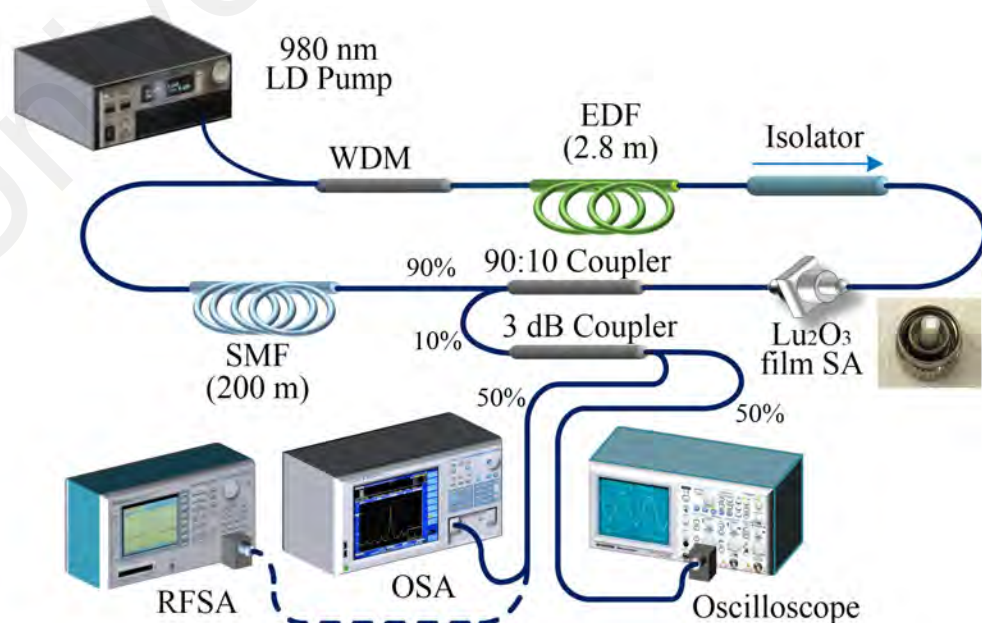


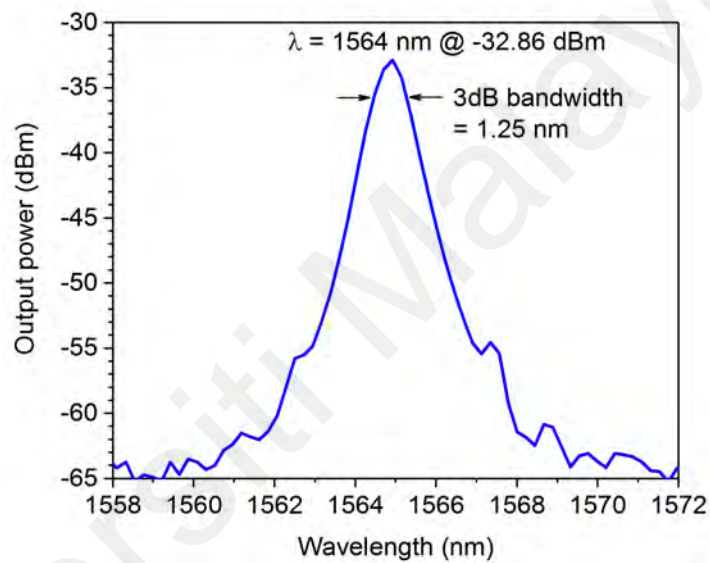
Figure 4.10: The proposed EDFL mode-locked experimental setup.

The EDFL cavity was observed to operate in the anomalous dispersion regime with a group velocity dispersion (GVD) of $\sim 21.9 \text{ ps}^2/\text{km}$. The total net dispersion was calculated to be approximately $\sim -4.464 \text{ ps}^2/\text{km}$. An OSA with a 0.07 nm resolution was utilized to investigate the laser optical spectrum. Meanwhile, a radio frequency spectrum analyzer (RFSA) and a digital oscilloscope (OSC) that pre-coupled with a fast photodetector (PD) was used to examine the presence and quality of the pulsed signal in the time domain and frequency domain, respectively. An optical power meter was also used to measure the laser output power.

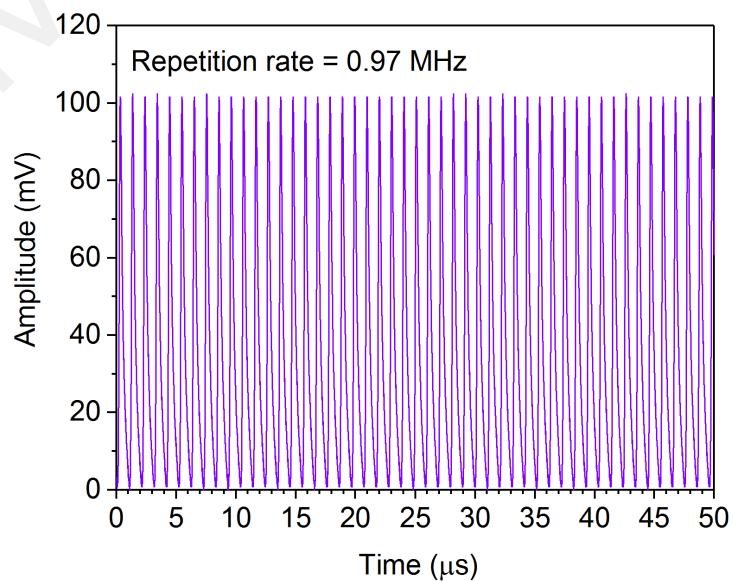
A stable self-starting mode-locking operation was observed, emerging at a threshold pump power of 145 mW. The mode-locked laser remained stable as the pump power rose to 187 mW. In the mode-locking process, Lu_2O_3 SA is utilized to obtain self-amplitude modulation (SAM) in the cavity. The film SA creates some loss inside the cavity, which is relatively large for low intensity, however, fairly small for a short pulse with high intensity. Hence, a short pulse creates a loss modulation due to high intensity at the pulse's peak saturates the absorber strongly than its low intensity wing (U. Keller, 2003).

Figure 4.11 shows the mode locked EDFL important characteristics examined at the threshold pump power of 145 mW. Figure 4.11 (a) illustrates the optical spectrum of the mode locked EDFL. The laser has a central wavelength of 1564 nm and a peak power intensity of -32.86 dBm. The 3dB spectral bandwidth is approximately 1.25 nm. The total net cavity dispersion is calculated as -4.34 ps^2 . The mode-locked pulses train as depicted in Figure 4.11 (b), has a nearly constant repetition rate of 0.97 MHz and has a considerably small amplitude fluctuation (below than 5%). The obtained repetition rate was examined, to be related with the overall EDFL cavity length of 206.18 m, indicating that the pulsed laser was a mode-locked laser. The autocorrelator trace of the mode locked EDFL along with the sech^2 fitting is illustrated in Figure 4.11 (c). The pulse width after deconvolution is 2.12 ps. Based on the obtained 1.25 nm (153 GHz) spectral

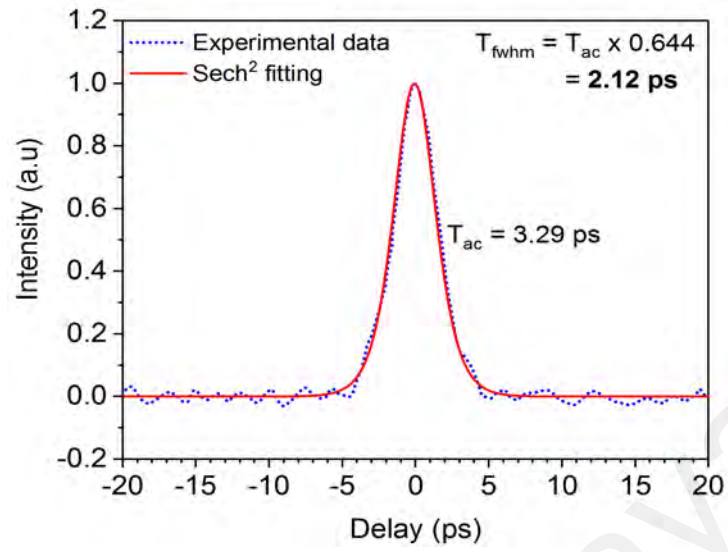
bandwidth, the time-bandwidth product (TBP) is calculated as 0.325. The transform limit derived from the obtained bandwidth is around 2.05 ps, which suggests that the output pulses are slightly chirped. Figure 4.11 (d) depicts the radio frequency (RF) spectrum of the mode-locked laser in the span of 50 MHz and taken at resolution bandwidth (RBW) of 3 kHz. The presence of many harmonics within the span, confirms that the generated pulse is considerably narrow. As shown in the inset of Figure 4.11 (d), the signal to noise ratio (SNR) is around 61 dB, which affirms the stability of the mode-locked pulses.



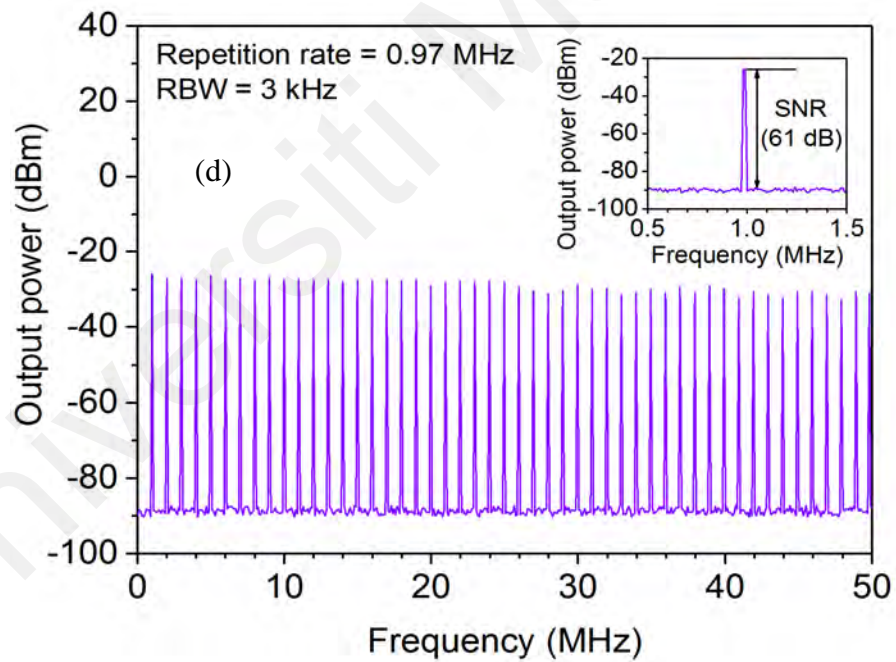
(a)



(b)



(c)



(d)

Figure 4.11: Mode-locked EDFL via Lu₂O₃ film SA important characteristics at 145 pump power (a) Output spectrum (b) Oscilloscope trace (c) Autocorrelator trace (d) RF spectrum, while the inset shows the fundamental frequency in detail.

Figure 4.12 shows the mode locked EDFL performances. The output power increases almost linearly from 3.88 mW to the maximum of 7.42 mW, as the pump power increased from 145 mW to 187 mW. The corresponding slope efficiency is obtained as 8.65%. The increase of the pump power causes the pulse energy and peak power to rise accordingly, to reach the maximum value of 7.64 nJ and 3.61 kW, respectively. The mode-locked operation was examined for 1 hr duration at room temperature. Observation of the laser output showed no significant fluctuations in the optical spectrum and pulse amplitude, thus validating the long stability of the designed system. This also suggests that the SA was still in good condition, indicating that the SA has higher thermal damage threshold than the laser output.

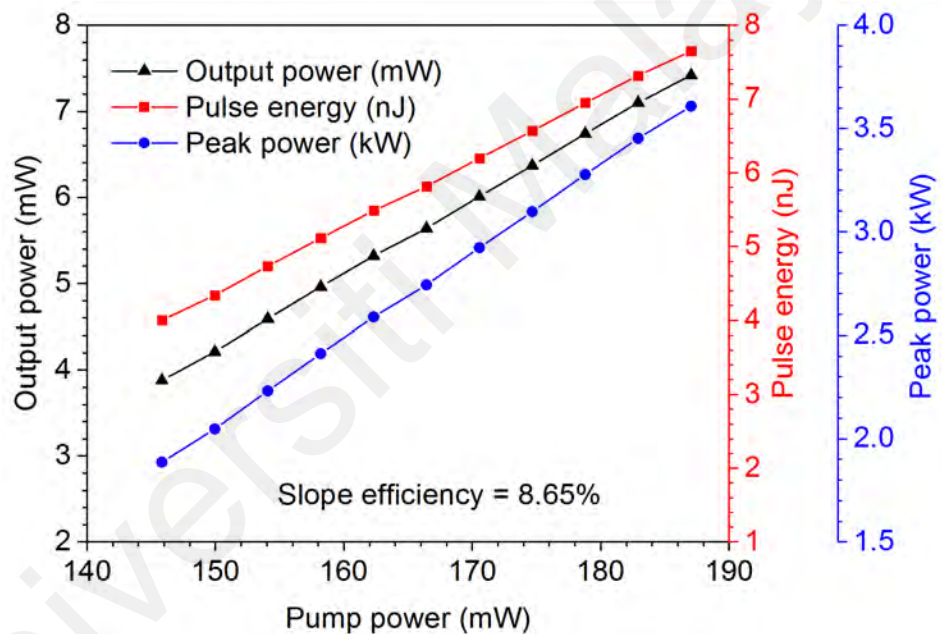


Figure 4.12: The output power, pulse energy and peak power of the mode-locked EDFL as a function of pump power (145-187 mW).

4.6 Summary

Stable and reliable Q-switched and mode-locked fiber lasers were successfully demonstrated by integrating a Lu_2O_3 thin film SA (with a thickness of around 30 μm). At first, a Q-switched EDFL was demonstrated. It was stably operating at 1570 nm, within a frequency range of 18.4-30.4 kHz, for a pump power of 26.3 mW - 71.6 mW. At the maximum pump power, the highest output power and pulse energy of 2.32 mW and 76 nJ were attained respectively. Additionally, the maximum peak power of 8.98 mW, the shortest pulse width of 8.47 μs and the highest pulse frequency of 30.4 kHz were observed at the pump power of 71.6 mW. A compact Q-switched YDFL was also successfully reported by integrating a thin film Lu_2O_3 SA. The proposed YDFL has a centre wavelength at 1067.8 nm. The pulsed laser preserved stably within a tunable frequency range of 26 to 46 kHz throughout an input pump power range of 116 to 151 mW. The maximum peak power and the highest pulse energy recorded as 28 mW and 128 nJ, respectively. Besides, the shortest pulse width assessed as 4.6 μs . The optical signal to noise ratio (OSNR) of ~42 dB. Finally, a stable and reliable mode-locked EDFL has been demonstrated by integrating Lu_2O_3 thin film SA in the extended EDFL cavity. The pulsed laser has a repetition rate of 0.97 MHz and stably operated at 1564 nm wavelength within a pump power range of 145-187 mW. The highest attainable output power, pulse energy and peak power were 7.42 mW, 7.64 nJ and 3.61 kW, respectively, and were achieved at the maximum pump power of 187 mW. Additionally, the pulse width was 2.12 ps, while the RF signal possessed a considerably high signal to noise ratio of 61 dB. Lu_2O_3 SAs thin film with all-fiber connections offered a robust, reliable, compact and highly thermal damage threshold pulsed laser in research, medical, military, and industrial applications.

CHAPTER 5: MICROSECOND AND FEMTOSECOND PULSE GENERATION WITH NICKEL OXIDE SATURABLE ABSORBER

5.1 Introduction

Up to date, many SAs have been explored for Q-switched and mode locked pulse generation including semiconductor saturable absorber mirror (SESAM) (Okhotnikov et al., 2004), carbon nanotubes (Ahmed et al., 2015), graphene (Fu et al., 2014), topological insulator (N. Xu et al., 2018), transition metal di-chalcogenide (TMDs) (B. Chen et al., 2015) and black phosphorus (BP) (Ismail et al., 2016). These materials were reported to have ultrafast recovery time, and excellent saturable absorption characteristics, which are important for Q-switching and mode-locking. However, there are also some optical restrictions for these materials, and the investigation for new SA candidates with better performance is still a very attractive topic for the researchers. Lately, the interest on new kind of metal nanoparticles materials such as gold, silver nanoparticles, titanium dioxide and cobalt oxide are also increasing for Q-switched and mode-locked fiber lasers (Al-Masoodi et al., 2018; Lokman et al., 2018; Reddy et al., 2018; Rosol et al., 2020). These types of SAs gained attraction due to their unique properties such as proper modulation depth, low saturation intensity and fast response time.

However, there are not many reports on Nickel oxide (NiO), which has an appropriate modulation depth and low saturation intensity as a SA. Band-gap energy of NiO is reported to be within a range from 3.6 to 4.0 eV, which equivalent to wavelength of 309 to 344 nm (Wang et al., 2015). However, Duan et. al reported that the nanoparticle absorption can be red shifted by increasing the nanoparticle size (Duan et al., 2012). Therefore, NiO nanoparticle could be used as an SA in near infrared region. In this chapter, a new SA based on NiO nanoparticles is developed for Q-switching and mode-locking applications.

5.2 Preparation of Characterization of Nickel Oxide Film SA

SA thin film was fabricated using NiO nanoparticles, which was synthesized in the laboratory using nickel chloride hexahydrate ($\text{NiCl}_2 \cdot 6\text{H}_2\text{O}$) and sodium hydroxide (NaOH) as the main materials. The fabrication process involved two steps: synthesis of NiO nanoparticles powder and embedding the nanoparticles into polyethylene glycol (PEG) film as described in Figures 5.1 (a) and (b), respectively. At first, 1 mol/l of $\text{NiCl}_2 \cdot 6\text{H}_2\text{O}$ was dissolved in 50 ml of deionized water under constant stirring for 10 minutes. After that, a freshly prepared solution of NaOH (2 mol/l) was added dropwise to the above solution and consequently, subjected to sonication using a horn sonicator for one hour. The product was collected via centrifugation and washed several times with deionized water. Finally, the obtained sample was calcinated in an electrical furnace at 350°C for 3 hours to form a NiO nanoparticles powder.

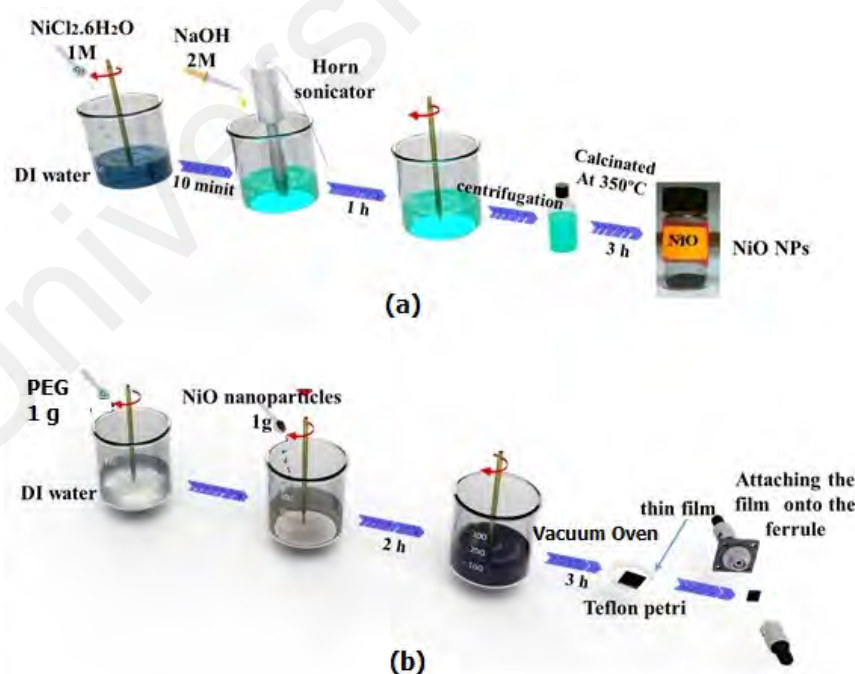


Figure 5.1: The fabrication process of NiO nanoparticles thin film (a) synthesis of NiO nanoparticles (b) Embedding the nanoparticles into the PEG film

After that, the obtained NiO nanoparticles powder was mixed with the PEG solution to fabricate the thin film as described in Figure 5.1 (b). The PEO solution was prepared earlier by dissolving 1 g of PEG in 120 ml of deionized water. Then, the mixture was stirred for 2 hours. After that, the uniformly mixed slurry was cast on Teflon petri and dried at 60 °C in a vacuum oven to fabricate the film as shown in Figure 5.2 (a). The NiO film thickness was measured to be around 40 μm. Figures 5.2 (b) shows the field emission scanning electron microcopy (FESEM) image of NiO film. It indicates that the film has a smooth morphology, which consists of a highly dense nanoparticles with size of less than 50 nm. Figure 5.2 (c) show the XRD pattern of the NiO film, which was obtained to investigate the phases as well as the crystalline orientation of the nanostructure. As shown in the figure, the pattern obviously indicates three peaks located at 37.28°, 43.28°, and 62.88°, which correspond to crystalline planes of (111), (200), and (220). The observed crystalline planes correspond to the face centered cubic structure of NiO. A small piece of the prepared film was then placed onto a fiber ferrule tip as shown in Figure 5.2 (d). It was then connected to another fresh ferrule via a fiber adaptor to fabricate the NiO based SA. Index matching gel is applied at the connection to minimize parasitic reflections.

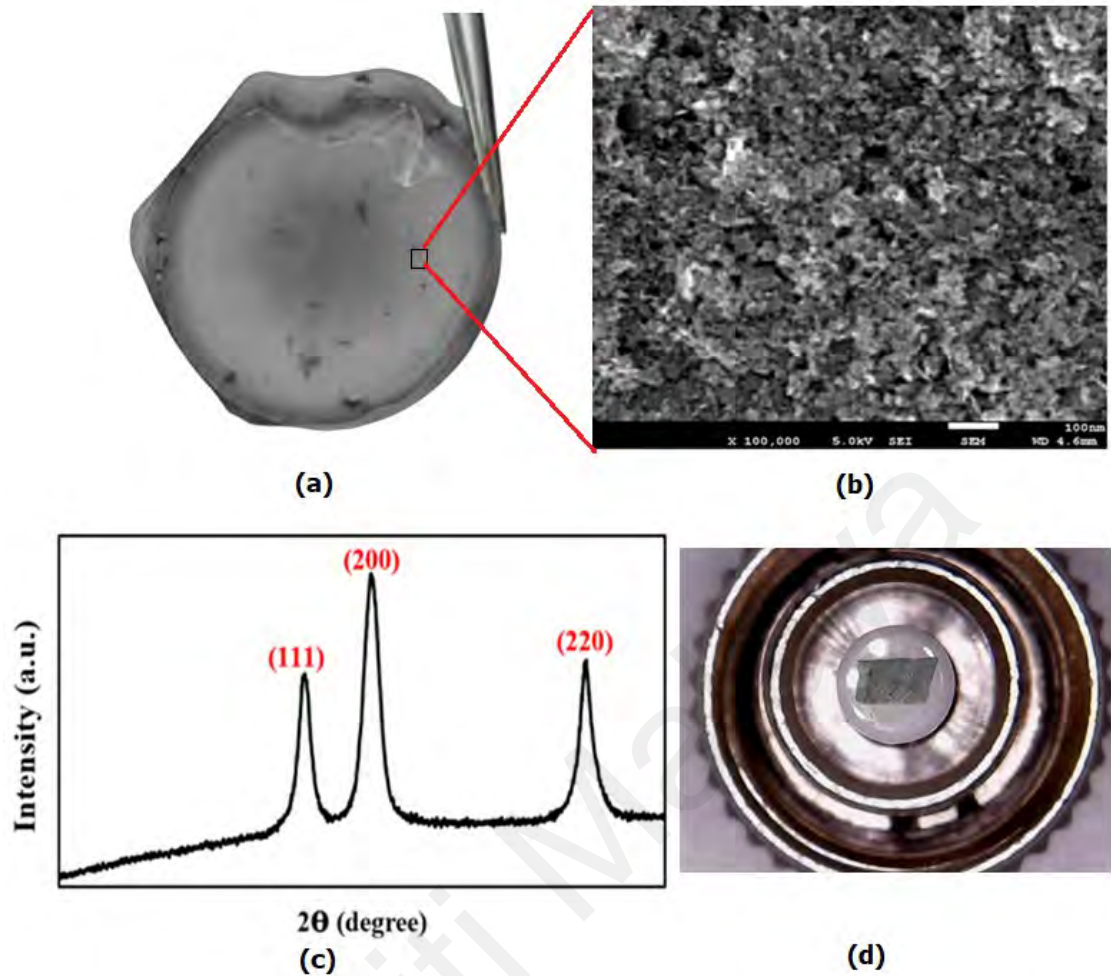


Figure 5.2: (a) Image of the fabricated NiO PEG thin film image (b) FESEM image (c) XRD pattern of the NiO nanoparticles embedded on the PEG thin film (d) The NiO film attached onto a fiber ferrule tip.

The nonlinear optical absorption of the NiO PEG thin film was also investigated. This was accomplished by employing a twin-detection technique as described in the previous chapter. Figure 5.3 shows the measured nonlinear absorption profile, which indicates that the saturation intensity of the NiO PEG film SA is 2.5 MW/cm^2 whereas its non-saturable absorption and modulation depth are 76 % and 9 %, respectively.

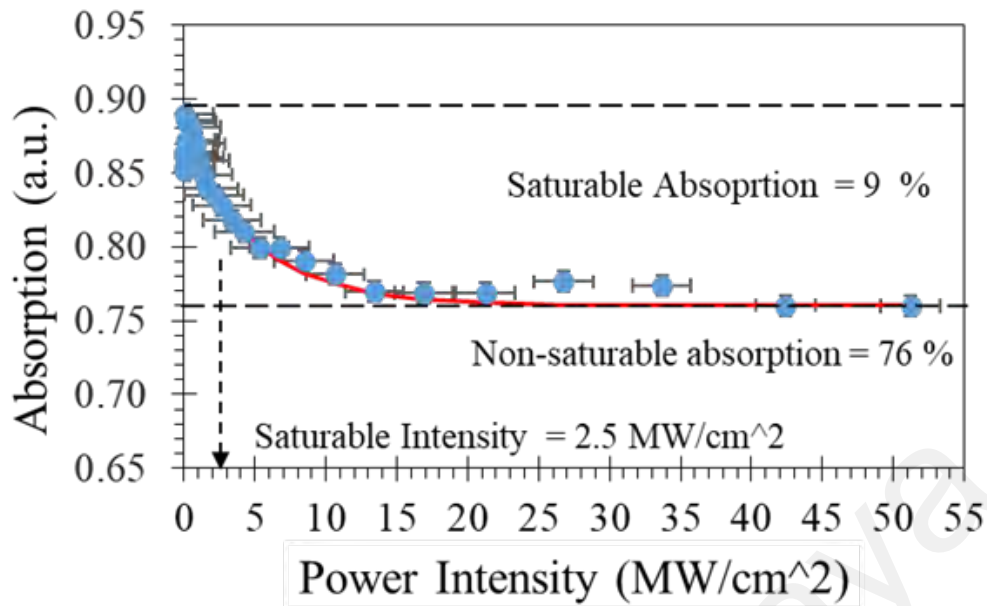


Figure 5.3: The nonlinear saturable absorption curve for the NiO PEG film

5.3 Microsecond Q-switched Pulse Generation in 1-Micron region Nickel Oxide Nanoparticles Saturable Absorber

The fabricated NiO SA device is incorporated into an YDFL cavity to produce a Q-switching pulse train operating at 1-micron region as shown in Figure 5.4. The laser ring cavity consists of a 980 nm / 1064 nm wavelength division multiplexer (WDM), a 1.5 m long Ytterbium-doped fiber (YDF), 3 dB output coupler, the constructed SA device and optical isolator. The YDF was used as a gain medium and was pumped by a 980 nm laser diode (LD) through a 980/1064 nm wavelength division multiplexer (WDM). The YDF has core and cladding diameters of 4 μm and 125 μm respectively, with numerical aperture of 0.20, as well as cut-off wavelength of 950 nm and ion absorption of 280 dB/m at 920 nm. An isolator is integrated into the optical ring cavity to ensure unidirectional operation. The YDF was connected to the 3 dB output coupler, which allows half of the oscillating laser power to be extracted for analysis. Another half of light was channelled to the SA device and kept in the cavity to oscillate for laser generation. The output laser

is analysed by an optical spectrum analyzer (OSA) with a spectral resolution of 0.02 nm, an optical power meter and a 2 GHz photodetector together with a 350 MHz oscilloscope or 7.8 GHz radio frequency (RF) spectrum analyzer.

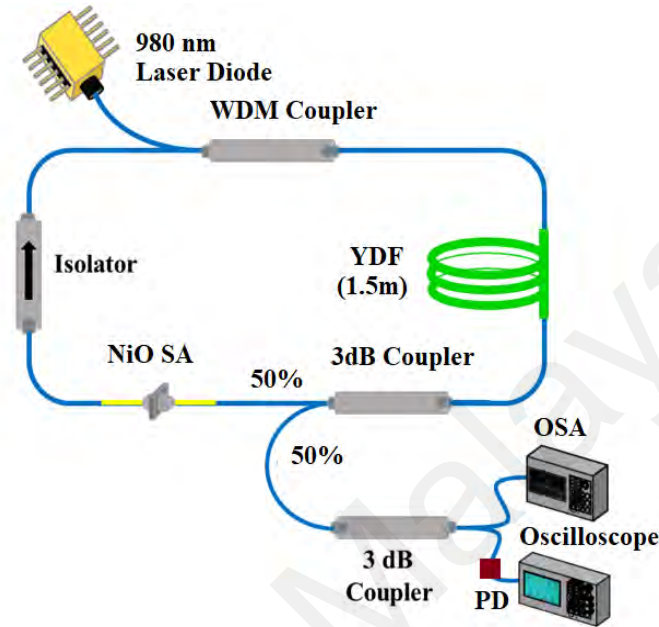


Figure 5.4: The schematic diagram of the proposed Q-switched YDFL with NiO based SA

Q-switching operation was realized as the prepared NiO PEG film was placed inside the resonant cavity while increasing the pump power above the threshold level of 89.2 mW. The Q-switching operation was maintained up to the maximum pump power of 226 mW. Figure 5.5 shows the attenuated emission spectrum of the laser at threshold pump power of 89.2 mW. As shown in the figure, the output wavelength was centred at 1064.2 nm with an FWHM of 1.3 nm. As we removed the SA from the cavity, no Q-switched pulses were observed, even when the output power reached 226 mW. It is worthy to note that the Q-switching operation was started and sustained by the saturable absorption effect of the NiO PEG film. Without the SA, the continuous wave (CW) laser was obtained, which operated at a longer wavelength of 1072 nm.

The operation wavelength of the Q-switched laser was blue-shifted when the SA was inside the cavity. The change of output wavelength was attributed to the insertion loss induced by the NiO SA.

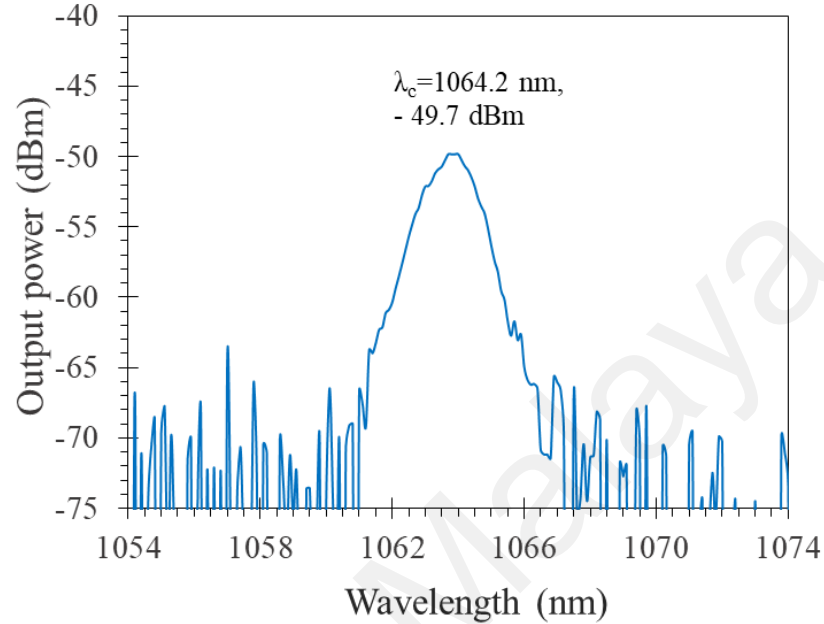
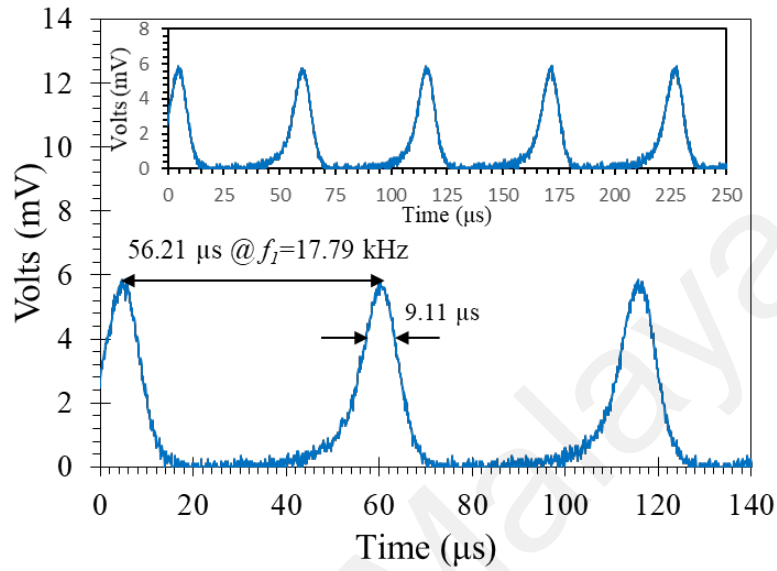


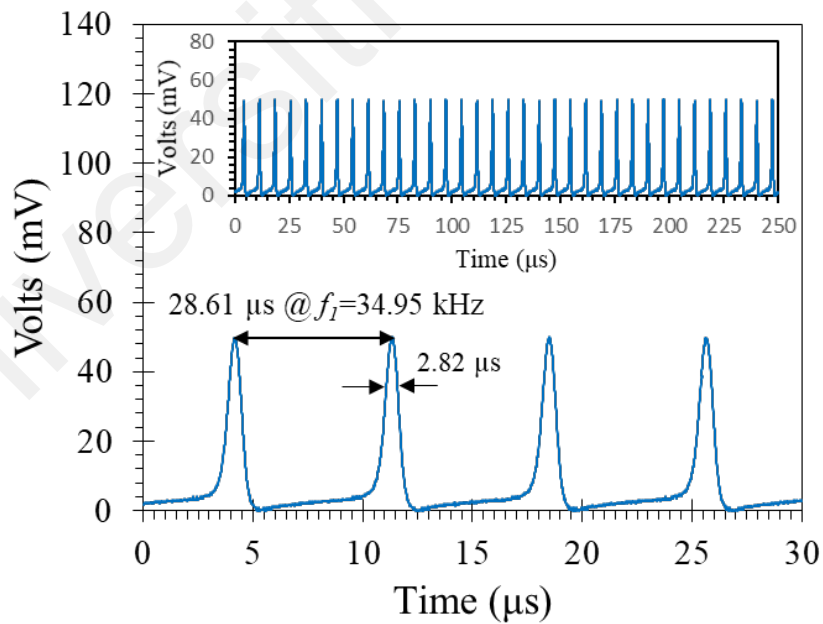
Figure 5.5: Output spectrum of the Q-switched YDFL at 89.2 mW pump power

Figures. 5.6 (a), (b) and (c) show the Q-switched pulse trains obtained at three different pump powers of 89.2, 158.7, and 226 mW, respectively. As the pump power increases, more energy can be stored in the laser cavity and this contributes to the rise in the repetition rate accompanied by the reduction in pulse duration. The pulses have the repetition rates of 17.79, 34.5, and 54.35 kHz at 89.2, 158.7, and 226 mW, respectively as shown in the figures. The corresponding pulse durations are 9.11, 2.90 and 2.27 μ s at pump power of 89.2, 158.7, and 226 mW, respectively. Besides, it can be clearly seen the pulse profile is asymmetric with a slow rise time and a fast-falling edge. The result is caused by the nonlinear absorption of NiO nanoparticles. During the initial Q-switched pulse build-up stage, the single-photon absorption of NiO dominates the interaction due to the low intra-cavity photon density, so the pulse has a slow rise time. However, two-

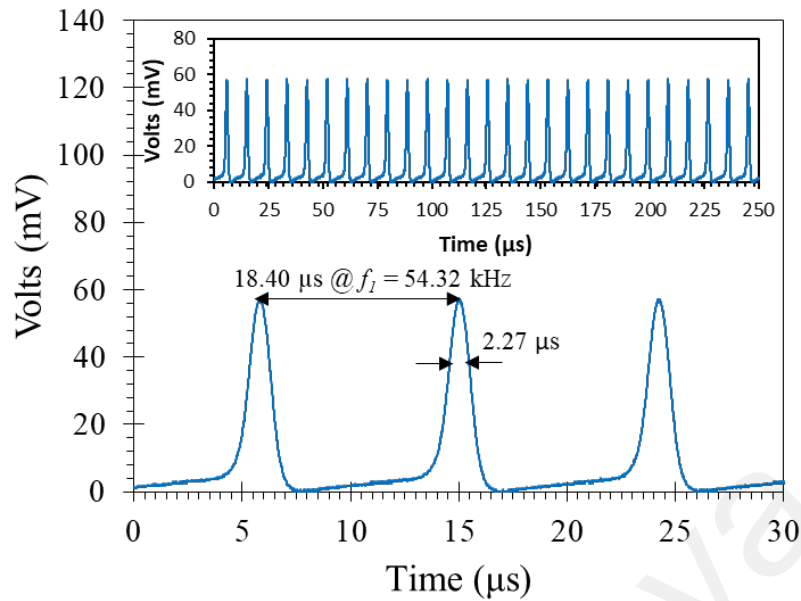
photon absorption of NiO occurs with the accumulation of photon number, which will cause the sudden decrease of transmittance. The cavity photon density reduces abruptly, leading to a fast-falling edge of the Q-switched pulse.



(a)



(b)

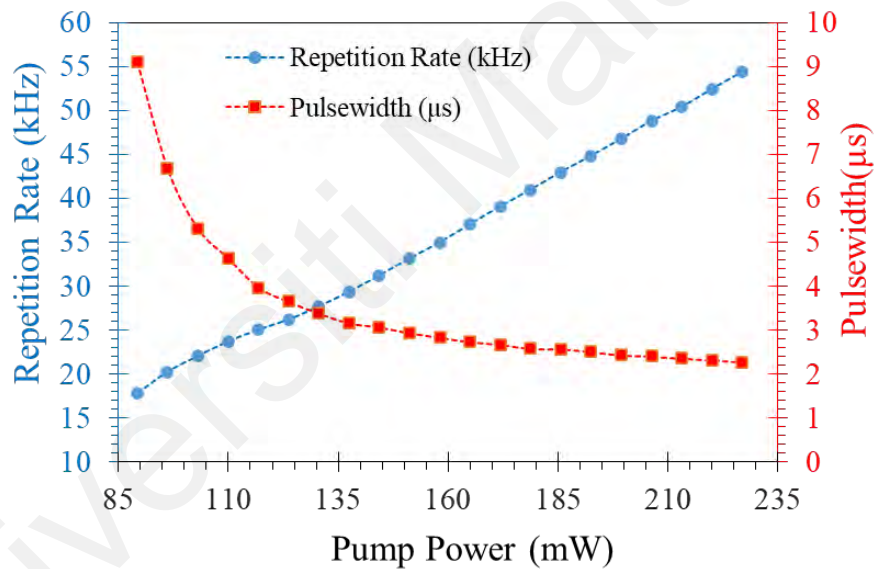


(c)

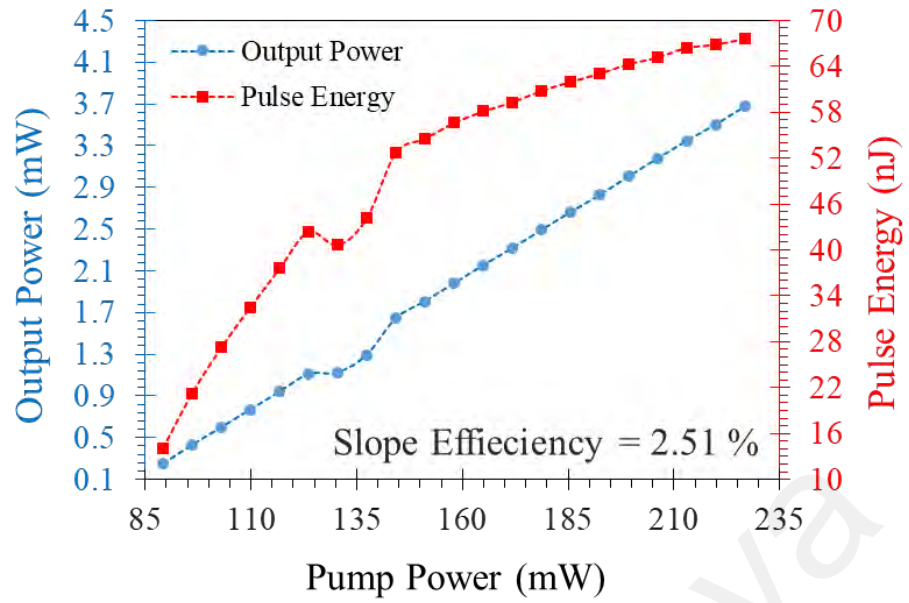
Figure 5.6: Temporal characteristics of the Q-switched YDFL at pump powers of (a) 89.2 mW (b) 158.7 mW and (c) 226 Mw

The properties of the Q-switching laser principally rely on upon the gain medium, SA property and pump power. Unlike settled repetition rate determined by cavity length of mode-locked, Q-switched laser has a variable repetition. Figure 5.7 (a) showed the pulse repetition rate and pulse width of the Q-switched laser as functions of the pump power. When pump power increased from 89.2 to 226.0 mW, the repetition rate raised from 17.79 to 54.32 kHz, while the pulse width reduced from 9.1 to 2.27 μ s. These phenomena can be explained as follows: the larger the pump power, the more the electrons accumulated on the upper energy level. So, the rise time and falling time of the pulse both become shorter. As a result, the repetition rate increased, and pulse width decreased as the pump power raised. Figure 5.7 (b) shows the obtained output power and single pulse energy against the pump power. The single pulse energy can be easily calculated from the measured output power and repetition rate. It is found that the output power almost linearly increased with the pump power with a slope efficiency of 2.51%. The average

output power increased from 0.25 to 3.68 mW as the pump power increased from the threshold pump power of 89.2 mW to the maximum pump power of 226 mW. The pulse energy also had an increasing trend with pump power and the maximum pulse energy of 69 nJ was obtained at the maximum pump power. However, the single pulse energy increment is slower at higher pump power, which may be attributed by the saturation of NiO material. The RF spectrum with 900 kHz span was measured at pump power of 226 mW as shown in Figure 5.8. The pulse repetition rate was 54.32 kHz, matching with the oscilloscope data. The RF signal-to-noise ratio (SNR) is about 41.1 dB with no spectral modulation, indicating that the Q-switching operation is stable.



(a)



(b)

Figure 5.7: The Qwitching performance of the YDFL (a) Repetition rate and pulse width (b) average pump power and single pulse energy against the pump power.

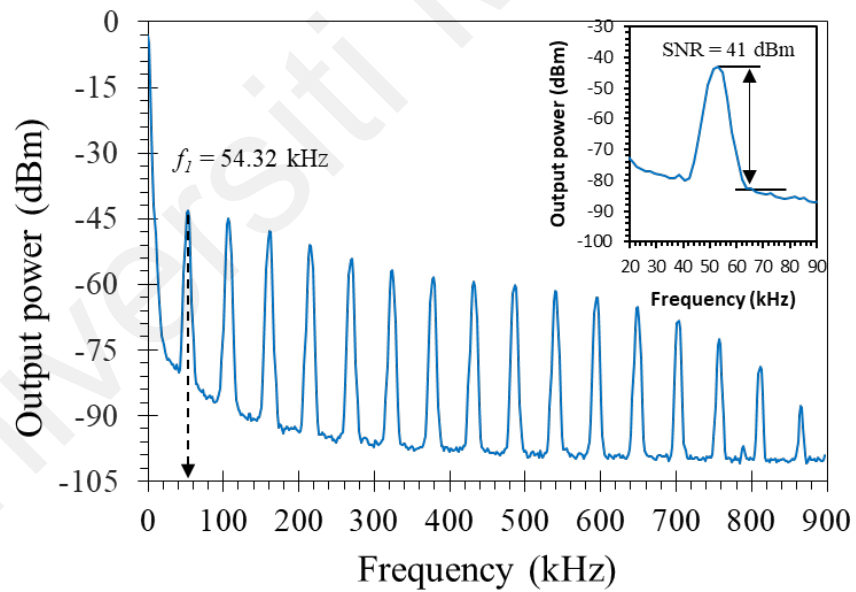
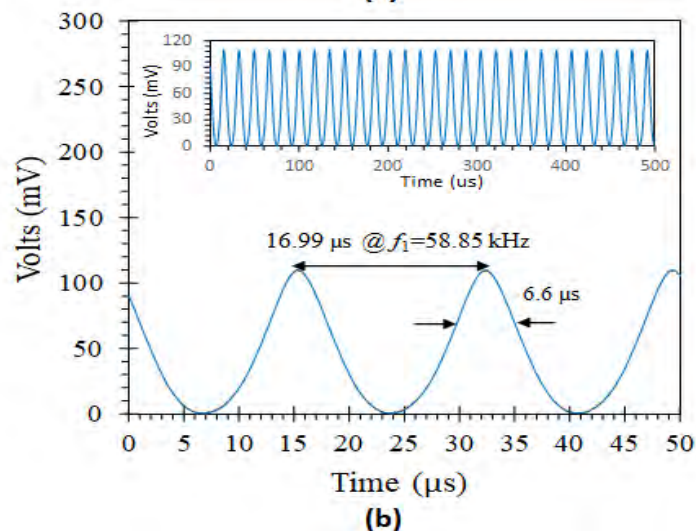
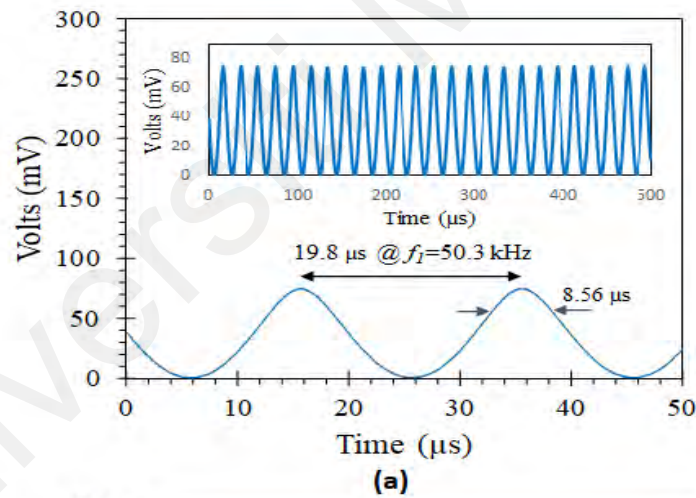


Figure 5.8: RF spectrum at 226 mW pump power

After inserting the fabricated NiO film SA into the EDFL cavity, a continuous wave (CW) laser is firstly generated at threshold pump power of 80 mW. By further increasing the pump power over 143.8 mW, self-starting Q-switched laser was obtained from the ring EDFL, generating a stable train of microsecond pulses, centered at 1570.6 nm. Typical output oscilloscope trace, at three different pump powers of 143.8 mW, 191 mW, 239.6 mW are shown in Figures 5.10 (a), (b) and (c), respectively. Pulses are generated with a spacing of 19.8 μs , 16.99 μs and 15.16 μs , corresponding to repetition rates of 50.3 kHz, 57.87 kHz and 65.96 kHz, respectively. The pulse width of 8.56 μs , 6.6 μs and 5.59 μs were obtained at pump powers of 143.8 mW, 191 mW, 239.6 mW, respectively. With the pump power rising, the repetition frequency increases, and the pulse width reduces, which is a typical phenomenon of passively Q-switched lasers.



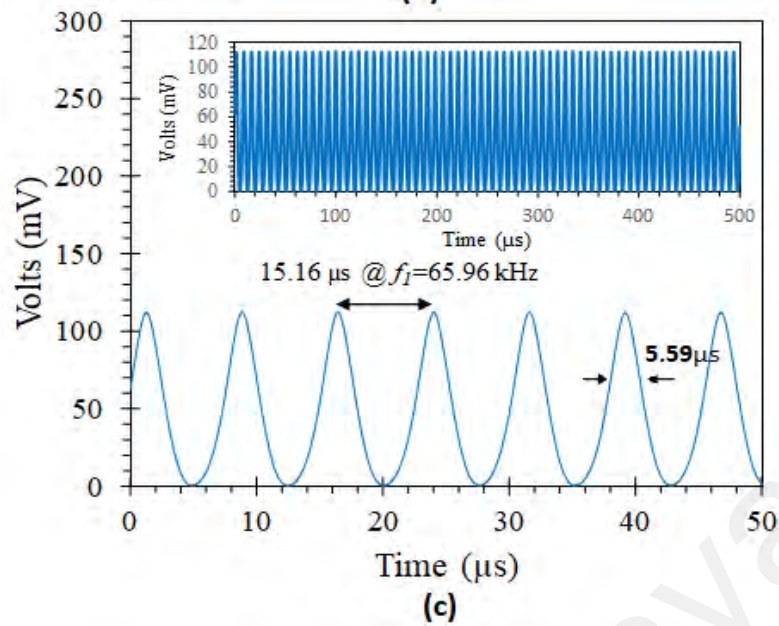


Figure 5.10: Typical output pulse train at pump powers of (a) 143.8 mW, 191 mW and (c) 239.6 mW

Typical output spectral characteristic of the laser, at 191 mW pump power, is illustrated in Figure 5.11 (a). It shows the laser spectrum centered at 1570.6 nm with the full width at half maximum (FWHM) of 1.3 nm. Relative to CW laser, the FWHM of the Q-switched laser spectrum was widened and the center wavelength was slightly red-shifted. This is attributed to an insertion loss introduced by the NiO PEG SA, which causes the adjustment of the mode competition condition of the Q-switching operation as compared to the mode competition condition of CW operation. The radio frequency (RF) spectrum of the output laser shows a high signal-to-background contrast of 73.42 dB (Figure 5.11 (b)), indicating good pulse train stability, comparable to Q-switched fiber lasers based on other materials (Al-Hayali et al., 2017; H. Chen et al., 2016). Following stable Q-switching results obtained by using the NiO SA at 1570.6 nm, the same experiment is conducted with a ~40 μm thick pure PEG film (fabrication process like that used for NiO PEG SA fabrication, but without the NiO nanoparticles). No Q-switching is

observed at any pump power level, confirming that the Q-switching pulse arises from the NiO nanoparticles.

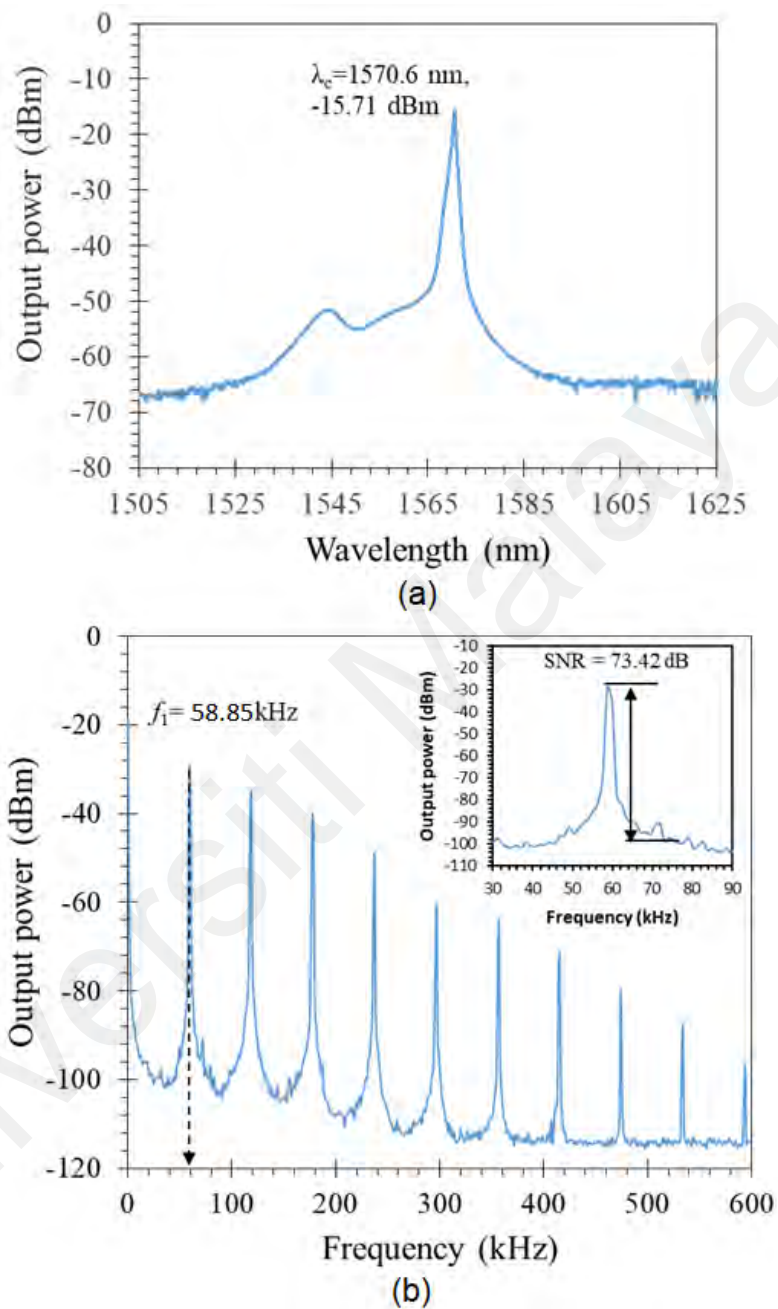
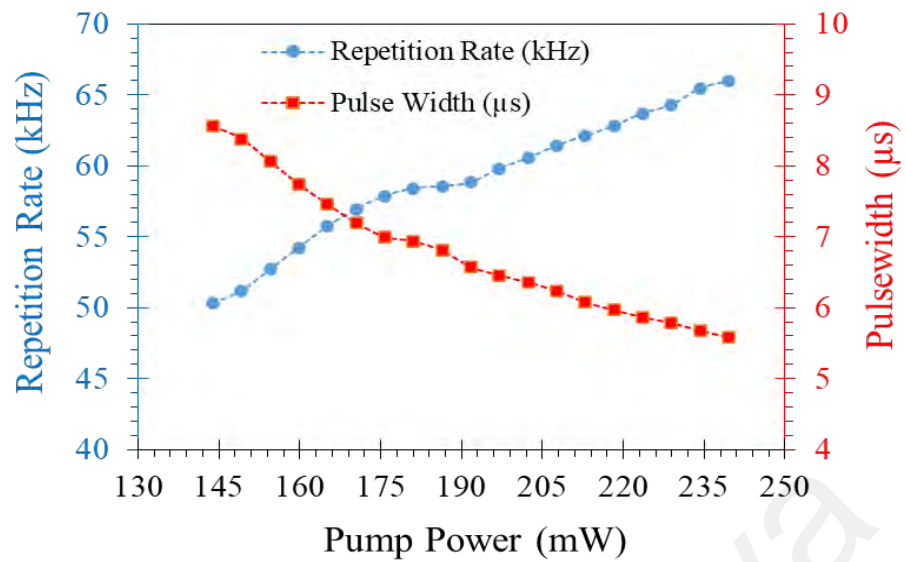


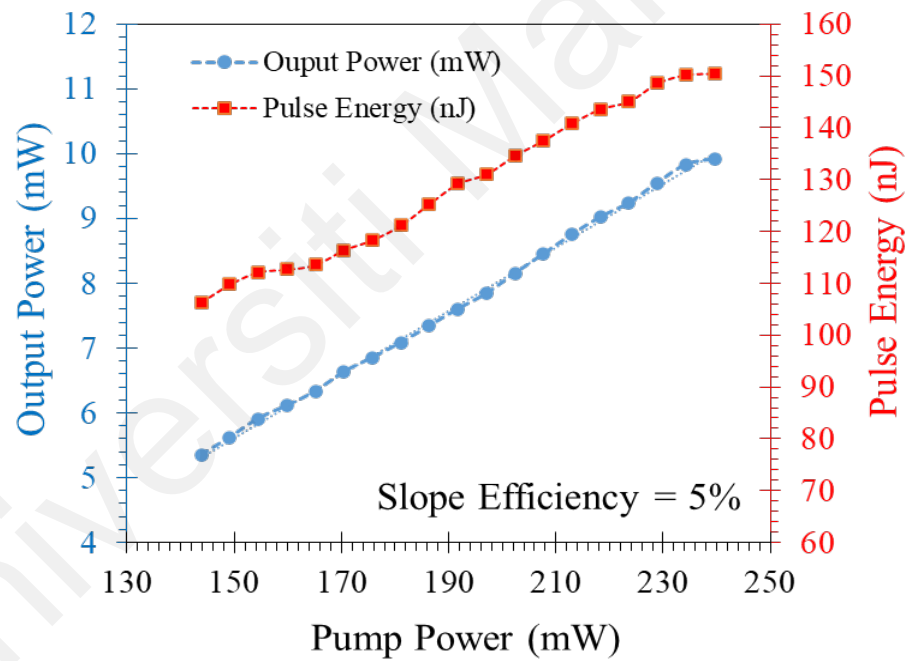
Figure 5.11: Spectral and temporal characteristics of the Q-switched EDFL (a) Measured optical spectrum (b) RF spectrum on a 600 kHz span where the fundamental frequency is 58.85 kHz. Inset of (b) indicates the RF spectrum of fundamental frequency on a 60 kHz span.

The pulse properties in a passively Q-switched laser relies on nonlinear dynamics in the gain medium and SA. This leads to a dependence of output laser repetition rate and pulse width on pump power. The repetition rate and pulse width were recorded by an oscilloscope and their relations with pump power are plotted in Figure 5.12 (a). A laser pulse is emitted once the storage energy of the cavity reaches a certain threshold. Therefore, a greater pump power enables higher repetition rates and results in shorter pulse widths. This is experimentally observed by changing the pump power from the threshold of 143.8 mW to 239.6 mW as the cavity repetition rate is rose from 50.3 kHz to 65.96 kHz and the pulse width is decreased from 8.56 μ s to 5.59 μ s (Figure 5.12 (a)). The pulse width could be further shortened by reducing the length of the laser cavity.

The Q-switched laser output power and pulse energy versus pump power are shown in Figure 5.12 (b). An average output power of 5.35 mW was achieved at threshold pump power of 143.8 mW and a maximum power of 9.92 mW was obtained at the pump power of 239.6 mW, delivering a slope efficiency of about 5 %. On the other hand, the pulse energy increased from 106.36 nJ to 150.4 nJ as the pump power was raised from 143.8 mW to 239.6 mW. We believe that higher pulse energies could be realized by further optimizing the laser cavity. It is worthy to note that we did not find any optical damage on the NiO PEG film in the laser experiment.



(a)



(b)

Figure 5.12: Q-switching performance of the NiO based EDFL (a) Variation of the repetition rate and pulse width with pump power (b) Variation of the average output power and pulse energy with pump power

5.5 Mode-locked femtosecond pulse in 1.5-micron spectral range with NiO SA

Ultrafast fiber lasers have become a mature technology, facilitating a broad range of applications, including high-capacity and high-rate wavelength division multiplexing fiber communication systems, high-precision fiber sensing technology, and high-power lasers for micromachining (U. Keller, 2003). While many schemes exist to generate ultrashort pulses in fiber lasers, SAs, an ultrafast optical switch exhibiting an intensity-dependent transmission, have been widely deployed in many systems as they enable a wide space of parameters to be accessed without the implementation of complicated and expensive external modulators. Various types of saturated absorbing materials are used for ultrafast laser generation as discussed in the previous chapters and literatures (Glubokov et al., 2014; Jin et al., 2018). In this section, a femtosecond pulse generation is demonstrated from a soliton mode locked EDFL based on a NiO SA. The NiO-based device exhibits strong nonlinear saturable absorption with an optical modulation depth of 9 % and saturation intensity of 2.5 MW/cm^2 at 1550 nm. Using the newly developed NiO PEG thin film in an extended cavity EDFL, a stable mode-locked operation was achieved at 1561.4 nm, with 710 fs pulses and 3.3 MHz repetition rate.

The mode locked EDFL was realized in an EDFL ring cavity shown in Figure 5.13. The laser resonator is almost similar with the previous Q-switched laser of Figure 5.9 except for the addition of 10 m long single mode fiber (SMF) inside the cavity to compensate the dispersion so that the cavity dispersion becomes anomalous. The laser cavity is based on ring configuration and consists of a polarization independent optical isolator, NiO SA device, 10 dB output coupler, 10 m long additional SMF section and a fiber amplifier. The fiber amplifier was constructed from a 0.5m long highly doped EDF, co-pumped by a 980 nm pump diode via a 980/1550 nm WDM. The optical isolator ensures unidirectional propagation of the oscillating laser inside the cavity and an output coupler with a splitting ratio of 10:90 was used, so that 10% of the power was used to

measure the output of the mode-locked pulses in the spectral, time and frequency domains. The total cavity length is 14 m, which consists of 13 m SMF, 0.5 m WDM fiber and 0.5 m EDF. The group velocity dispersions of the SMF, WDM and EDF are $-21.7 \text{ ps}^2/\text{km}$, $-7 \text{ ps}^2/\text{km}$ and $7.65 \text{ ps}^2/\text{km}$, respectively. The net cavity dispersion is calculated to be -0.282 ps^2 , which ensures that the laser operates in the anomalous dispersion regime. The performance of the mode locked laser was gauged using an OSA, an autocorrelator, a digital oscilloscope, and a RF spectrum analyser with a high-speed photodetector.

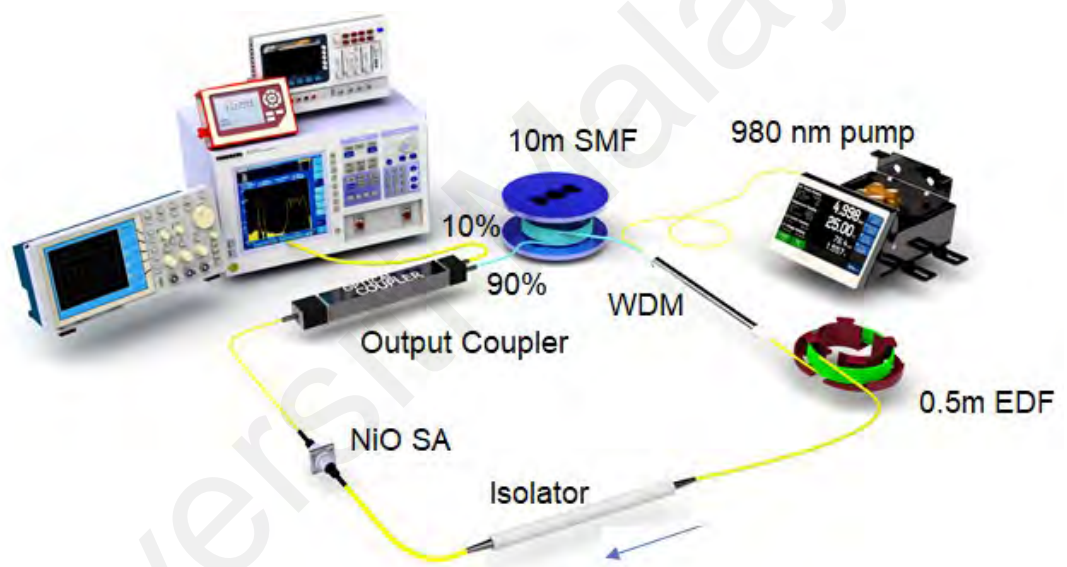
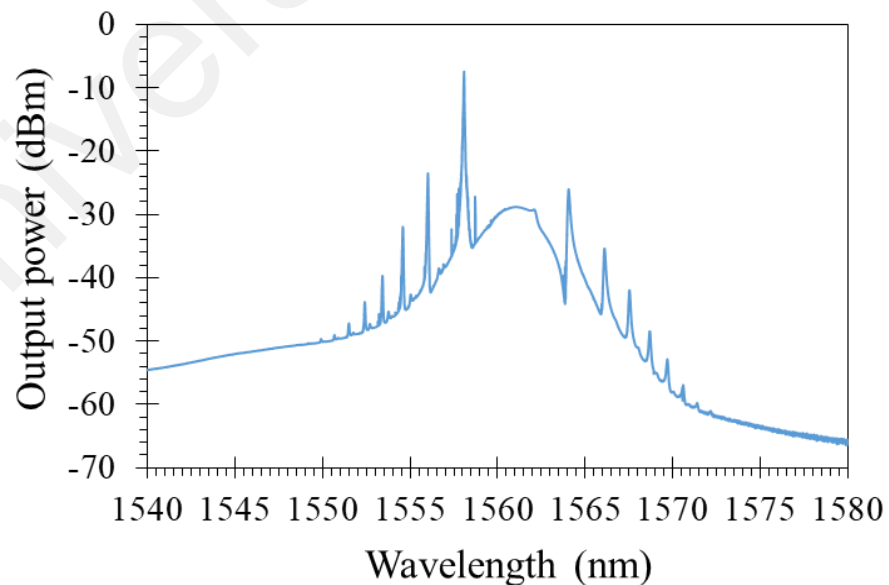


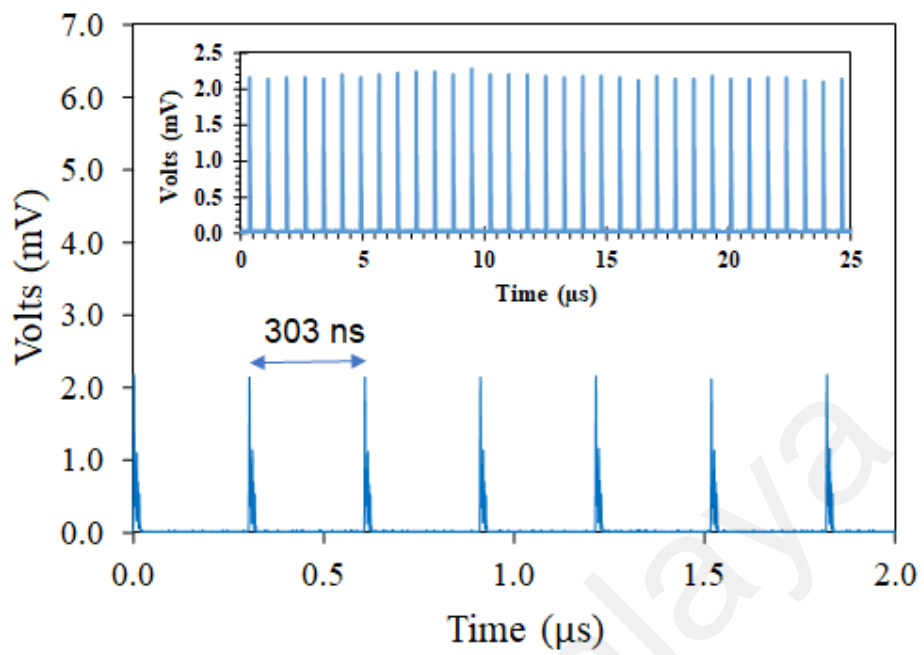
Figure 5.13: Configuration of the soliton mode-locked femtosecond EDFL

Through intracavity dispersion management, a soliton mode-locked fiber laser generates 710 fs pulses with a 3 dB spectral bandwidth of 3.7 nm. By tuning the 980 nm pump power the CW laser operation was firstly obtained at a pump power of 90 mW while the mode-locking start-up threshold was 159.8 mW. Stable pulse output was maintained as the pump power was increased up to 186.4 mW. Figure 5.14 (a) records the spectral profile of the output laser at a pump power of 186.4 mW. The center wavelength of the output spectrum is approximately 1561.4 nm with a full width at half-

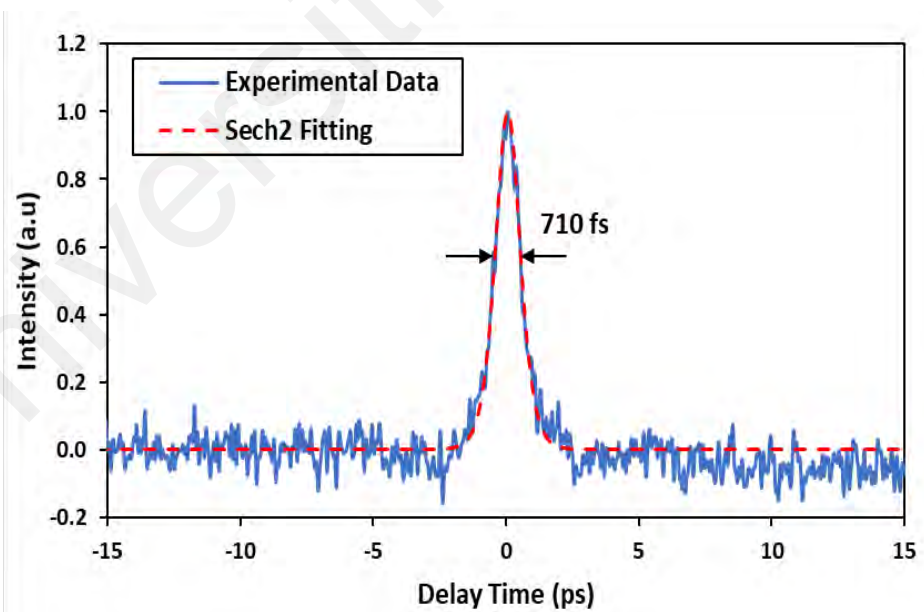
maximum (FWHM) of 3.7 nm. The spectrum exhibits Kelly sidebands, demonstrating the formation of conventional solitons. Soliton mode-locking was achieved in the anomalous dispersion regime utilizing NiO-SA. The pulse sequence diagram is shown in Figure 5.14 (b), and the pulse interval is about 303 ns, which corresponds to 3.3 MHz repetition rate. The intensity of the pulse sequence does not fluctuate, indicating that the mode-locked pulses are steady. Figure 5.14 (c) shows the measured mode-locked pulse autocorrelator trajectory. The sech^2 function is used to fit the output pulse, and the pulse width is about 710 fs from the autocorrelation trace. The time-bandwidth product (TBP) was calculated to be 0.323, which is slightly larger than that of the transform-limited pulse, indicating that the intracavity pulse has only a slight chirp. To investigate the stability of the mode-locked laser, the RF spectrum in the 100 MHz range is monitored as illustrated in Figure 5.14 (d). The fundamental frequency of the pulse is obtained at 3.3 MHz, which is consistent with the oscilloscope trace and laser cavity length. The SNR of the fundamental frequency is 72 dB, which indicates the high stability of the mode-locked pulses.



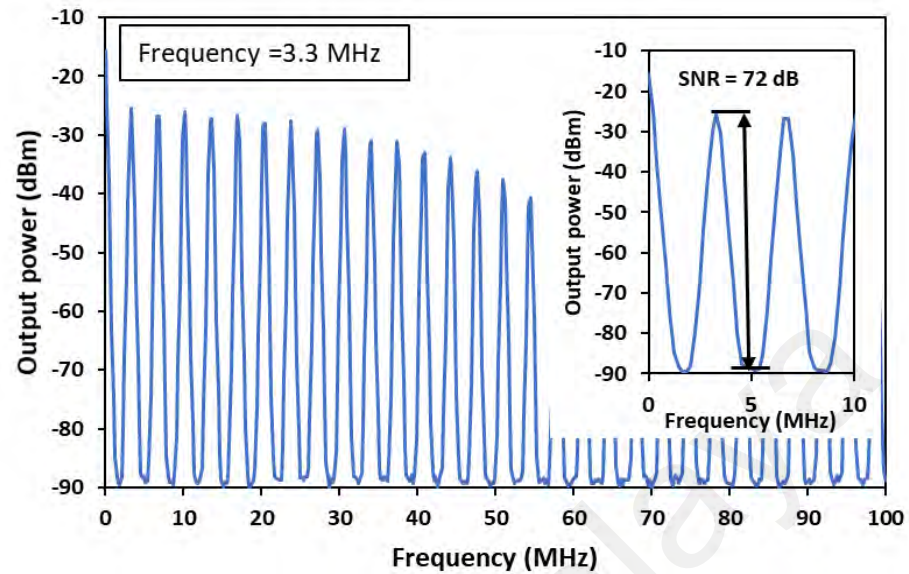
(a)



(b)



(c)



(d)

Figure 5.14: Output performance of the soliton EDFL based on NiO PEG film SA: (a) measured optical spectrum centred at 1561.4 nm (b) typical output pulse train with a spacing of 303 ns; (b) (c) autocorrelation trace of the 710 fs output pulses together with a sech^2 fit; (d) RF spectrum showing the signal-to-background contrast of 72 dB.

Figure 5.15 records the change in output power and pulse energy with increasing pump power of the mode locked EDFL. As shown in the figure, both average output power and single pulse energy of the fiber laser increases linearly with the augment of the pump power. At the maximum pump power of 186.4 mW, the average output power and pulse energy is 7.42 mW and 2.27 nJ, respectively. The SA works stably under the maximum output power, indicating that SA can withstand high power illumination and has good operation stability. We have also tried to take the NiO SA out of the cavity or tried to replace the SA with pure PEG film without NiO. In these two cases, no matter how the pump power was adjusted, mode locking could not be achieved. However, insertion the NiO SA into the cavity again can restore the mode-locked operation of the EDFL, so it is

verified that the mode-locking operation depends on the NiO material. These results fully indicate that the NiO film-based SA has good application prospects in obtaining femtosecond pulse lasers.

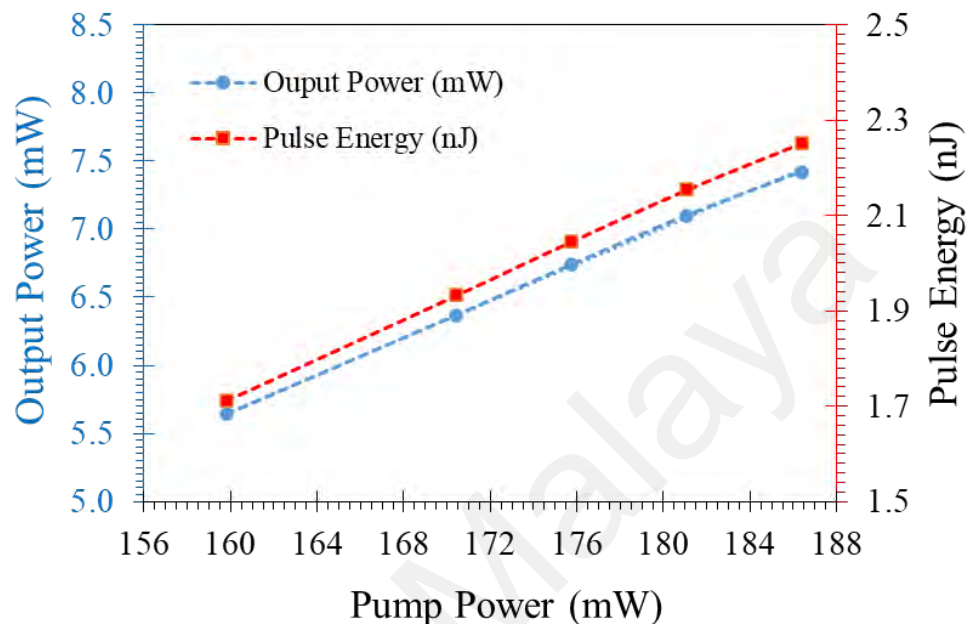


Figure 5.15: Average output power and pulse energy as functions of pump power.

5.6 Summary

Q-switched and mode-locked fiber lasers operated in microsecond and femtosecond regime, respectively were successfully demonstrated using a saturable absorption property of NiO nanoparticles. The NiO PEG film was prepared by drop and dry method, and it was sandwiched between two fiber ferrule connectors with a fiber adapter to form a fiber compatible NiO SA. The modulation depth of the SA device was 9 % at 1550 nm. By inserting NiO into a YDFL cavity, the stable Q-switched pulses appeared at the pump power of 89.2 mW. With the increase of the pump power from 89.2 to 226 mW, the repetition frequency raised from 17.79 to 54.35 kHz, while the pulse width reduced from 9.1 to 2.27 μ s. The maximum single pulse energy is calculated to be 0.69 nJ. The YDFL also exhibits a high SNR for the RF spectrum and long-term stability. Efficient passive Q-switching of an EDFL with NiO SA has also been demonstrated at a threshold pump

power of 143.8 mW. The laser operated at 1570.6 nm. Under a pump power of 239.6 mW, stable Q-switched laser pulses of 5.59 μ s in duration, 9.92 mW in average output power and 150.4 nJ in energy were obtained.

A mode locked EDFL with a soliton pulse of 710 fs was also realized in a modified laser cavity with anomalous cavity dispersion of -0.282 ps^2 with a use of NiO based SA device. A self-starting stable mode-locked pulse operated at 1561.4 nm was obtained within a pump power range from 159.8 to 186.4 mW. It generated the maximum output power and pulse energy of 7.42 mW and 2.27 nJ, respectively at 186.4 mW pump power. This study reveals that the NiO PEG film is a promising laser SA in achieving efficient and stable microsecond and femtosecond pulses. This work opens a new route for the application of NiO to nonlinear photonics, emphasizing the application in Q-switched and mode-locked lasers.

CHAPTER 6: CONCLUSION AND OUTLOOK

6.1 Conclusion

In this work, novel saturable absorber devices based on lanthanoid and metal oxides were studied for developing Q-switched and mode-locked fiber lasers at ~ 1 and $1.5 \mu\text{m}$ regions. These lasers could facilitate a broad range of applications, including laser material processing, telecommunications, and medical diagnostics. The main achievements and findings of the present work can be summarized as follows:

- Successful fabricate and complete characterization for new passive SAs based on three different materials: vanadium pentoxide (V_2O_5), lutetium oxide (Lu_2O_3) and nickel oxide (NiO).
- Successful demonstrate various Q-switched fiber lasers based on the newly developed SAs in both 1- and 1.5-micron regimes.
- Successful demonstrate various mode-locked fiber lasers based on the newly developed SAs.
- A soliton mode-locked Erbium-doped fiber laser (EDFL) operating at 1561.4 nm with a pulse width as short as 710 fs was successfully realized using the NiO based SA by optimizing the cavity design to operate at anomalous cavity dispersion of -0.282 ps^2 .

Vanadium pentoxide (V_2O_5) is one of the most important transition metal oxides, which have an excellent nonlinear optical absorption characteristic. In this study, Q-switched and mode-locked fiber lasers were demonstrated using the newly developed V_2O_5 SA as described in Chapter 3. The SA was prepared by the embedding of V_2O_5 material into polyethylene glycol (PEG) to compose a film absorber, which was then inserted between two fiber ferrules to form a fiber compatible SA device. The V_2O_5 PEG

film was characterized to have modulation depth, saturation intensity and non-saturable absorption of 7 %, 90 MW/cm² and 49 %, respectively.

A Q-switched Ytterbium-doped fiber laser operating at 1068.2 nm was firstly realized by incorporating the SA in a YDFL cavity as the pump power was set above the threshold of 96.1 mW. The maximum output pulse energy of 0.59 nJ and minimum pulse width of 2.97 μ s were obtained at the repetition rate of 43.57 kHz from the laser cavity when the input pump power is 171.8 mW. By incorporating V₂O₅ film into an EDFL, Q-switched pulses were also obtained within a pump power range of 110.9 – 166.5 mW. The pulse repetition rate of the laser has showed an increasing trend from 91.7 kHz to 128.2 kHz, whereas the pulse width exhibited a decreasing trend from 10.90 μ s to 7.81 μ s with the increase of pump power within the range. The highest pulse energy of 3.2 nJ is obtained at pump power of 166.5 mW. An ultrashort pulse laser operating in L-band region (1595.4 nm) was also experimentally achieved by incorporating the V₂O₅ film inside an EDFL cavity configured with 4 m long EDF and 50 m long additional SMF. The soliton mode locked pulses were successfully generated within a pump power of 80.0 mW to 106.6 mW. It operated at a repetition rate of 9.4 MHz and pulse width of 1.40 ps and produced a maximum output power of 1.93 mW and maximum pulse energy of 205.3 pJ. The signal to noise ratio (SNR) of the repetition rate frequency was measured to be 40.66 dB, which indicates the pulses generated was stable.

Lutetium oxide (Lu₂O₃) is one of the lanthanoid oxide materials, which were widely used as cracking, alkylation, hydrogenation, polymerization, X-ray application as well as the starting material in the production of laser crystals. Experimentally, it has been tested to have sufficient optical absorption in both 1 and 1.5- μ m wavelength region, suggesting a suitability to be used as a potential SA candidate. By properly embedding the Lu₂O₃ element into the polyvinyl alcohol (PVA), a very thin Lu₂O₃ PVA film with a thickness

of around 30 μm was successfully realized. In this study, the newly developed Lu_2O_3 PVA composite thin film with a modulation depth of 10% was integrated into fiber laser ring cavity for realizing both Q-switched and mode-locked pulses as described in Chapter 4.

A Q-switched EDFL was stably operating at 1570 nm, within a pump power range between 26.3 and 71.6 mW. At 71.6 mW pump power, the laser operated at 30.4 kHz repetition rate and 8.47 μs pulse width while generating the highest energy of 76 nJ. A stable Q-switched YDFL operating at 1067.8 nm was also successfully obtained with the use of Lu_2O_3 SA. The pulsed laser preserved stably within a tunable frequency range of 26 to 46 kHz throughout an input pump power range of 116 to 151 mW. The maximum peak power, the highest pulse energy and the shortest pulse width were recorded as 28 mW, 128 nJ and 4.6 μs , respectively. Finally, a stable mode locked EDFL operating at 1564 nm wavelength and 0.97 MHz repetition rate has been successfully demonstrated by integrating Lu_2O_3 thin film SA in the extended EDFL cavity within a pump power range of 145-187 mW. The highest attainable output power, pulse energy and peak power were 7.42 mW, 7.64 nJ and 3.61 kW, respectively. The pulse width was 2.12 ps, while the RF signal possessed a considerably high signal to noise ratio of 61 dB.

In chapter 5, Q-switched and mode-locked fiber lasers operated in microsecond and femtosecond regime, respectively were successfully demonstrated using a saturable absorption property of NiO nanoparticles, another metal oxide material. The NiO PEG film was prepared by drop and dry method, and it was sandwiched between two fiber ferrule connectors with a fiber adapter to form a fiber compatible NiO SA. The SA has a modulation depth of about 9 % at 1550 nm. By inserting NiO into a YDFL cavity, the stable Q-switched pulses were successfully obtained as the pump power exceeded the threshold of 89.2 mW. With the increase of the pump power from 89.2 to 226 mW, the repetition frequency raised from 17.79 to 54.35 kHz, while the pulse width reduced from

9.1 to 2.27 μs . The maximum single pulse energy is calculated to be 0.69 nJ. As the NiO SA was incorporated into EDFL cavity, an efficient passive Q-switching has also been demonstrated at a threshold pump power of 143.8 mW. The laser operated at 1570.6 nm. Under a pump power of 239.6 mW, stable Q-switched laser pulses of 5.59 μs in duration, 9.92 mW in average output power and 150.4 nJ in energy were obtained. In a modified EDFL cavity with anomalous cavity dispersion of -0.282 ps^2 , soliton mode-locked pulses operating at 710 fs regime was also realized with a use of NiO based SA device. A self-starting stable mode-locked pulse operated at 1561.4 nm was obtained within a pump power range from 159.8 to 186.4 mW. It generated the maximum output power and pulse energy of 7.42 mW and 2.27 nJ, respectively at 186.4 mW pump power.

The performances of the Q-switched and mode-locked lasers explored in this thesis are summarized in Tables 6.1 and 6.2, respectively. In summary, this study reveals that the V_2O_5 , Lu_2O_3 and NiO films are the promising laser SAs in achieving efficient and stable Q-switched and mode-locked pulses. These SA devices with all-fiber connections offered a robust, reliable, compact, and highly thermal damage threshold pulsed laser in research, medical, military, and industrial applications. In addition, they will facilitate many more potential nonlinear photonic applications, which are expected to work towards ultrafast photonics and play key role in various optical telecommunications and measurement applications.

Table 6.1: Comparison of Q-switching performances

SA	V ₂ O ₅	V ₂ O ₅	Lu ₂ O ₃	Lu ₂ O ₃	NiO	NiO
Center Wavelength (nm)	1068.2	1562.4	1570	1067.8	1064.2	1570.6
Pump Power (mW)	91.1 – 171.8	110.9 – 166.5	26.3 - 71.6	116- 151	89.2 - 226	143 - 239.6
Repetition Rate (kHz)	21.21 – 43.57	91.66 – 128.2	18.4 - 30.4	26.25 - 46.68	17.79 - 54.35	50.3 - 65.96
Output Power (mW)	0.65– 2.58	0.24 – 0.40	0.36 – 2.32	2.2 – 6.0	0.25 – 3.68	5.35 – 9.92
Pulse Width (µs)	5.89 - 2.97	10.6 – 4.71	14.6 – 8.47	9.36 – 4.59	9.1 - 2.27	8.56 – 5.59
Pulse Energy (nJ)	29 - 56	2.6 – 3.2	19.4 - 76	85 - 128	16 - 69	106.36 – 150.4
SNR (dB)	45.84	45.84	40	42	41.1	73.42

Table 6.2: Comparison of mode-locking performances

SA	V ₂ O ₅	Lu ₂ O ₃	NiO
Center Wavelength (nm)	1595.4	1564	1561.4
Spectral Bandwidth (nm)	2.7	1.25	3.7
Pump Power (mW)	80 – 106.6	145 – 187	159.8 - 186.4
Repetition Rate (MHz)	9.4	0.97	3.3
Max. Output Power (mW)	1.93	7.42	7.42
Pulse Width	1.40 ps	2.12 ps	710 fs
Max. Pulse Energy	205.3 pJ	7.64 nJ	2.27 nJ
SNR (dB)	40.66	61	72

6.2 Future Work

All the proposed objectives have been successfully implemented. However, the demonstration of the lanthanoid and metal oxides materials in pulsed fiber laser technology can be further explored. These materials have a great potential as alternative SA. Further work should be devoted to enhancing the performance of the proposed fiber laser in terms of shorting the pulse width as well as increasing the repetition rate, output power and pulse energy. This can be achieved by addressing a shorter cavity length and enhanced gain medium. Additionally, a future work should focus on exploring the developed SAs in other wavelength region such as 2 μm and 3 μm using Thulium-doped fiber (TDF) and ZBLAN EDF, respectively, as the gain medium. Q-switched and mode-locked fiber laser operating in 3.0 μm region will be a very interesting area to investigate. As to the best of our knowledge, there is no affords have been made so far to address the application of the lanthanoid and metal oxides-based SA in this wavelength region. On the other hand, developing new set of lanthanoid and metal-oxide materials for fiber laser application will be interesting research as well. As through this research work, we found that these materials have very attractive performance in fiber laser technology.

REFERENCES

- Ab Rahman, M. F., Latiff, A. A., Rosol, A. H. A., Dimyati, K., Wang, P., & Harun, S. W. (2018). Ultrashort Pulse Soliton Fiber Laser Generation With Integration of Antimony Film Saturable Absorber. *Journal of Lightwave Technology*, 36(16), 3522-3527.
- Adachi, S., & Koyamada, Y. (2002). Analysis and design of Q-switched erbium-doped fiber lasers and their application to OTDR. *Journal of Lightwave Technology*, 20(8), 1506.
- Agrawal, G. P. (2013). *Semiconductor lasers*: Springer Science & Business Media.
- Ahmad, H., Lee, C., Ismail, M., Ali, Z., Reduan, S., Ruslan, N., . . . Harun, S. W. (2016). Zinc oxide (ZnO) nanoparticles as saturable absorber in passively Q-switched fiber laser. *Optics Communications*, 381, 72-76.
- Ahmad, H., Muhammad, F., Zulkifli, M., & Harun, S. J. I. P. J. (2012). Graphene-oxide-based saturable absorber for all-fiber Q-switching with a simple optical deposition technique. 4(6), 2205-2213.
- Ahmad, H., Reduan, S. A., Ali, Z. A., Ismail, M., Ruslan, N., Lee, C., . . . Harun, S. W. J. I. P. J. (2016). C-band Q-switched fiber laser using titanium dioxide (TiO₂) as saturable absorber. 8(1), 1-7.
- Ahmad, H., Ruslan, N., Ismail, M., Reduan, S., Lee, C., Sathiyam, S., . . . Harun, S. W. (2016). Passively Q-switched erbium-doped fiber laser at C-band region based on WS₂ saturable absorber. *Applied optics*, 55(5), 1001-1005.
- Ahmad, H., Samion, M. Z., Kamely, A., Ismail, M. F. J. I. P., & Technology. (2019). Mode-locked thulium doped fiber laser with zinc oxide saturable absorber for 2 μ m operation. 97, 142-148.
- Ahmed, M., Ali, N., Salleh, Z., Rahman, A., Harun, S., Manaf, M., . . . Technology, L. (2014). All fiber mode-locked Erbium-doped fiber laser using single-walled

carbon nanotubes embedded into polyvinyl alcohol film as saturable absorber. *62*, 40-43.

Ahmed, M., Ali, N., Salleh, Z., Rahman, A. A., Harun, S. W., Manaf, M., & Arof, H. (2015). Q-switched erbium doped fiber laser based on single and multiple walled carbon nanotubes embedded in polyethylene oxide film as saturable absorber. *Optics & Laser Technology*, *65*, 25-28.

Al-Hayali, S. K. M., Mohammed, D. Z., Khaleel, W. A., & Al-Janabi, A. H. (2017). Aluminum oxide nanoparticles as saturable absorber for C-band passively Q-switched fiber laser. *Applied optics*, *56*(16), 4720-4726.

Al-Hiti, A. S., Rahman, M. F. A., Harun, S. W., Yupapin, P., & Yasin, M. (2019). Holmium oxide thin film as a saturable absorber for generating Q-switched and mode-locked erbium-doped fiber lasers. *Optical Fiber Technology*, *52*, 101996.

Al-Masoodi, A. H. H., Alani, I. A., Ahmed, M. H. M., Al-Masoodi, A. H., Alani, A. A., Wang, P., & Harun, S. W. (2018). Cobalt oxide nanocubes thin film as saturable absorber for generating Q-switched fiber lasers at 1 and 1.5 μm in ring cavity configuration. *Optical Fiber Technology*, *45*, 128-136.

Alani, I. A., Lokman, M. Q., Ahmed, M. H. M., Al-Masoodi, A. H. H., Latiff, A. A., & Harun, S. W. J. L. P. (2018). A few-picosecond and high-peak-power passively mode-locked erbium-doped fibre laser based on zinc oxide polyvinyl alcohol film saturable absorber. *28*(7), 075105.

Alcock, I., Tropper, A., Ferguson, A., & Hanna, D. J. E. L. (1986). Q-switched operation of a neodymium-doped monomode fibre laser. *22*(2), 84-85.

Alexy, M., Kundrat, J., & Shannon, G. J. B. I. S. w. G. (2017). Resistance Welding and Laser Welding for Electrical Contacting and Micro Joining Solutions. *61*.

Angamuthu, M., & Ramalingam, A. (2011). Balanced key tree management for multi-privileged groups using (N, T) policy. *Security and Communication Networks*.

- Aydın, Y. O. (2014). *Development of a 60 w pulsed fiber laser amplifier for materials processing*.
- Bachmann, F. J. A. s. s. (2003). Industrial applications of high power diode lasers in materials processing. *208*, 125-136.
- Bao, Q., Zhang, H., Ni, Z., Wang, Y., Polavarapu, L., Shen, Z., . . . Loh, K. P. (2011). Monolayer graphene as a saturable absorber in a mode-locked laser. *Nano Research*, *4*(3), 297-307.
- Bouessay, I., Rougier, A., Beaudoin, B., & Leriche, J. J. A. S. S. (2002). Pulsed laser-deposited nickel oxide thin films as electrochromic anodic materials. *186*(1-4), 490-495.
- Bourzeix, S., Plimmer, M., Nez, F., Julien, L., & Biraben, F. (1993). Efficient frequency doubling of a continuous wave titanium: sapphire laser in an external enhancement cavity. *Optics communications*, *99*(1-2), 89-94.
- Chen, B., Zhang, X., Wu, K., Wang, H., Wang, J., & Chen, J. (2015). Q-switched fiber laser based on transition metal dichalcogenides MoS₂, MoSe₂, WS₂, and WSe₂. *Optics express*, *23*(20), 26723-26737.
- Chen, H., Chen, Y., Yin, J., Zhang, X., Guo, T., & Yan, P. (2016). High-damage-resistant tungsten disulfide saturable absorber mirror for passively Q-switched fiber laser. *Optics express*, *24*(15), 16287-16296.
- Chen, R., Tang, Y., Zheng, X., & Jiang, T. J. A. O. (2016). Giant nonlinear absorption and excited carrier dynamics of black phosphorus few-layer nanosheets in broadband spectra. *55*(36), 10307-10312.
- Chen, Y.-F., Tsai, S., & Wang, S. J. O. I. (2000). High-power diode-pumped Q-switched and mode-locked Nd: YVO₄ laser with a Cr⁴⁺: YAG saturable absorber. *25*(19), 1442-1444.
- Chen, Y., Jiang, G., Chen, S., Guo, Z., Yu, X., Zhao, C., . . . Tang, D. (2015). Mechanically exfoliated black phosphorus as a new saturable absorber for both

Q-switching and mode-locking laser operation. *Optics express*, 23(10), 12823-12833.

Chen, Y., Zhao, C., Chen, S., Du, J., Tang, P., Jiang, G., . . . Tang, D. (2014). Large energy, wavelength widely tunable, topological insulator Q-switched erbium-doped fiber laser. *IEEE Journal of Selected Topics in Quantum Electronics*, 20(5), 315-322.

Chen, Y. C., & Fan, X. J. A. O. M. (2019). Biological lasers for biomedical applications. 7(17), 1900377.

Clowes, J. (2008). Next generation light sources for biomedical applications: fibre lasers—compact, cost-effective, turnkey solutions. *Optik & Photonik*, 3(1), 36-38.

Desurvire, E. J. P. T. (1994). The golden age of optical fiber amplifiers. 47(1), 20-27.

Diao Li^{1;2}, H. X., Mei Qi, Yadong Wang, Sinan Aksimsek, Nikolain Chekurov, Wonjae Kim, Changfeng Li, Juha Riikonen, Fangwei Ye, Qing Dai⁶, Zhaoyu Ren, Jintao Bai, Taw que Hasan, Harri Lipsanen and Zhipei Sun. (2017). Graphene actively Q-switched lasers. *IOPscience*, 4(2).

Digonnet, M. J. (2001). *Rare-earth-doped fiber lasers and amplifiers, revised and expanded*: CRC press.

Du, J., Wang, Q., Jiang, G., Xu, C., Zhao, C., Xiang, Y., . . . Zhang, H. (2014). Ytterbium-doped fiber laser passively mode locked by few-layer Molybdenum Disulfide (MoS₂) saturable absorber functioned with evanescent field interaction. *Scientific reports*, 4, 6346.

Duan, W., Lu, S., Wu, Z., & Wang, Y. (2012). Size effects on properties of NiO nanoparticles grown in alkalisalts. *The Journal of Physical Chemistry C*, 116(49), 26043-26051.

- Eichhorn, M., & Jackson, S. D. J. O. L. (2007). High-pulse-energy actively Q-switched Tm³⁺-doped silica 2 μm fiber laser pumped at 792 nm. *32*(19), 2780-2782.
- Eigenwillig, C. M., Biedermann, B. R., Palte, G., & Huber, R. (2008). K-space linear Fourier domain mode locked laser and applications for optical coherence tomography. *Optics express*, *16*(12), 8916-8937.
- El-Sherif, A. F., & King, T. A. (2003). High-energy, high-brightness Q-switched Tm³⁺-doped fiber laser using an electro-optic modulator. *Optics communications*, *218*(4-6), 337-344.
- Etzel, H., Gandy, H., & Ginther, R. J. A. O. (1962). Stimulated emission of infrared radiation from ytterbium activated silicate glass. *1*(4), 534-536.
- Franken, e. P., Hill, A. E., Peters, C., & Weinreich, G. J. P. R. L. (1961). Generation of optical harmonics. *7*(4), 118.
- Freudiger, C. W., Yang, W., Holtom, G. R., Peyghambarian, N., Xie, X. S., & Kieu, K. Q. J. N. p. (2014). Stimulated Raman scattering microscopy with a robust fibre laser source. *8*(2), 153.
- Fu, B., Hua, Y., Xiao, X., Zhu, H., Sun, Z., & Yang, C. (2014). Broadband graphene saturable absorber for pulsed fiber lasers at 1, 1.5, and 2 μm. *IEEE Journal of Selected Topics in Quantum Electronics*, *20*(5), 411-415.
- Gandy, H., Ginther, R., & Weller, J. J. A. P. L. (1965). Energy transfer in triply activated glasses. *6*(3), 46-49.
- Gangwar, R., Singh, S. P., & Singh, N. J. P. I. E. R. (2007). Soliton based optical communication. *74*, 157-166.
- Garmire, E. (2000). Resonant optical nonlinearities in semiconductors. *IEEE Journal of Selected Topics in Quantum Electronics*, *6*(6), 1094-1110.

- Gattass, R. R., & Mazur, E. J. N. p. (2008). Femtosecond laser micromachining in transparent materials. *2*(4), 219-225.
- Geim, A. K., & Grigorieva, I. V. J. N. (2013). Van der Waals heterostructures. *499*(7459), 419-425.
- Geusic, J., Marcos, H., & Van Uitert, L. J. A. P. L. (1964). Laser oscillations in Nd-doped yttrium aluminum, yttrium gallium and gadolinium garnets. *4*(10), 182-184.
- Glubokov, D. A. e., Sychev, V. V. e., Mikhailov, A. S., Korolkov, A. E. e., Chubich, D. A. e., Shapiro, B. I., & Vitukhnovskii, A. G. e. (2014). Saturable absorber based on silver nanoparticles for passively mode-locked lasers. *Quantum Electronics*, *44*(4), 314.
- Gomez, L. A. J. I. J. o. s. t. i. Q. e. (2004). Picosecond SESAM-Baed Ytterbium Mode-Locked Fiber Laser. *10*(1), 129.136.
- Guo, B., Wang, S.-H., Wu, Z.-X., Wang, Z.-X., Wang, D.-H., Huang, H., . . . Zhang, H. (2018). Sub-200 fs soliton mode-locked fiber laser based on bismuthene saturable absorber. *Optics express*, *26*(18), 22750-22760.
- Hakulinen, T., & Okhotnikov, O. G. (2007). 8 ns fiber laser Q switched by the resonant saturable absorber mirror. *Optics letters*, *32*(18), 2677-2679.
- Haris, H., Harun, S. W., Yupapin, P., Arof, H., & Apsari, R. (2020). Generation of Vector Soliton Pulses with Graphene Oxide Film in Mode-locked Erbium-doped Fiber Laser Cavity. *Nonlinear Optics Quantum Optics-Concepts in Modern Optics*, *52*(1-2), 111-118.
- Harun, S. W., Ismail, M., Ahmad, F., Ismail, M., Nor, R. M., Zulkepely, N., & Ahmad, H. J. C. P. L. (2012). A Q-switched erbium-doped fiber laser with a carbon nanotube based saturable absorber. *29*(11), 114202.

- Haus, H. A. (2000). Mode-locking of lasers. *IEEE Journal of Selected Topics in Quantum Electronics*, 6(6), 1173-1185.
- Hecht, J. (2010). The First Half-Century of Laser Development: How a solution that once was looking for a problem has become part of everyday life. In: Wiley Online Library.
- Herda, R., Kivistö, S., & Okhotnikov, O. G. J. O. I. (2008). Dynamic gain induced pulse shortening in Q-switched lasers. 33(9), 1011-1013.
- Hermens, F., Flin, R., & Ahmed, I. J. J. o. E. m. r. (2013). Eye movements in surgery: A literature review. 6(4).
- Hjelme, D. R., & Mickelson, A. R. J. I. j. o. q. e. (1992). Theory of timing jitter in actively mode-locked lasers. 28(6), 1594-1606.
- Huang, S.-L., Tsui, T.-Y., Wang, C.-H., & Kao, F.-J. J. J. j. o. a. p. (1999). Timing jitter reduction of a passively Q-switched laser. 38(3A), L239.
- Island, J. O., Steele, G. A., van der Zant, H. S., & Castellanos-Gomez, A. (2015). Environmental instability of few-layer black phosphorus. *2D Materials*, 2(1), 011002.
- Ismail, E., Kadir, N., Latiff, A., Ahmad, H., & Harun, S. (2016). Black phosphorus crystal as a saturable absorber for both a Q-switched and mode-locked erbium-doped fiber laser. *RSC advances*, 6(76), 72692-72697.
- Jackson, S. D., Bugge, F., & Erbert, G. J. O. I. (2007). Directly diode-pumped holmium fiber lasers. 32(17), 2496-2498.
- Jackson, S. D. J. A. o. (2007). Passively Q-switched Tm 3+-doped silica fiber lasers. 46(16), 3311-3317.

- Javan, A., Bennett Jr, W. R., & Herriott, D. R. J. P. R. L. (1961). Population inversion and continuous optical maser oscillation in a gas discharge containing a He-Ne mixture. *6*(3), 106.
- Jiang, M., Ahn, K., Cao, X.-D., Dasika, P., Liang, Y., Islam, M., . . . Weidman, D. (1997). Synchronization of passively mode-locked erbium-doped fiber lasers and its application to optical communication networks. *Journal of Lightwave Technology*, *15*(11), 2020-2028.
- Jiang, X., Liu, S., Liang, W., Luo, S., He, Z., Ge, Y., . . . Wen, Q. (2018). Broadband nonlinear photonics in few-layer MXene Ti₃C₂T_x (T= F, O, or OH). *Laser & Photonics Reviews*, *12*(2), 1700229.
- Jiang, Y., Narushima, T., & Okamoto, H. J. N. P. (2010). Nonlinear optical effects in trapping nanoparticles with femtosecond pulses. *6*(12), 1005-1009.
- Jin, X., Hu, G., Zhang, M., Hu, Y., Albrow-Owen, T., Howe, R. C., . . . Hasan, T. (2018). 102 fs pulse generation from a long-term stable, inkjet-printed black phosphorus-mode-locked fiber laser. *Optics express*, *26*(10), 12506-12513.
- Johnson, L., Boyd, G., Nassau, K., & Soden, R. J. P. R. (1962). Continuous operation of a solid-state optical maser. *126*(4), 1406.
- Kang, Z., Liu, M., Li, Z., Li, S., Jia, Z., Liu, C., . . . Qin, G. (2018). Passively Q-switched erbium doped fiber laser using a gold nanostars based saturable absorber. *Photonics Research*, *6*(6), 549-553.
- Kao, K. C., & Hockham, G. A. (1966). *Dielectric-fibre surface waveguides for optical frequencies*. Paper presented at the Proceedings of the Institution of Electrical Engineers.
- Keiser, G., Xiong, F., Cui, Y., & Shum, P. P. J. J. o. b. o. (2014). Review of diverse optical fibers used in biomedical research and clinical practice. *19*(8), 080902.

- Keller, U. (2003a). Recent developments in compact ultrafast lasers. *Nature Photonics*, 424, 831-838.
- Keller, U. (2003b). Recent developments in compact ultrafast lasers. *nature*, 424(6950), 831-838.
- Keller, U., Miller, D., Boyd, G., Chiu, T., Ferguson, J., & Asom, M. (1992). Solid-state low-loss intracavity saturable absorber for Nd: YLF lasers: an antiresonant semiconductor Fabry–Perot saturable absorber. *Optics letters*, 17(7), 505-507.
- Keller, U. J. n. (2003). Recent developments in compact ultrafast lasers. 424(6950), 831-838.
- Koester, C. J., & Snitzer, E. J. A. o. (1964). Amplification in a fiber laser. 3(10), 1182-1186.
- Kong, C., Pilger, C., Hachmeister, H., Wei, X., Cheung, T. H., Lai, C. S., . . . Wong, K. K. J. B. o. e. (2017). Compact fs ytterbium fiber laser at 1010 nm for biomedical applications. 8(11), 4921-4932.
- Koponen, J. J., Söderlund, M. J., Hoffman, H. J., & Tammela, S. K. J. O. E. (2006). Measuring photodarkening from single-mode ytterbium doped silica fibers. 14(24), 11539-11544.
- Kumar, A., Gupta, M. P., Banerjee, J., Neogy, S., Keskar, N., Bhatt, R., . . . Processing, M. (2019). Micro-Welding of Stainless Steel and Copper Foils Using a Nano-Second Pulsed Fiber Laser. 6(2), 158-172.
- Kurkov, A. J. L. P. L. (2011). Q-switched all-fiber lasers with saturable absorbers. 8(5), 335-342.
- Latiff, A., Rusdi, M., Hisyam, M., Ahmad, H., & Harun, S. (2016). *Black phosphorus as a saturable absorber for generating mode-locked fiber laser in normal dispersion*

regime. Paper presented at the Second International Seminar on Photonics, Optics, and Its Applications (ISPhOA 2016).

- Lee, J., Koo, J., Jhon, Y. M., & Lee, J. H. J. O. e. (2015). Femtosecond harmonic mode-locking of a fiber laser based on a bulk-structured Bi₂Te₃ topological insulator. *23*(5), 6359-6369.
- Li, H., Shi, Y., Chiu, M.-H., & Li, L.-J. J. N. E. (2015). Emerging energy applications of two-dimensional layered transition metal dichalcogenides. *18*, 293-305.
- Li, H., Xia, H., Lan, C., Li, C., Zhang, X., Li, J., & Liu, Y. (2015). Passively Q-switched erbium-doped fiber laser based on few-layer MoS₂ saturable absorber. *IEEE Photonics Technology Letters*, *27*(1), 69-72.
- Li, J., Luo, H., Zhai, B., Lu, R., Guo, Z., Zhang, H., & Liu, Y. (2016). Black phosphorus: a two-dimension saturable absorption material for mid-infrared Q-switched and mode-locked fiber lasers. *Scientific reports*, *6*, 30361.
- Lin, J., Hu, Y., Chen, C., Gu, C., & Xu, L. J. O. e. (2015). Wavelength-tunable Yb-doped passively Q-switching fiber laser based on WS₂ saturable absorber. *23*(22), 29059-29064.
- Liu, J., Xu, J., & Wang, P. (2012). Graphene-based passively Q-switched 2 μ m thulium-doped fiber laser. *Optics Communications*, *285*(24), 5319-5322.
- Liu, X., Han, D., Sun, Z., Zeng, C., Lu, H., Mao, D., . . . Wang, F. J. S. r. (2013). Versatile multi-wavelength ultrafast fiber laser mode-locked by carbon nanotubes. *3*(1), 1-6.
- Lokman, M. Q., Yusoff, S. F. A. Z., Ahmad, F., Zakaria, R., Yahaya, H., Shafie, S., . . . Harun, S. W. (2018). Deposition of silver nanoparticles on polyvinyl alcohol film using electron beam evaporation and its application as a passive saturable absorber. *Results in Physics*, *11*, 232-236.

- Lu, L., Liang, Z., Wu, L., Chen, Y., Song, Y., Dhanabalan, S. C., . . . Xing, F. (2018). Few-layer Bismuthene: Sonochemical Exfoliation, Nonlinear Optics and Applications for Ultrafast Photonics with Enhanced Stability. *Laser & Photonics Reviews*, 12(1), 1700221.
- Lucas, L., & Zhang, J. (2012). Femtosecond laser micromachining: a back-to-basics primer. *Industrial laser solutions*.
- Luo, Z.-C., Luo, A.-P., & Xu, W.-C. J. I. P. J. (2010). Tunable and switchable multiwavelength passively mode-locked fiber laser based on SESAM and inline birefringence comb filter. 3(1), 64-70.
- Luo, Z., Huang, Y., Zhong, M., Li, Y., Wu, J., Xu, B., . . . Weng, J. J. J. o. L. T. (2014). 1-, 1.5-, and 2- μm fiber lasers Q-switched by a broadband few-layer MoS₂ saturable absorber. 32(24), 4077-4084.
- Luo, Z., Zhou, M., Weng, J., Huang, G., Xu, H., Ye, C., & Cai, Z. (2010). Graphene-based passively Q-switched dual-wavelength erbium-doped fiber laser. *Optics letters*, 35(21), 3709-3711.
- Ma, J., Lu, S., Guo, Z., Xu, X., Zhang, H., Tang, D., & Fan, D. (2015). Few-layer black phosphorus based saturable absorber mirror for pulsed solid-state lasers. *Optics express*, 23(17), 22643-22648.
- Maiman, T. H. (1960). Stimulated optical radiation in ruby.
- Manzeli, S., Ovchinnikov, D., Pasquier, D., Yazyev, O. V., & Kis, A. J. N. R. M. (2017). 2D transition metal dichalcogenides. 2(8), 17033.
- Mao, D., Cui, X., He, Z., Lu, H., Zhang, W., Wang, L., . . . Zhao, J. J. N. (2018). Broadband polarization-insensitive saturable absorption of Fe₂O₃ nanoparticles. 10(45), 21219-21224.

- Mao, D., She, X., Du, B., Yang, D., Zhang, W., Song, K., . . . Zhao, J. (2016). Erbium-doped fiber laser passively mode locked with few-layer WSe₂/MoSe₂ nanosheets. *Scientific reports*, 6, 23583.
- Mao, D., Wang, Y., Ma, C., Han, L., Jiang, B., Gan, X., . . . Zhao, J. (2015a). WS₂ mode-locked ultrafast fiber laser. *Scientific reports*, 5, 7965.
- Mao, D., Wang, Y., Ma, C., Han, L., Jiang, B., Gan, X., . . . Zhao, J. J. S. r. (2015b). WS₂ mode-locked ultrafast fiber laser. 5, 7965.
- Martin E. Fermann, I. H. (2009). Ultrafast Fiber Laser Technology. *IEEE JOURNAL OF SELECTED TOPICS IN QUANTUM ELECTRONICS*, 15(1), 191-206.
- Mears, R. J., Reekie, L., Jauncey, I., & Payne, D. N. J. E. L. (1987). Low-noise erbium-doped fibre amplifier operating at 1.54 μm . 23(19), 1026-1028.
- Minoshima, K., Kowalevich, A. M., Hartl, I., Ippen, E. P., & Fujimoto, J. G. J. O. L. (2001). Photonic device fabrication in glass by use of nonlinear materials processing with a femtosecond laser oscillator. 26(19), 1516-1518.
- Moghissi, K., & Dixon, K. J. F. O. (2017). Image-guided surgery and therapy for lung cancer: a critical review. 13(26), 2383-2394.
- Molli, M., Bhat Kademane, A., Pradhan, P., & Sai Muthukumar, V. (2016). Study of nonlinear optical absorption properties of V₂O₅ nanoparticles in the femtosecond excitation regime. *Applied Physics A*, 122(8), 757. doi:10.1007/s00339-016-0290-6
- Moulton, P. F. J. J. B. (1986). Spectroscopic and laser characteristics of Ti: Al₂O₃. 3(1), 125-133.
- Nagy, Z., Takacs, A., Filkorn, T., & Sarayba, M. J. J. o. r. s. (2009). Initial clinical evaluation of an intraocular femtosecond laser in cataract surgery. 25(12), 1053-1060.

- Nikodem, M. P., Sergeant, H., Kaczmarek, P., & Abramski, K. M. (2008). *Actively mode-locked fiber laser using acousto-optic modulator*. Paper presented at the 16th Polish-Slovak-Czech Optical Conference on Wave and Quantum Aspects of Contemporary Optics.
- Niu, K., Chen, Q., Sun, R., Man, B., & Zhang, H. (2017). Passively Q-switched erbium-doped fiber laser based on SnS 2 saturable absorber. *Optical Materials Express*, 7(11), 3934-3943.
- Nizamani, B., Salam, S., Jafry, A. A. A., Zahir, N. M., Jurami, N., Khudus, M., . . . Harun, S. W. (2020). Indium Tin Oxide Coated D-Shape Fiber as a Saturable Absorber for Generating a Dark Pulse Mode-Locked Laser. *Chinese Physics Letters*, 37(5). doi:10.1088/0256-307x/37/5/054202
- Okhotnikov, O., Grudinin, A., & Pessa, M. (2004). Ultra-fast fibre laser systems based on SESAM technology: new horizons and applications. *New journal of physics*, 6(1), 177.
- Ordin, S., & Shelykh, A. J. S. (2010). Optical and dielectric characteristics of the rare-earth metal oxide Lu 2 O 3. *44(5)*, 558-563.
- Osellame, R., Cerullo, G., & Ramponi, R. (2012). *Femtosecond laser micromachining: photonic and microfluidic devices in transparent materials* (Vol. 123): Springer Science & Business Media.
- Pang, L., Song, C., Lv, R., Chen, Z., Liu, S., Wu, R., . . . Technology, L. (2019). High stable polarization-insensitive Er-doped Q-switched fiber laser with iron oxide nanoparticles as saturable absorber. *113*, 379-383.
- Paschotta, R., Häring, R., Gini, E., Melchior, H., Keller, U., Offerhaus, H., & Richardson, D. (1999). Passively Q-switched 0.1-mJ fiber laser system at 1.53 μm. *Optics letters*, 24(6), 388-390.

- Paschotta, R., Nilsson, J., Tropper, A. C., & Hanna, D. C. J. I. J. o. q. e. (1997). Ytterbium-doped fiber amplifiers. *33*(7), 1049-1056.
- Patel, C. K. N. J. P. r. (1964). Continuous-wave laser action on vibrational-rotational transitions of C O 2. *136*(5A), A1187.
- Pepe, Y., Karatay, A., Donar, Y. O., Yildiz, E. A., Sınağ, A., Unver, H., & Elmali, A. J. O. (2021). Enhanced nonlinear absorption coefficient and low optical limiting threshold of NiO nanocomposite films. *227*, 165975.
- Peter, W., Milonni, J., & Eberly, H. (2010). Text book of Laser physics.
- Plamann, K., Aptel, F., Arnold, C., Courjaud, A., Crotti, C., Deloison, F., . . . Legeais, J.-M. J. J. o. O. (2010). Ultrashort pulse laser surgery of the cornea and the sclera. *12*(8), 084002.
- Popa, D., Sun, Z., Hasan, T., Torrisi, F., Wang, F., & Ferrari, A. C. (2011). Graphene Q-switched, tunable fiber laser. *Applied Physics Letters*, *98*(7), 073106.
- Rahimi-Nasrabadi, M., Pourmortazavi, S. M., Ganjali, M. R., & Norouzi, P. J. J. o. M. S. M. i. E. (2017). Optimized synthesis and characterization of lutetium carbonate and oxide nanoparticles and their use as degradation photocatalyst. *28*(22), 17078-17088.
- Rahman, M., Rusdi, M., Lokman, M., Mahyuddin, M., Latiff, A., Rosol, A., . . . Harun, S. J. C. P. L. (2017). Holmium Oxide Film as a Saturable Absorber for 2 μ m Q-Switched Fiber Laser. *34*(5), 054201.
- Reddy, P. H., Rahman, M. F. A., Paul, M. C., Latiff, A. A., Rosol, A. H. A., Das, S., . . . Harun, S. W. (2018). Titanium dioxide doped fiber as a new saturable absorber for generating mode-locked erbium doped fiber laser. *Optik*, *158*, 1327-1333.

- Rosol, A. H. A., Latiff, A. A., Khudus, M., & Harun, S. W. (2020). Nanosecond pulses generation with rose gold nanoparticles saturable absorber. *Indian Journal of Physics*, 94(7), 1079-1083. doi:10.1007/s12648-019-01541-4
- Rusdi, M., Rosol, A., Rahman, M., Mahyuddin, M., Latiff, A., Ahmad, H., . . . Yasin, M. (2019). Q-switched and mode-locked thulium doped fiber lasers with nickel oxide film saturable absorber. *Optics Communications*, 447, 6-12.
- Rusdi, M. F. M., Latiff, A. A., Paul, M. C., Das, S., Dhar, A., Ahmad, H., . . . Technology, L. (2017). Titanium dioxide (TiO₂) film as a new saturable absorber for generating mode-locked thulium-holmium doped all-fiber laser. 89, 16-20.
- Sadeq, S. A., Harun, S. W., & Al-Janabi, A. H. J. A. O. (2018). Ultrashort pulse generation with an erbium-doped fiber laser ring cavity based on a copper oxide saturable absorber. 57(18), 5180-5185.
- Salehi, J. A., Weiner, A. M., & Heritage, J. P. J. J. o. L. T. (1990). Coherent ultrashort light pulse code-division multiple access communication systems. 8(3), 478-491.
- Set, S. Y., Yaguchi, H., Tanaka, Y., & Jablonski, M. (2004a). Laser mode locking using a saturable absorber incorporating carbon nanotubes. *Journal of Lightwave Technology*, 22(1), 51.
- Set, S. Y., Yaguchi, H., Tanaka, Y., & Jablonski, M. J. J. o. L. T. (2004b). Laser mode locking using a saturable absorber incorporating carbon nanotubes. 22(1), 51.
- Snitzer, E. J. P. o. t. I. (1966). Glass lasers. 54(10), 1249-1261.
- Sobon, G. J. P. R. (2015). Mode-locking of fiber lasers using novel two-dimensional nanomaterials: graphene and topological insulators. 3(2), A56-A63.
- Sorokin, P. P., Lankard, J. J. I. J. o. R., & Development. (1966). Stimulated emission observed from an organic dye, chloro-aluminum phthalocyanine. 10(2), 162-163.

- Spühler, G., Paschotta, R., Fluck, R., Braun, B., Moser, M., Zhang, G., . . . Keller, U. J. B. (1999). Experimentally confirmed design guidelines for passively Q-switched microchip lasers using semiconductor saturable absorbers. *16*(3), 376-388.
- Srilakshmi, P., Maheswari, A., Sajeew, V., & Sivakumar, M. (2019). Tuning the optical bandgap of V₂O₅ nanoparticles by doping transition metal ions. *Materials Today: Proceedings*, *18*, 1375-1379.
- Steen, W. M., & Mazumder, J. (2010). *Laser material processing*: springer science & business media.
- Sun, B., Zhang, Y., Zhang, R., Yu, H., Zhou, G., Zhang, H., & Wang, J. J. O. e. (2018). Nonlinear optical response during the electron transition process originated from 3D spin-orbit splitting in NiO nanosheets. *26*(2), 1230-1236.
- Sun, R., Zhang, H., & Xu, N. (2018). High-power passively Q-switched Yb-doped fiber laser based on Tin selenide as a saturable absorber. *Laser Physics*, *28*(8), 085105.
- Sun, Z., Hasan, T., Torrisi, F., Popa, D., Privitera, G., Wang, F., . . . Ferrari, A. (2010). Graphene mode-locked ultrafast laser. *ACS Nano* *4* (2): 803–810. In.
- Tan, C., Huang, X., & Zhang, H. J. M. T. (2013). Synthesis and applications of graphene-based noble metal nanostructures. *16*(1-2), 29-36.
- Tanabe, S. J. C. R. C. (2002). Rare-earth-doped glasses for fiber amplifiers in broadband telecommunication. *5*(12), 815-824.
- Tsai, T.-Y., & Birnbaum, M. J. J. o. a. p. (2000). Co²⁺: ZnS and Co²⁺: ZnSe saturable absorber Q switches. *87*(1), 25-29.

- Usha, V., Vettumperumal, R., Kalyanaraman, S., & Thangavel, R. J. I. J. o. N. (2018). Analysis of linear and nonlinear optical properties of NiO nanoparticles by sol-gel method. *17*(05), 1850003.
- Walsh, T., Ilkov, F., & Chin, S. (1997). The dynamical behaviour of and in a strong, femtosecond, titanium: sapphire laser field. *Journal of Physics B: Atomic, Molecular and Optical Physics*, *30*(9), 2167.
- Wang, J., Yang, P., Wei, X., & Zhou, Z. (2015). Preparation of NiO two-dimensional grainy films and their high-performance gas sensors for ammonia detection. *Nanoscale research letters*, *10*(1), 119.
- Wang, W., Yue, W., Liu, Z., Shi, T., Du, J., Leng, Y., . . . Liu, X. J. A. O. M. (2018). Ultrafast Nonlinear Optical Response in Plasmonic 2D Molybdenum Oxide Nanosheets for Mode-Locked Pulse Generation. *6*(17), 1700948.
- Wang, Z., Molina-Sanchez, A., Altmann, P., Sangalli, D., De Fazio, D., Soavi, G., . . . Finazzi, M. J. N. I. (2018). Intravalley spin-flip relaxation dynamics in single-layer WS₂. *18*(11), 6882-6891.
- Watanabe, S., & Takahashi, H. J. N. E. J. o. M. (1994). Treatment of nevus of Ota with the Q-switched ruby laser. *331*(26), 1745-1750.
- Weber, M., Lynch, J., Blackburn, D., & Cronin, D. J. I. J. o. q. e. (1983). Dependence of the stimulated emission cross section of Yb³⁺ on host glass composition. *19*(10), 1600-1608.
- Wiktorczyk, T. J. O. A. (2001). Optical properties of electron beam deposited. *31*(1).
- Woodward, R. I., & Kelleher, E. J. J. A. S. (2015). 2D saturable absorbers for fibre lasers. *5*(4), 1440-1456.
- Xu, C., & Wise, F. J. N. p. (2013). Recent advances in fibre lasers for nonlinear microscopy. *7*(11), 875.

- Xu, N., Zhang, H., Yang, W., Han, X., & Man, B. (2018). High-efficiency passively Q-switched neodymium-doped fiber laser operation at 1360.61 nm with bismuth selenide as saturable absorber. *Laser physics*, 28(12), 125801.
- Yan, B., Liao, L., You, Y., Xu, X., Zheng, Z., Shen, Z., . . . Yu, T. (2009). Single-Crystalline V2O5 Ultralong Nanoribbon Waveguides. *Advanced materials*, 21(23), 2436-2440.
- Yang, H., & Liu, X. (2017). Nonlinear optical response and applications of tin disulfide in the near-and mid-infrared. *Applied Physics Letters*, 110(17), 171106.
- Yuan, L., Ge, J., Peng, X., Zhang, Q., Wu, Z., Jian, Y., . . . Han, J. J. A. A. (2016). A reliable way of mechanical exfoliation of large scale two dimensional materials with high quality. *6*(12), 125201.
- Zayhowski, J., & Dill, C. J. O. I. (1995). Coupled-cavity electro-optically Q-switched Nd:YVO 4 microchip lasers. *20*(7), 716-718.
- Zayhowski, J., & Kelley, P. J. I. j. o. q. e. (1991). Optimization of Q-switched lasers. *27*(9), 2220-2225.
- Zayhowski, J. J., & Dill, C. J. O. I. (1994). Diode-pumped passively Q-switched picosecond microchip lasers. *19*(18), 1427-1429.
- Zervas, M. N., & Codemard, C. A. J. I. J. o. s. t. i. Q. E. (2014). High power fiber lasers: a review. *20*(5), 219-241.
- Zhang, H., Tang, D., Zhao, L., Bao, Q., & Loh, K. J. O. E. (2009). Large energy mode locking of an erbium-doped fiber laser with atomic layer graphene. *17*(20), 17630-17635.

Zhao, C., Zhang, H., Qi, X., Chen, Y., Wang, Z., Wen, S., & Tang, D. (2012). Ultra-short pulse generation by a topological insulator based saturable absorber. *Applied Physics Letters*, 101(21), 211106.

Zhou, D.-P., Wei, L., Dong, B., & Liu, W.-K. (2010). Tunable passively Q-switched erbium-doped fiber laser with carbon nanotubes as a saturable absorber. *IEEE Photonics Technology Letters*, 22(1), 9-11.

Zitter, R. N. J. A. P. L. (1969). Saturated optical absorption through band filling in semiconductors. *14*(2), 73-74.

Universiti Malaysia

LIST OF PUBLICATIONS AND PAPERS PRESENTED

Journal Publications (ISI)

- a) **MF Baharom**, MFA Rahman, AA Latiff, P Wang, H Arof, SW Harun. (2019). Lutetium oxide film as a passive saturable absorber for generating Q-switched fiber laser at 1570 nm wavelength. *Optical Fiber Technology*, Vol 50 pp (82-86).
- b) **MF Baharom**, MFA Rahman, AA Latiff, P Wang, SW Harun. (2019). Lutetium (III) oxide film as passive mode locker device for erbium-doped fibre laser cavity. *Optics Communications* 446, 51-55.
- c) **MF Baharom**, MFA Rahman, AA Latiff, R Apsari, SW Harun. (2020). Inducing Q-switching operation at 1-micron all-fiber laser via lutetium oxide film saturable absorber” *Optik*,pp 165267.
- d) A Nady, **MF Baharom**, AA Latiff, SW Harun. (2018). Mode-Locked Erbium-Doped Fiber Laser Using Vanadium Oxide as Saturable Absorber. *Chinese Physics Letters*, Vol 35 pp(4).
- e) A Jannifar, **MF Baharom**, J Bakri, SW Harun. (2018). Q-Switched Ytterbium-Doped Fiber Laser Using V₂O₅ Polymer film as Saturable Absorber. *Nonlinear Optics, Quantum Optics: Concepts in Modern Optics*, Vol 49.
- f) A Jannifar, **MF Baharom**, NF Zulkipli, J Bakri, SW Harun. (2018). Q-switched Ytterbium-doped Fiber Laser with Nickel Oxide Nanoparticles Saturable Absorber. *Nonlinear Optics, Quantum Optics: Concepts in Modern Optics*, Vol 49.

- g) M.F.A. Rahman, P. H. Reddy, M. C. Paul, S. Das, A.Dhar, **M.F.Baharom**, A.A. Latiff, M.F.M. Rusdi, P. Wang, K. Dimyati, S. W. Harun. (2019).Titanium dioxide fiber saturable absorber for Q-switched fiber laser generation in the 1-micrometer region. Applied optics, Vol. 3, 3495-3500.

Paper Presented at Conference

- a) **M.F. Baharom**, N.F. Zulkeffli, A.A. Latif, S.W. Harun. (2018). Erbium Oxide as New Saturable Absorber for Short-Pulse Generation at 1.55-Micron Region. Newton Researcher Links Workshop: 2018 Bio-Photonics for Medical Technologies, Malacca, Malaysia